X-10 REACTOR FORENSIC ANALYSIS AND EVALUATION USING A SUITE OF NEUTRON TRANSPORT CODES

A Thesis
Presented to
The Academic Faculty

by

Evan Maxwell Redd

In Partial Fulfillment
of the Requirements for the Degree
Master of Science in Nuclear Engineering in the
George W. Woodruff School of Mechanical Engineering

Georgia Institute of Technology
August 2015

X-10 REACTOR FORENSIC ANALYSIS AND EVALUATION USING A SUITE OF NEUTRON TRANSPORT CODES

Approved by:

Dr. Anna Erickson, Advisor
School of Mechanical Engineering
Georgia Institute of Technology

Dr. Ce Yi
School of Mechanical Engineering
Georgia Institute of Technology

Dr. Glenn Sjoden
Air Force Technical Applications Center
U.S. Air Force

Dr. Kevin Manalo
High Performance Computing
Alabama School System HPC

Date Approved: March 25, 2015

This thesis work is dedicated to my family. To my father, Alan, who taught me to never give up and to never stop learning. My late mother, Linda, who instilled the importance of happiness and selflessness. My sister, Lindsay, who showed me strong resolve and persistence in achieving happiness. Last but not least, my beautiful wife Michelle, who unconditionally supported and encouraged me throughout my academic career and life.

ACKNOWLEDGEMENTS

First, I would like to thank Dr. Glenn Sjoden for his career/research guidance and challenging reactor physics courses that imparted the skills needed for becoming a successful nuclear engineer. I would also like to thank Dr. Anna Erickson, who provided a smooth transition in advisement and was instrumental in shaping this research. Last and certainly not least, I would like to thank the former CRiTCEL team. Specifically, Dr. Kevin Manalo, Dr. Ce Yi, Dr. Chris Edgar, Mike Chin, Dr. Jessica Paul and Matt Molinar for assistance and most importantly the patience for fielding my endless questions.

This material is based upon work supported by the U.S. Department of Homeland Security under Grant Award Number, 2012-DN-130-NF0001. The views and conclusions contained in this document are those of the author(s) and should not be interpreted as representing the official policies, either expressed or implied, of the U.S. Department of Homeland Security.

TABLE OF CONTENTS

LIST OF TABLES

LIST OF FIGURES

SUMMARY

X-10, the genesis production reactor for the U.S. paved the way for all weapons material production. This feat offers a unique fundamental opportunity of nuclear forensic analysis and popular neutron code package evaluation. Production reactor nuclear forensic signatures and characteristics are emphasized throughout this work. These underlying production characteristics are reported and analyzed for potential in-core zone provenance and axial slug location coupled with how the nuclear data uncertainties affect these conclusions. Material attribution with respect to commercial versus military reactor applications is also featured in this study. Three nuclear code packages are examined including Scale 6.1 (Scale 6.2 beta-3 for nuclear data uncertainty reporting and evaluation), Monte Carlo N-Particle (MCNP) and Parallel Environment Neutral-particle TRANsport (PENTRAN). Each of these code packages employs different neutron transport methods and cross-section evaluation. These code results are compared and contrasted for the researcher to gain perspective into if and how nuclear forensic analysis is affected by these relative outcomes from the neutronics packages. Notably, Scale 6.2 beta-3 offers perspective on the nuclear data uncertainty and how it affects final conclusions on isotopic reporting and material provenance.

CHAPTER 1

INTRODUCTION

Since the militarization of fissile isotopes, proliferation of special nuclear material has become a cause of great concern for sponsored weapons states, especially with regards to global terrorism. Consequently, weaponizable material disposition is highly interesting to the non-proliferation and forensic communities. Strong nuclear security and responsible behavior are the overall goals regarding this material for these weapon states. These goals can be achieved through deterrence using nuclear forensic material attribution methods. Forensic measures can be employed in the field if a sample is collected for either destructive or nondestructive analysis. The forensic analytical techniques can be divided into two major categories, which include chemical/physical and radioanalytical methods. Both methods can provide tremendous insight into the material in question.[1] These methods can provide deterrence against potential proliferators by enabling a detailed characterization of the material and eventual attribution to an originating country. The downside to these analysis methods is the necessity of access to comparison data (e.g. Pu isotopics) for the attribution process. Otherwise, analysis can be achieved computationally and signatures can be developed or characterized to attribute fissile material from different operating nuclear reactors in the past and present.

In 1942, President Franklin D. Roosevelt authorized the United States to conduct research into building the atomic bomb—the Manhattan Project. The reactors used today for fissile material production are not grossly advanced from the genesis reactors of the Manhattan Project due to their relatively simple and well-known designs. The study of these original reactors can provide deep insight and characteristics/signatures of reactors operating today. One such reactor from the Manhattan Project era was the X-10 (Clinton Pile) located in Oak Ridge Tennessee.

1.1 History of the X-10 Graphite Reactor

The "Manhattan Project" would bring together the most prestigious scientists of the Twentieth Century. The Manhattan Project was named after the Manhattan Engineer District, set up by the Army Corps of Engineering to develop and manufacture the atomic bomb. Oak Ridge, Tennessee would become the site of the experimental facilities used for the production and research necessary to build the first atomic bomb. This Manhattan pilot site would contain the air-cooled experimental pile, a separation plant and many supporting facilities. The secrecy surrounding Oak Ridge was of such importance to national security that the Governor of Tennessee was unaware of its existence. The X-10 graphite reactor was built at the Oak Ridge location, together with similar reactors at the Hanford site in Washington State, supplied the Los Alamos Scientific Laboratory with the plutonium necessary for the Manhattan Project. Los Alamos conducted studies on these samples which heavily influenced weapon design. It is also noteworthy that neutron-cross-section studies, radiation-damage studies, and biological radiation-effect studies were conducted at these Oak Ridge facilities.

The X-10 reactor sustained the fission reaction on November 4, 1943 using natural uranium fuel from the natural abundance of the fissile atom U-235. Since natural uranium contains 0.72 atom percent U-235, with the remainder of the uranium as U-238 with a very small fraction of U-234, natural uranium is excellent fuel for the manufacture of plutonium, which results from neutron capture in U-238 and transmutation through decay to result in Pu-239 . The excess neutrons produced from the fission of the U-235 atom are used in the production of Pu-239. .

The reactor was designed and built in approximately 10 months by the du Pont de Nemours Company ("DuPont") assisted by the University of Chicago. The short time of conception to completion presented an overdesign of most of the components involved with the reactor. The air-cooling system allowed continuous operation at One Mega-Watt (MW) power level. There were also many openings throughout the graphite matrix that served as research openings for the studies cited above.

After the critical loading of the reactor was completed, the plutonium production started. The overdesigned pile was recognized within the first few days of operation, and a redesign in fuel loading, cladding for the fuel slugs, and larger air cooling fans was installed. These changes raised the power level to approximately 3.6 MW in 1944.[2]

1.1.1 X-10 Graphite Reactor Structure and Fuel Elements

Figure 1.1 shows a schematic of the X-10 Graphite Reactor. The external dimension of the reactor from north-to-south is 38 feet, from east-to-west is 47 feet, and the height is approximately 35 feet resting on a concrete pad. None of the internal parts

are visible from the laboratory. Explanation and figures of the internal components of the pile are shown below in the accompanying figures.

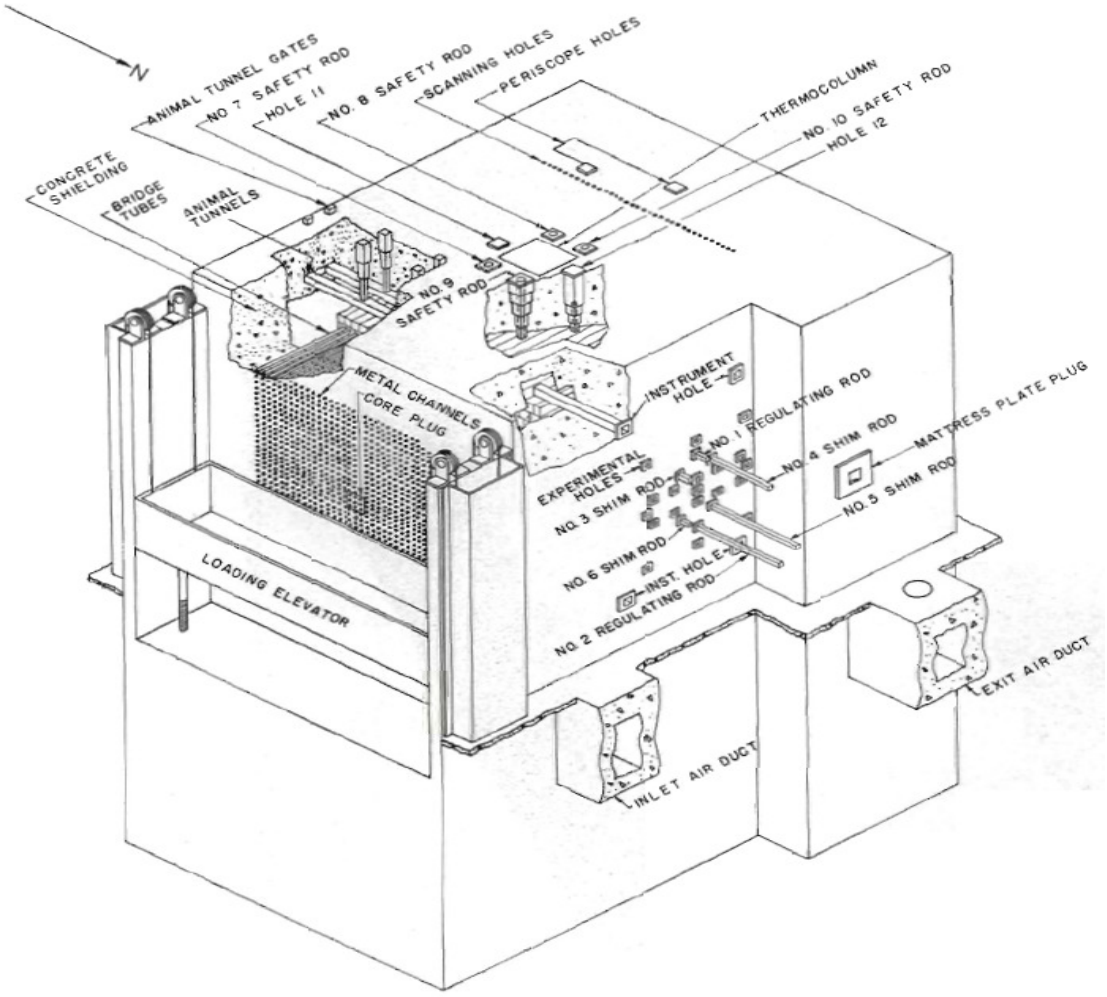

Figure 1.1: X-10 schematic showing reactor face and experiment holes.

The internal portion not seen from the laboratory is a 24 foot cube of graphite blocks. The graphite blocks are 4 inches by 4 inches (10.32 x 10.32 cm) and keyed together throughout the core. Diamond shaped holes are formed in the graphite blocks manufactured using V-cuts. The reactor core has 1248 of these diamond shaped holes, spaced on 8 inch centers (20.32 cm). Graphite is not only a good neutron moderator, but a

good lubricant as well. This lubricative quality aided the reactor worker(s) that physically pushed the fuel slugs down the fuel channel. Also, the absorption cross-section is very low for nuclear grade graphite (approximately 4.5 millibarns; note nuclear grade graphite is virtually boron free).[2] One of the main overdesigns of this project was the concrete shield surrounding the reactor. The shield is 7 feet thick surrounding the graphite completely.[2] Figure 1.2 shows the placement of the graphite blocks that made up the internal core region of the reactor.

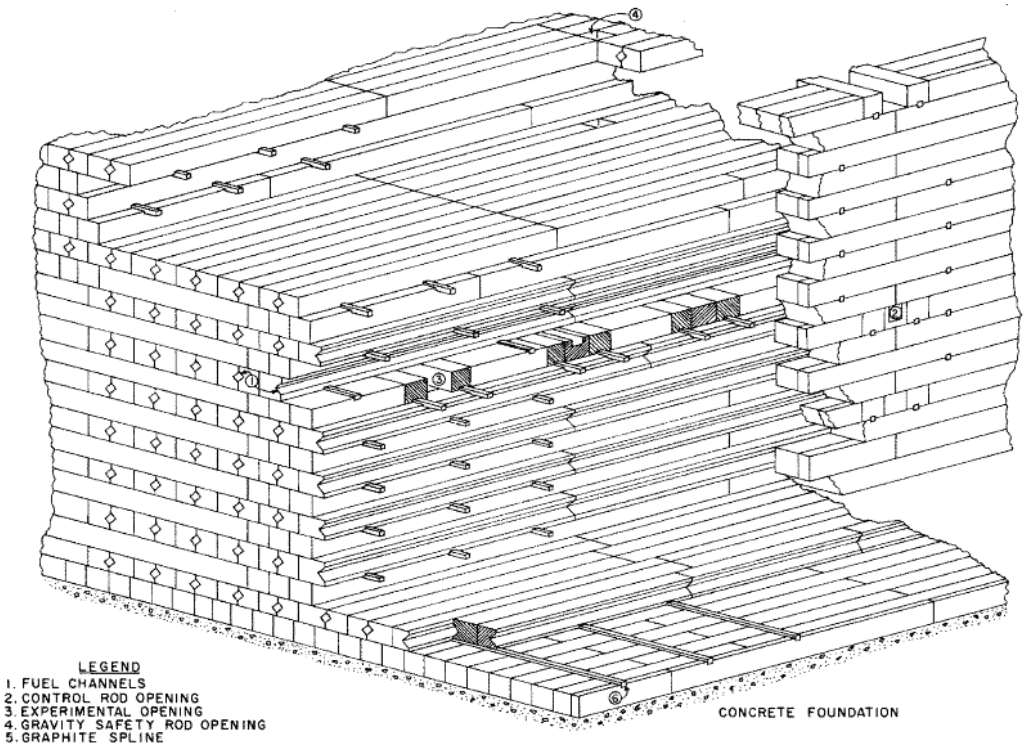

Figure 1.2: Placement of graphite blocks that made up core region of the reactor.

The fuel elements design in the graphite pile changed througout the operation history (bonding methods with the cladding and natural uranium metal). Mainly due to heating problems, the fuel elements would rupture. For the purpose of this research, the

uranium slug measured 1.1 inches in diameter and 4 inches in length. This equates to approximately 1170 grams of natural uranium per slug.[3] An aluminum can surrounding the slug was used as the fuel cladding which protected the uranium metal from oxidizing. Slugs were arranged end-to-end to mimic a long fuel rod. As previously mentioned, the addition of the slug required reactor workers to physically push the slugs into position. Discharge from the reactor required workers to push the fuel slugs into the exit air manifold which fed into a 20-foot deep water pit below the ground floor level and then transported away for processing.[2]

The X-10 reactor was cooled by outside air drawn in through filtering fans. Air was drawn through the reactor in order to achieve a negative pressure while in operation. Due to the dependence on the outside air temperature, the reactor core would have drastic temperature fluctuations from the summer to winter months. Early operating summer measurements show with the inlet air temperature at 32ºC, the temperature in the center position of the reactor is 138ºC. This same position measurement in the winter months was 53ºC lower.[4] These shifting temperatures due to the outside weather conditions would cause the isotopics to differ slightly depending on the time of year, and the associated Doppler behavior of the resonance cross sections of the fissile material. Temperature changes would mainly affect the Pu-239 absorption and fission cross-sections due to a high thermal resonance in Pu-239; work by Westcott reflected the dramatic increase in thermal neutron cross section as a result of “Non-1/v” characterized behavior via a multiplier, the “g-factor,” with respect to temperature.[5] As an example of the effect of temperature between a cross-section at 138 ºC in summer and the winter temperature of 85 ºC, the U-238 microscopic capture cross-section is approximately 10%

higher in the summer months. This effect would be vastly greater for Pu-239, up to an order of magnitude, depending upon the fuel channel conditions.

1.2 Forensic Relevance of X-10 Reactor Study

With the advancement of nuclear technology and proliferation becoming a growing concern throughout the world, accurate reactor analysis and characterization is needed within the nonproliferation and forensic communities. Computational forensic reactor physics is a good tool in combating potential proliferate countries by exposing unique fuel attributes or signatures based on assumed operating parameters. Ideally, the physical fuel elements could be examined through destructive and non-destructive techniques but access to many countries nuclear inventories is restricted.

Nuclear forensics offers a unique perspective into nuclear attribution. The field uses an abundant amount of analyses and knowledge that characterize unique attributes of nuclear material. A knowledge of the nuclear power cycle, nuclear weapons development, environmental indicators, radiochemical signatures and gathered intellegence on nuclear activities are some of the necessary tools of a forensic researcher. Using this knowledge to determine the origin of the nuclear material and potentially the use of this material is the basis for nuclear attribution.

Special Nuclear Material (SNM) contains significant amounts of fissile isotopes and can potentially be used to create a nuclear weapon; specifically, U-235 that has been enriched to greater than 20% and a quality of 93% Pu-239. These isotopes are prime candidates for clandestine production of a nuclear weapon by a terrorist organization or nations without nuclear capabilities.[6]

Plutonium is continuously bred in the fuel while the reactor is in operation from the neutron capture of uranium and subsequent beta decay. Pu-239 is produced by neutron capture of U-238 (U-239 compound nucleus formation) which then beta decays to Np-239 followed by another beta decay to Pu-239. The heavier plutonium elements are produced from extended neutron captures.

Weapons grade plutonium had to contain less than 7% Pu-240 because of the atom having a proclivity to spontaneous fission which could cause the weapon to "fizzle." A fizzle was the result of the spontaneous fission injecting neutrons into the system and prematurely causing the chain reaction before the optimal fissile configuration is achieved. This characteristic causes the yield of the weapon to significantly drop.

Early production reactors were developed for the specific purpose of weapons production. Examining the Manhattan era reactors can provide insight into other countries weapons development due to the similar, simple design. For example, North Korea adopted the Calder Hall type reactor built in the 1950's by the United Kingdom. This was a graphite moderated gas cooled reactor similar to the X-10 reactor modeled in this study. The main difference was the power levels the reactors operated. X-10 operated between 3.5 MW thermal to 4.0 MW while the Calder Hall type operated between 180 and 240 MW thermal for accelerated weapons material production. X-10 was also a pilot plant for the Hanford-B design which was used by the Russian and Chinese production programs. The main differences between these reactors was the cooling mechanism and the power level. Hanford-B reactor types operated around 250 MW thermal power level and were cooled by light water.[7] Similarities in design to the other graphite moderated

production reactors mimicked by other countries offers a stand-a-far forensic attribution study.

Although the natural uranium fuel of the X-10 reactor cannot be made into an improvised nuclear device (IND), chemical separation of the produced plutonium could provide material for a weapon. The plutonium would have to contain a low level of Pu-240 and Pu-242, which is characteristic of the reactors of this time. Highly irradiated fuel would be less desirable due to the overabundance of these isotopes because of the high spontaneous fission (neutron emission) rates. Although the fuel slugs of the X-10 reactor could not be fashioned into an IND directly, a radiological dispersal device (RDD) could be assembled due to the high radioactivity after discharge. Full characterization of reactor isotopics and signature development are necessary for the nonproliferation and forensic communities fight against the nuclear terrorism mission.

It is worthy of mention, that the uranium ore used in the production of the natural uranium metal for U.S. production reactors was mined in the Belgian Congo. The uranium mined from this region powered the Hiroshima bomb. Uranium ore from Africa was a main source for many countries weapons programs, estimated to make up one fifth to one half of the Western world's uranium supply.[8] Leveraging the history of African uranium ore trade can lead to specific forensic signatures by analyzing materials found from this region. For example, from the Unpublished Writings of Enrico Fermi by Salvatore, the prevalent uranium impurities from this mine in the Belgian Congo included magnesium, sodium, iron (all containing < 50 ppm), and manganese (containing < 200 ppm). These impurities, with the average carbon content found in uranium metal of the time (discussed in Chapter 3) make interesting forensic markers for the subsequent fuel

made for these early production reactors that eventually produced the first atomic weapons by the United States.

1.3 Problem Statement

United States policy is pushing towards an increase in nuclear attribution as it ultimately leads to deterrence of weapons states sponsoring terrorist organizations. This attribution of source materials will also create an accountability of the nation states to secure these materials in the appropriate manner.[9] Having the ability to attribute state or terrorist sponsored nuclear weapons and SNM (potentially used in RDD or IND) is the key in deterrence. Without attribution, retaliation or political sanctions levied against the sponsored state(s) is not possible. If there are no tangible consequences of a terrorist orchestrated event the concept of deterrence is meaningless. Quoted from "Deterring State Sponsorship of Nuclear Terrorism":

"*U.S. attribution capabilities are and will always be limited. A series of authoritative reports have called for increased investment in nuclear forensics, and, more importantly, have flagged incomplete signature databases as a fundamental limitation to U.S. capabilites…one of the most critical areas for improved attribution capabilities is an enhanced database of nuclear signatures.*"

Obtaining these attributes and signatures from these production reactors can be problematic because of limited access to nuclear military or civilian facilities. Subsequent speculation of the intentions of a nuclear program can create geopolitical tensions. Speculation can be mitigated (and some tension) by computationally analyzing production reactors used by state-sponsored weapons states.

One such reactor and the focus of this research was the X-10 (Clinton Pile). X-10 was the genesis reactor of U.S. weapons campaign. This reactor was simply designed but paved the way for understanding the required reactor physics for weapons grade material production still used today. Modeling and forensic analysis of the X-10 reactor will highlight the spectral characteristics of production reactors and show the effect on fuel isotopics. A selection of neutron code packages will also be compared and contrasted to investigate potential sources of inaccuracies across dissimilar neutron transport methods. This analysis will display the predictive capabilities of these advanced codes and will enable future researchers to tap into actinide and fission product data from a production reactor with a simple and effective design. Nuclear data uncertainty is also generated to add another perspective to nuclear forensic quantities and isotopic reporting. The uncertainty in isotopics showcases challenges for determining in-core material provenance (loading zones and axially). This nuclear forensic isotopic reporting also aids in distinguishing reactor intent (commercial versus military). Collectively, these results should highlight distinct characteristics and forensic signatures of early production reactors and emphasize the underlying physics (and effects) required for weapons material production to this day.

CHAPTER 2

FORENSIC ANALYSIS ISOTOPES/RATIOS OF INTEREST

Computational and destructive analysis of production/power nuclear fuel is vital in forensic analysis. These analyses allow the nuclear forensics community to characterize different aspects of the nuclear fuel cycle whether for weapon or commercial power use. Leveraging the known fission product distributions, in respect to different fission types, aids in the forensic analysis of fuel elements from a reactor. Examining fission products along with the heavy element constituents produced in a reactor cycle highlights the operating characteristics of the reactor.

2.1 Operating Reactor Neutron Spectrum and Enrichment from Plutonium Isotopics

Reactors across the world operate at differing levels of power and U-235 enrichment for production of plutonium, commercial uses and research. Mayer, Wallenius and Ray state a correlation between main reactor types has been found by Pu-238 content and the Pu-242/Pu-240 ratio. The higher uranium enrichment in the fuel affects the Pu-238 abundance. Also, the softer the spectrum the higher the ratio of Pu-242/Pu-240. These characteristics can be a minor indicator of reactor intention.[1]

The level of enrichment can be determined by the amount of Pu-238 a fuel element contains due to the chain of neutron captures required to produce this isotope.

Correspondingly, the higher the U-235 content, the higher the Pu-238 content due to the requirement of subsequent captures of U-236 and U-237 which then beta decays to neptunium-237. Capture of a neutron by the neptunium-237 nucleus and the beta decay of neptunium-238 eventually produce the end product of Pu-238 (pathway chain found in Figure 2.1 below).

Another indicator of reactor operation is the Pu-242/Pu-240 ratio. This ratio will show the type of neutron spectrum at which the reactor operated. As shown below, are the principle neutron capture reactions in reactor operation.[10]

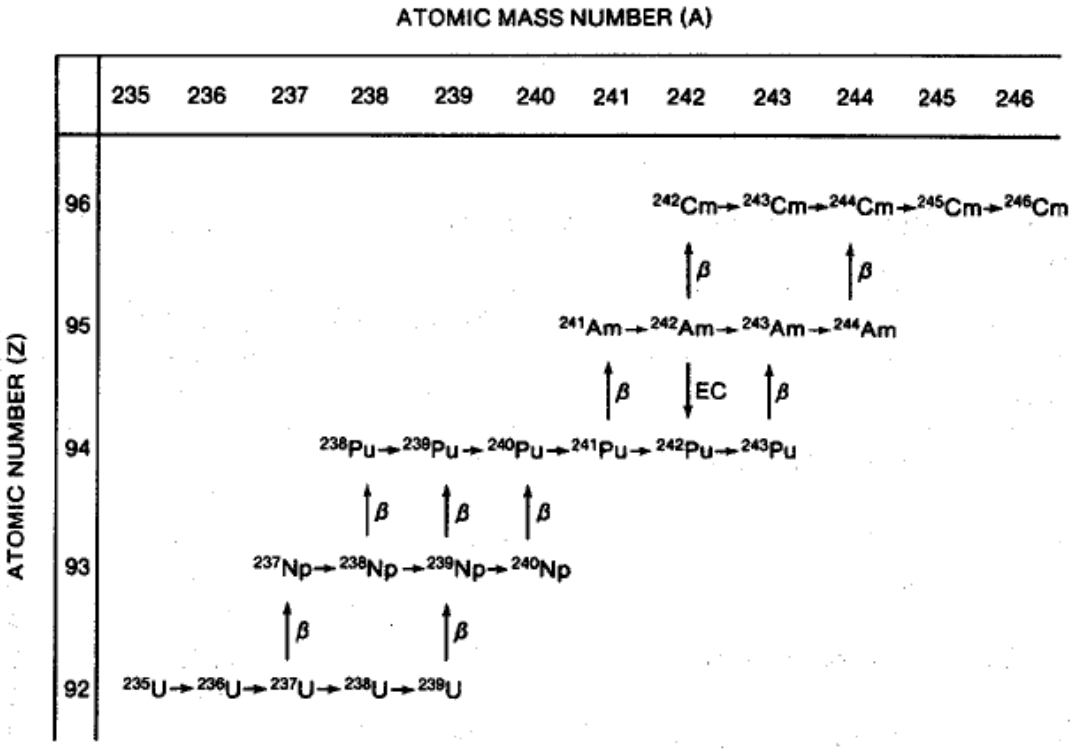

Figure 2.1: Principle neutron capture reactions found in fuel elements.

As shown in Figure 2.1, there are many pathways to the higher order plutonium isotopes. Pu-240 and Pu-241 are required to capture a thermal neutron for the production of Pu-

242. The fission-to-capture ratios for Pu-240 and Pu-241 are, 2.03E-04 and 2.80 respectively. Statistically, Pu-240 will almost always capture a thermal neutron while Pu-241 will fission. This is due to the binding energy of the captured neutron, which is enough to cause fission (overcome fission barrier) in certain odd numbered heavy nuclei.[5] The buildup of Pu-242 will depend on how much Pu-239 is bred. Typically, the reactor fuel will be removed once the Pu-240 content has reached between 5% and 7% with respect to Pu-239 content.[11] Figure 2.2 shows the radiative capture cross-section for Pu-240 and the total fission cross-section for Pu-241.

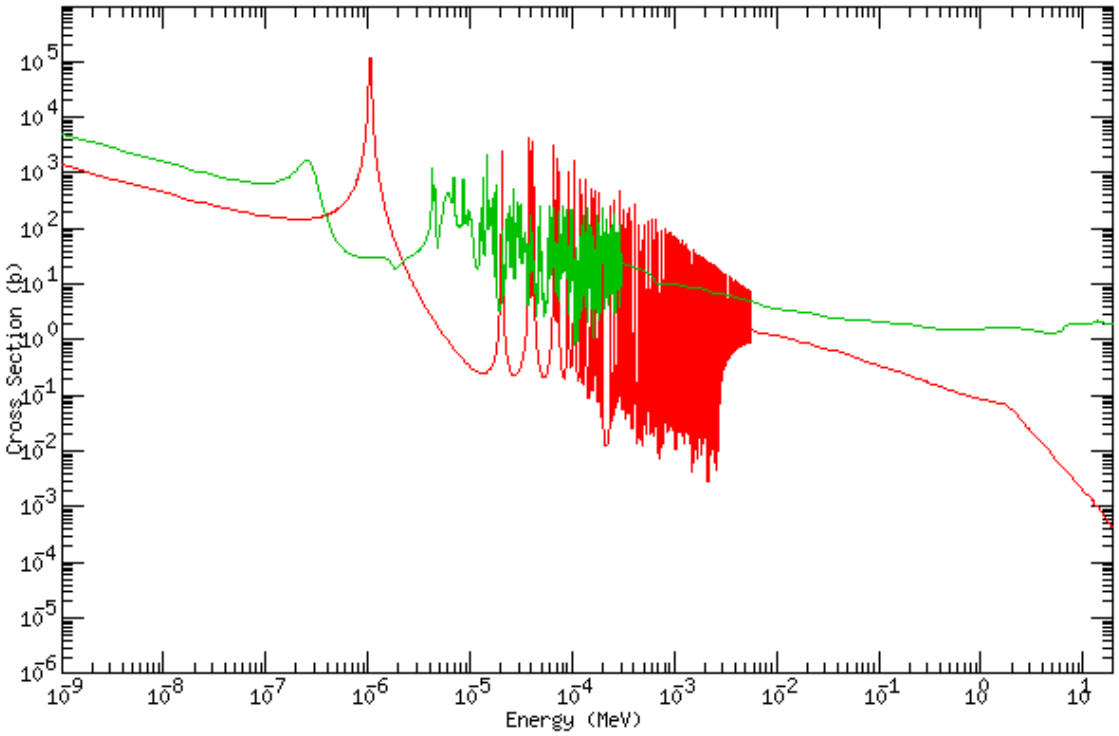

Figure 2.2: Radiative capture cross-section for Pu-240 (red) and total fission cross-section for Pu-241 (green).[24]

The above cross-section relationships show how Pu-241 is built up within the fuel due to the overwhelming capture cross-section. After the resonance in the neutron capture reaction of Pu-240, the cross-section drops off considerably. This drastic drop-off explains the behavior of the Pu-242/Pu-240 ratio. The softer the spectrum becomes the higher the ratio due to the capture cross-section dominating which translates to less Pu-240. Consequently, the harder the spectrum the lower the ratio will become due to the drastic drop of the Pu-240 capture cross-section. This relationship is a good indicator of the energy at which the fuel was exposed to in the reactor. It is noteworthy, Pu-240 has a high fission yield (1020 n/s-g) and is usually the major neutron-emitting plutonium isotope present which is not desired in weapon design.[10]

2.2 Relative Fuel Type Fissions in Reactor Operation

Fission reactions are what drive a nuclear reactor. At the beginning of the cycle, U-235 dominates the majority of fission reactions. As plutonium is bred into the fuel, the fission reactions are shared by the Pu-239 and Pu-241 produced from capture in U-238. Illustrated below in Figure 2.3 are the total fission cross-sections of U-235 (shown in red), Pu-239 (shown in green) and Pu-241 (shown in blue). It is also worth mentioning that U-238 contributes to fissions within the system by fast fission neutrons (high neutron energy).

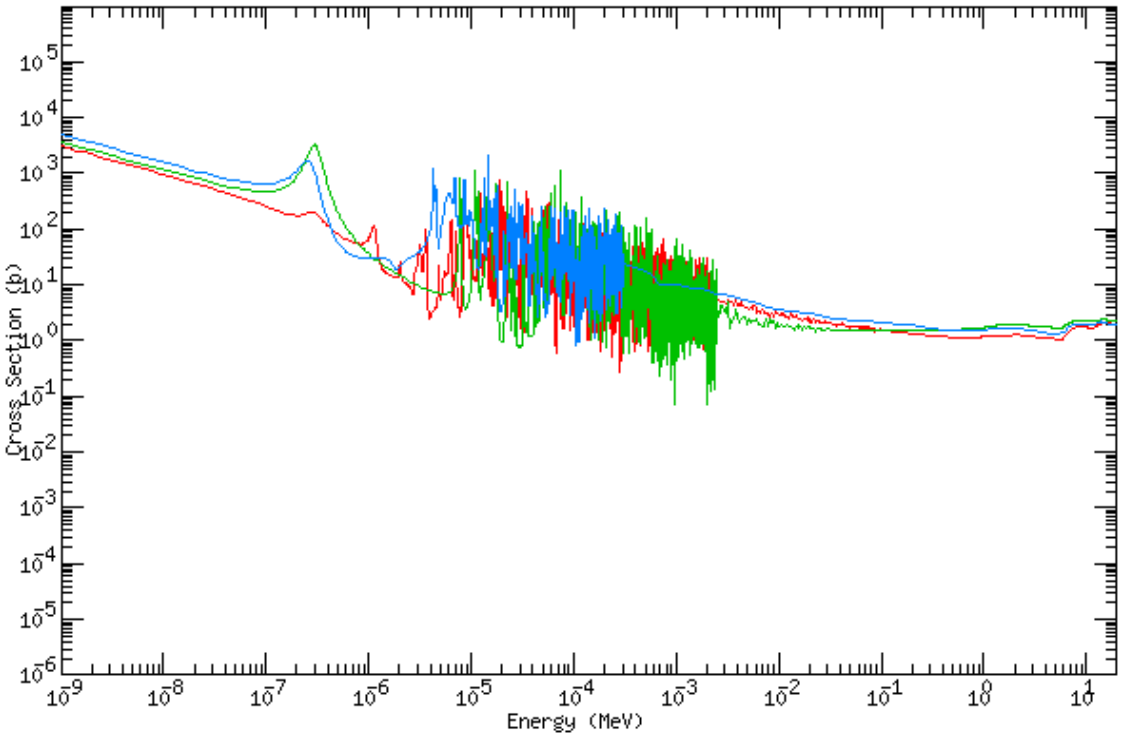

Figure 2.3: U-235 (red), Pu-239 (green) and Pu-241 (blue) total fission cross-sections. Note high thermal resonance at approximately 10^{-7} MeV.[24]

The high fission cross-section of these main constituents of nuclear fuel create an opportunity of forensic interest. Fissioning these atoms of interest creates fission products. Fission by-products are, depending on the fission product mass, distributed in similar and dissimilar ways depending on the fissioning fuel. Shown below in Figure 2.4 is the mass distribution of fission products for U-235 and Pu-239.

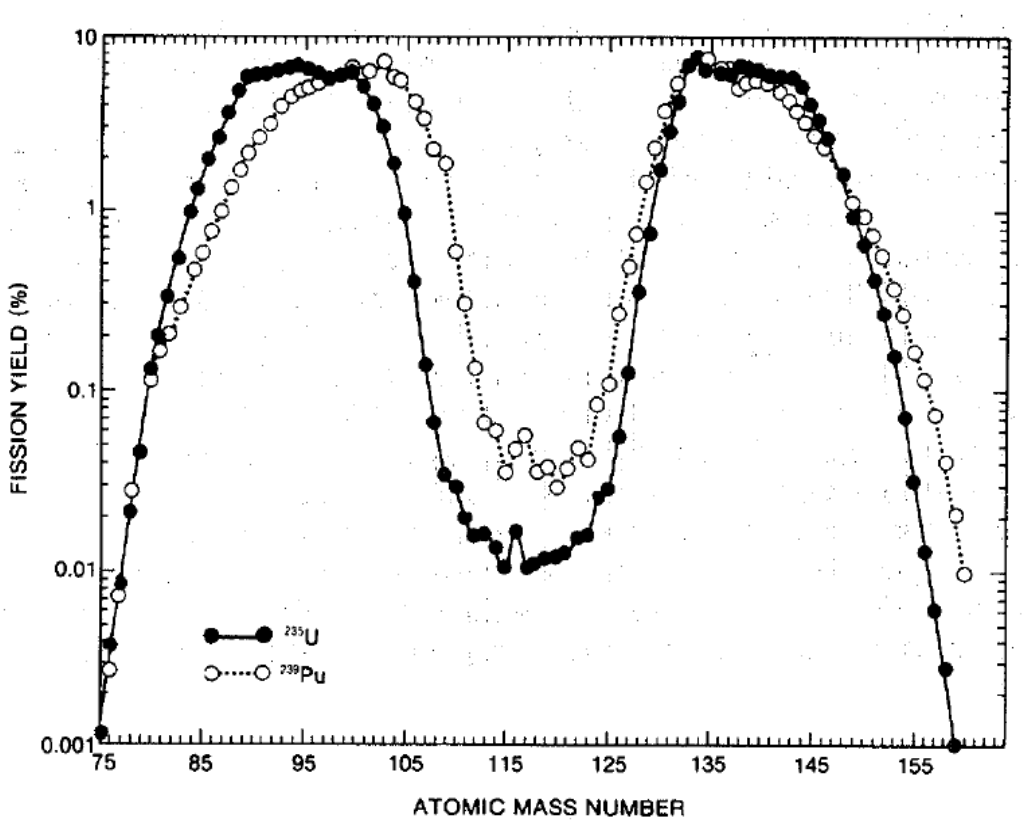

Figure 2.4: Mass distribution of fission products between U-235 and Pu-239.[10]

Highlighting the similarities and dissimiliarties between these two fission curves is of forensic relevance.

One such mass chain of significance is mass chain 106: Ru-106 beta decays to Rh-106 which then beta decays to Pd-106. This mass chain has a 0.402 % U-235 fission yield while the Pu-239 fission yield is 4.4 %. Pu-239 fission creates 10.95 times more fission products corresponding to mass chain 106 products than U-235 fission. Cs-137 is a fission product that can be used for total fissions within the system due to the similarites between fission yields of the two fuel types. Ratioing these two isotopes of interests will reveal the relative Pu-239 fissions within the system to total fissions.

Also noteworthy are the potential analyses that can be performed on this mass chain. Ru-106 has a half-life of around 370 days and decays by beta emission to Rh-106. Rh-106 has a very short half-life and emits high energy gamma rays which indicates the presence of Ru-106. These high energy gamma rays can be used to characterize the amount of Pu-239 fissions relative to total fissions in the fuel element (using gamma rays from the decay of Ba-137m for total fissions—denominator). The Pd-106 fission product is stable, and can be used for analysis of the fuel pin at any point after discharge (due to the high cumulative yield from the decay of the 106 mass chain) as long as the ingrowth from the decay of Ru-106 is calculated.

Another candidate for total number of fissions occuring in reactor fuel is the mass chain 138. The stable product of this chain is Ba-138, which has similar cumulative thermal fission yields for U-235, Pu-239 and Pu-241. This isotope could serve as a stable replacement for Cs-137 on the denominator of the mass chain 106/mass chain 138 ratio to indicate relative plutonium fissions in the fuel slug. This mass chain will also serve as other indicators in forensic analysis.

Using ENDF/B-VII yield data, other candidates for total fissions in the fuel slug were analyzed using a custom script to examine thermal cumulative yield data between the fission products of Pu-239/241 and U-235. The following table shows the isotope ZAID of interest and the percent difference between the thermal fission fuels that mainly reside in reactor fuel. For thermal reactors the neutron radiative capture cross-section for Pu-240 has a large resonance around thermal energies. This would cause most of the fissions of the higher plutonium masses to be attributed from Pu-241.

Table 2.1: Isotopes of interest for total fissions in fuel slug (thermal cumulative yields)

ZAID	Pu-239/U-235 Percent Difference [%]	Pu-239/Pu-241 Percent Difference [%]	U-235/Pu-241 Percent Difference [%]	Averaged Cumulative Yield [%]
42099	1.672	4.105	2.434	6.094
43099	1.672	4.105	2.434	6.094
43099m	1.671	4.105	2.434	5.363
42100	7.376	7.978	0.603	3.182
44099	1.672	3.987	2.315	6.096
53133	4.045	3.578	0.467	6.799
54133	4.625	0.442	4.183	6.815
55133	4.625	4.183	0.442	6.815
54134	2.520	3.094	0.573	7.726
55137	6.550	0.653	7.202	6.482
56137	6.643	0.559	7.202	6.484

As shown in Table 2.1, the mass chains 99, 133, 134 and 137 are good indicators of total fissions within the thermal system. Most of the isotopes in the table are stable, which makes destructive analysis possible at any point in time after fuel discharge. Xenon-134 is a stable noble gas that can be examined at a distance by remote sensing/monitoring, and Xenon-133 has a 5 day half-life, which can also be examined at a distance by remote sensing gamma spectrometry from a stationary monitoring station. Another desirable

characteristic are the high cumulative fission yields of these mass chains. A high cumulative yield makes gaining statistics by counting methods easier which in turn lowers the error in the measurement.

Knowing the total amount of fissions in the reactor fuel reveals the power level at which the reactor operated. Isotopes with the most error between fission types can also be leveraged to reveal certain operating parameters such as enrichment or the amount of plutonium produced in the core. Table 2.2 shows the ratios of different fission types thermal cumulative yields.

Table 2.2: Isotopes of interest for different fission types in reactor fuel (with respect to thermal cumulative yield data).

ZAID	Isotope Ratio	Ratio Value	Fission Yield for Numerator [%]	Fission Yield for Denominator [%]
44105	Pu-239/U-235	5.853	5.643	0.964
45105	Pu-239/U-235	5.853	5.643	0.964
46105	Pu-239/U-235	5.853	5.643	0.964
44106	Pu-239/U-235	10.832	4.349	0.402
45106	Pu-239/U-235	10.833	4.349	0.402
46106	Pu-239/U-235	10.833	4.349	0.402
44107	Pu-239/U-235	22.257	3.254	0.146
45107	Pu-239/U-235	22.778	3.330	0.146
46107	Pu-239/U-235	22.778	3.330	0.146
47107	Pu-239/U-235	22.778	3.330	0.146

2.3 Xe-135/Xe-133 Ratio and Fission Spectrum Type

One ratio that demonstrates the difference between fission spectrums is the Xe-135/Xe-133. The amount of Xe-135 to Xe-133 can reveal a lot about the fission type, whether from reactor operation or a nuclear detonation. Remote monitoring stations can be used around the area (or country) of suspected nuclear activities (such as weapons testing or production of weapons material). Typical low burnup reactors will have mass ratios < 0.10, while nuclear weapons testing will create ratios of about 40.0 at early times and > 1.0 at less than a day after detonation.[12] For example, the activity ratio of a nuclear detonation at 2 hours is around 8.20 (from Pu-239 fast neutron spectrum and a 1 kiloton detonation) and at one day, the mass ratio is reported at 0.60, which is an order of magnitude greater than production reactors. This gross difference in the Xe-135/Xe-133 ratio is a good forensic indicator of what activities are being conducted. These isotopes are also volatile which makes remote monitoring of a nuclear site of interest easier, due to the transport of the isotopes through the atmosphere.

The difference of radioxenon in reactor versus a nuclear detonation is drastic at early times. Reactors running at steady state also have differences in the ratio due to the amount of burnup in the core. Contrasting different simulations with respect to the power level and amount of burnup is of forensic interst as well. The NRX reactor was powered between 20 MW and 42 MW, light-water cooled and heavy water moderated utilizing natural-uranium fuel. An NRX reactor design will display a lower ratio compared to an X-10 reactor design due to the power level the reactor operated, and the design of the

reactor. This will be highlighted later in this study when different reactor types and the respected ratios are examined.

2.4 Concluding Forensic Analysis Remarks

Whether deterring state sponsorship terrorism or lone terrorist actions involving SNM, one of the best methods of imputation is nuclear forensic analysis. Being aware of nuclear processes used to produce the SNM and the processes used to fashion a RDD or an IND can lead to subtle differences that can be exploited to make an informed and, most importantly, accurate decision should a nuclear/radiological event take place on United States soil. Nuclear policy has changed in order to adapt to the ever-present terror organizations across the world. Reporting and analyzing actinide, fission products and previously discussed forensic markers (and others) will showcase the unique isotopic signatures resulting from spectral characteristics required by production reactors even today.

CHAPTER 3

X-10 UNIT CELL SIMULATIONS AND IMPACT ON FORENSIC ANALYSIS

Once nuclear data is established, neutronics calculations are necessary to predict the production of isotopes throughout a reactor core. Neutronic "unit cell" calculations using radiation transport theory are often the first step to larger reactor model computations. Due to the repeated lattice structure of the reactor, these simplified models with all laterally reflected boundary conditions can provide an accurate representation of the reactor system as a whole and yield a basis for cross-section evaluation. In this chapter, a comparison of unit cell calculations is presented using various standard computational models and methods. The unit cell considered here is based upon the X-10 air-cooled-graphite-moderated reactor that operated at Oak Ridge National Laboratory during the Manhattan Project and post-World War II. The X-10 is particularly interesting because of the simple design using natural uranium slugs moderated by graphite. Early United States' plutonium production reactors were based on this design and are considered primitive today. The unit cell was modeled using the following radiation transport codes: Monte Carlo Neutral Particle (MCNP6) code system using continuous energy cross-sections developed by Los Alamos National Laboratory, Scale 6.1 using the CSAS6 control module with KENO-VI developed by Oak Ridge National Laboratory,

and the PENTRAN 3-D parallel discrete ordinates code using ENDF/B-VI cross-sections derived from Scale 6.1.

3.1 Unit Cell Parameters, Limiting Constraints and Fuel Characteristics

The X-10 reactor unit cell is based on 8 inch (20.32 cm) centering of the fuel channels repeated throughout the reactor which held the natural uranium slugs. This loading configuration led to a unit cell 20.32 x 20.32 cm (x and y dimension) with eigenvalue calculations completed with a z-axis length of 1.0 cm. The z-axis was mirror reflected in the front and back of the unit cell. The length in the z-axis (10.32 cm) was selected because of the span of the natural uranium within the aluminum cladding. The 1.0 cm length was chosen to demonstrate the infinitely repeated boundary conditions placed on the unit cell (axially). This reflected boundary condition most accurately represents the average environment a slug would experience in the reactor.[13] Moreover, this unit cell configuration provides a simple but effective benchmarking result across all transport codes.

Analyzing the uranium metal fuel within the X-10 reactor unit cell offers near term forensic value in quickly gathering average estimates of isotopic inventories. Potential fuel content variations can lead to unique signatures of forensic importance and interest. The natural uranium fuel of the Manhattan Project Era was mined at specific locations around the world, mostly in Africa. Review of the open literature yielded data of trace element analysis of the natural uranium fuel used in the Manhattan Project. The specific trace element values were not used in this study but could be examined more thoroughly in the future. Trace analysis could be accomplished computationally or

through chemical dissolution of the slug and subsequent mass spectrometry analysis of the low-Z value elements. Another focus of this unit cell study was the carbon content in the fuel. For the Manhattan era, carbon content in natural uranium metal was reported between 0.01 and 0.23%. Los Alamos National Laboratory reported between 0.05-0.06% carbon content in the alpha-phase natural uranium metal. The density of the natural uranium metal of the time was calculated by the following formula (19.05 being the theoretical alpha-phase uranium density in g/cm^3):

$$\rho\left(\frac{g}{cm^3}\right) = 19.05 - 2.14 * WTPT_{Carbon}; where\ WTPT \equiv Weight\ Percent$$

For this study, an average value of 0.12% carbon content in the natural uranium metal was used.[14] An ideal natural uranium metal case (ρ = 19.05 g/cm^3) was also examined through burnup analysis and eigenvalue calculation.

The moderating material used in X-10 was graphite. This standard moderating material of the time was used because of its high moderating power and significant abundance. Ultra-pure reactor grade graphite was used in the pile with an average density of 1.61 g/cm^3. The natural uranium slug was manually inserted into the fuel channel. When fuel loading of the pile was required, the reactor technicians would physically push the slugs along the channel. Cut graphite provides a natural lubricant for the fuel elements to slide along.

3.2 MCNP Unit Cell Calculations

The Monte Carlo method and code platform originated from scientists working at Los Alamos National Laboratory in the 1940s working on nuclear weapon design. MCNP uses combinatorial geometry, which allows the user to predefine and combine geometrical bodies. This geometry feature is used across several code packages such as KENO which will be discussed later. The nuclear data tables used in this study were: continuous-energy neutron interaction data, multi-group neutron and neutron S(α,β) thermal data. For clarification of multi-group neutron data tables, a three-group structure was chosen to represent multi-group calculations.[15] This lower group structure was chosen due to the agreement between the three-group and continuous-energy calculation run on the unit cell model (discussed later). A three group energy configuration partially agrees with the literature stating thermal reactors should use a two-group structure (essentially fast and slow neutrons).[5]

3.2.1 MCNP Eigenvalue Calculation

Unit cells containing average carbon content (0.12%), no carbon and max carbon (0.23%) were run and the data was subsequently examined. Each Monte Carlo unit cell simulated 10,000 particles with 1000 cycles, with 500 initial cycles skipped (necessary to generate fission sources). Calculation results are captured below in Table 3.1.

Table 3.1: Unit cell calculation results with varying carbon content in fuel.

Unit Cell Description (carbon content [%])	k_∞ value (at 95% confidence level)	Average neutron lethargy causing fission [MeV]	Average mean free path in fuel [cm]
0.0	1.09491 ± 0.00015	1.8036E-07	1.9759
0.12	1.09489 ± 0.00016	1.7767E-07	1.9840
0.23	1.09461 ± 0.00016	1.7438E-07	1.9920

For comparison, average neutron lethargy and the mean free path of a neutron in the fuel will be examined; as the energy of the neutron decreases the lethargy of the neutron increases in the system. Neutron lethargy is a good representation of spectrum within the system because of its relationships to energy and energy loss caused by collisions within the fuel. Lethargy is heavily relied on when corresponding to moderating power and the moderating ratio which are important within reactor design. Along with lethargy, fluxes within the fuel region and moderator volume will be examined. All fluxes are normalized per fission neutron generation within the problem and results are shown in Table 3.3 below. The 3-group energy ranges for the F4 tallies within MCNP were divided from 0.00 – 6.25E-07 MeV (thermal), 6.25E-07 – 1.01E+00 MeV (epithermal) and 1.01E+00 – 2.00E+01 MeV (fast).

For the unit cell with the average fuel carbon content (0.12%), the final k_∞ at the 95% confidence level was **1.09489 ± 0.00016.** Average neutron lethargy energy that caused fission within the unit cell was **1.7767E-07 MeV**. The mean free path of a neutron within the fuel region was calculated to be **1.9840 cm**. Normalized total flux in the fuel

and moderator were **1.42026 ± 0.0002** and **1.52365 ± 0.0002**, respectively. All thermal, epithermal and fast fluxes within the fuel and moderator volumes are presented in the tables below.

The unit cell with the no carbon content (0.0%), the final k_∞ value at the 95% confidence level, was **1.09491 ± 0.00015.** Normalized total flux in the fuel volume was calculated to be **1.41133E+00 ± 0.0002.** Correspondingly, the normalized flux in the moderator volume was calculated to be **1.51450E+00 ± 0.0002.**

For fuel in the unit cell with the max carbon content (0.23%), the final k_∞ value at the 95% confidence level, was **1.09461 ± 0.00016.** Normalized total flux in the fuel volume was calculated to be **1.42813E+00 ± 0.0002.** Similarly, the normalized flux in the moderator volume was calculated to be **1.52965E+00 ± 0.0002.**

These 3 unit cell calculations showed the k_∞ value decreasing with increasing carbon content within the fuel. With 0.0% carbon in the fuel the fast flux contributed to 15.02% of the total flux, while the max carbon (0.23%) content fast flux in the fuel only contributed 14.93%. Adding moderation (carbon) to the fuel element, in theory, would soften the neutron spectrum within the unit cell making the thermal flux contribution directly proportional to the carbon content. In table 3.2, the trends within the unit cell follow predicted behavior for neutrons due to the carbon content decreasing the number of fissionable uranium atoms within the fuel element.

Table 3.2: Energy ranges for caused fissions within unit cell.

Unit Cell Description [% carbon content]	Thermal energy caused fissions (<0.625 eV) [%]	Epithermal energy caused fissions (0.625 eV – 100 keV) [%]	Fast energy caused fissions (> 100 keV) [%]
0.0	90.43	3.56	6.01
0.12	90.51	3.54	5.96
0.23	90.62	3.49	5.88

Table 3.3: Normalized fluxes within fuel volume

Unit Cell Description [% carbon content]	Normalized thermal flux in fuel region	Normalized epithermal flux in fuel region	Normalized fast flux in fuel region	Total normalized flux in fuel region
0.0	5.55182E-01 ± 0.0004	6.44088E-01 ± 0.0004	2.12065E-01 ± 0.0006	1.41133E+00 ± 0.0002
0.12	5.62822E-01 ± 0.0004	6.44594E-01 ± 0.0004	2.12847E-01 ± 0.0006	1.42026 ± 0.0002
0.23	5.70254E-01 ± 0.0004	6.44703E-01 ± 0.0004	2.13174E-01 ± 0.0006	1.42813E+00 ± 0.0002

Table 3.4: Normalized fluxes within moderator volume

Unit Cell Description [% carbon content]	Normalized thermal flux in moderator region	Normalized epithermal flux in moderator region	Normalized fast flux in moderator region	Total normalized flux in moderator region
0.0	8.94475E-01 ± 0.0004	5.68754E-01 ± 0.0001	5.12678E-02 ± 0.0006	1.51450E+00 ± 0.0002
0.12	9.02400E-01 ± 0.0004	5.69818E-01 ± 0.0001	5.14316E-02 ± 0.0006	1.52365E+00 ± 0.0002
0.23	9.08444E-01 ± 0.0004	5.69691E-01 ± 0.0001	5.15105E-02 ± 0.0006	1.52965E+00 ± 0.0002

Fluxes within the fuel and moderator volumes follow expected neutron behavior within a thermal system. Thermal fluxes increase with increasing moderation within the system. The increased moderation is attributed to the presence of carbon within the fuel. The increased carbon presence in the fuel also affects the flux in the moderator region of the system as more neutrons are moderated in the fuel. If the thermal neutrons in the fuel are able to escape the fuel region they contribute to the moderator thermal flux.

3.2.2 MCNP Burnup

For MCNP burnup analyses varying carbon content was analyzed in the X-10 reactor fuel. The main analysis focuses around a single X-10 fuel element (10.32 cm length).

The X-10 reactor operated between 3.5 and 4.0 MW. For the unit cell burnup, a nominal power of 3.5 MW was selected and scaled down to represent a single pin output. The burnup schedule consisted of 31.4731 day burn steps with 2.0084 day cooling steps, totaling 1822 days. At the beginning of the burn schedule, times of 1, 3, and 14 days were added to capture the plutonium and xenon accumulation through the prompt power curve. These steps were selected because of the length of time a slug was burned within the reactor (~ 5 years for peripheral slugs). There were mandatory shut-down periods of the reactor per week (approximately 10 hours) for refueling, maintenance, experimental instrumentation shuffling and radioisotope removal/insertion.[16] Also, a cooling period of 22,630 days since the slugs have been discharged was added to the end of the burn schedule to gather the isotopics after a long period of slug cooling and for possible slug

dissolution in the future. The total burnup of the fuel slug was 123.6 MWd/MTU. In comparison to other reactor burnups of the time, this is considered very low.

Differences in the fission yield curves between Pu-239 and U-235 can mainly be seen in the slight shift to higher atomic mass number of the Pu-239 curve with respect to the U-235 curve. For example, this shift is seen in the fission yield of Ru-106. For analysis purposes, Ruthenium's concentration was examined for fuel slug isotopic analysis (along with others). Cs-137 is usually the most widely accepted indicator of fuel burnup because of its very small absorption cross-section and the fission yield from Pu-239 and U-235 are nearly identical. Moreover, the burnup of irradiated fuel can be determined by fission product ratios, the two most common being Cs-134/Cs-137 and Europium-154/Cs-137. These ratios will be examined although the times for this burnup are relatively long compared to other plutonium production reactors of that time.

In Figure 3.1 below, a representation of the k_∞ value for the unit cell is highlighted for the first 45.47 days of burnup. The initial drop in the k_∞ value can be explained by the ingrowth of Xe-135, which is a known neutron poison with a very large absorption cross section. This behavior is also illustrated below with a relationship of Xenon concentration and the effect on k_∞ value. Figure 3.3 represents the entire range of burnup and the $k\infty$ value trend. The inventory of Xe-135 remains rather constant across all burn steps (max value of 1.778 μg).

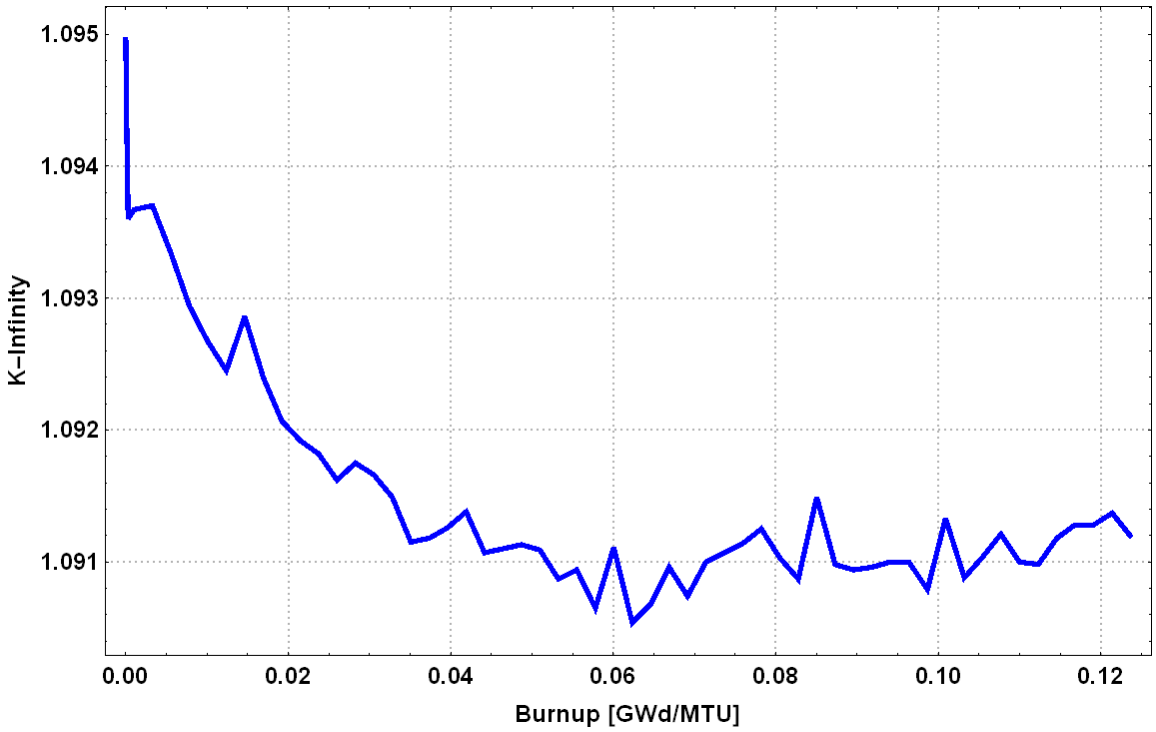

Figure 3.1: MCNP calculated k_{∞} value as a function of burnup with the stated assumed reactor operations schedule.

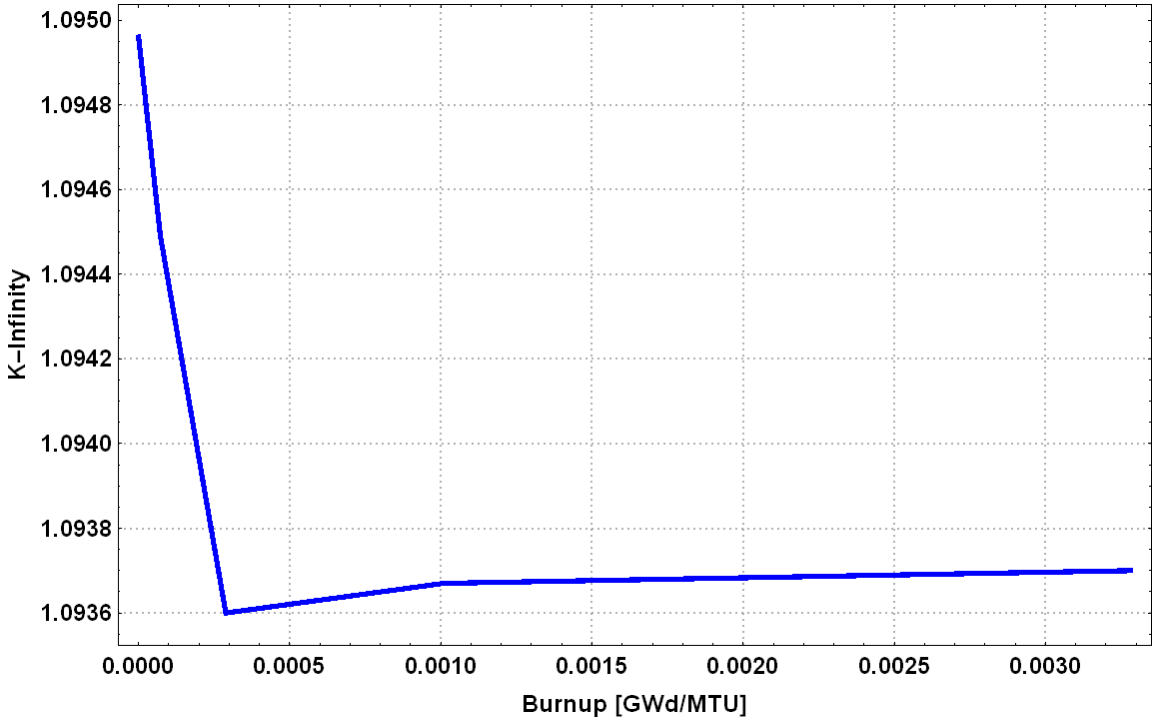

Figure 3.2: MCNP calculated k_∞ value behavior across first 45.47 days of burnup.

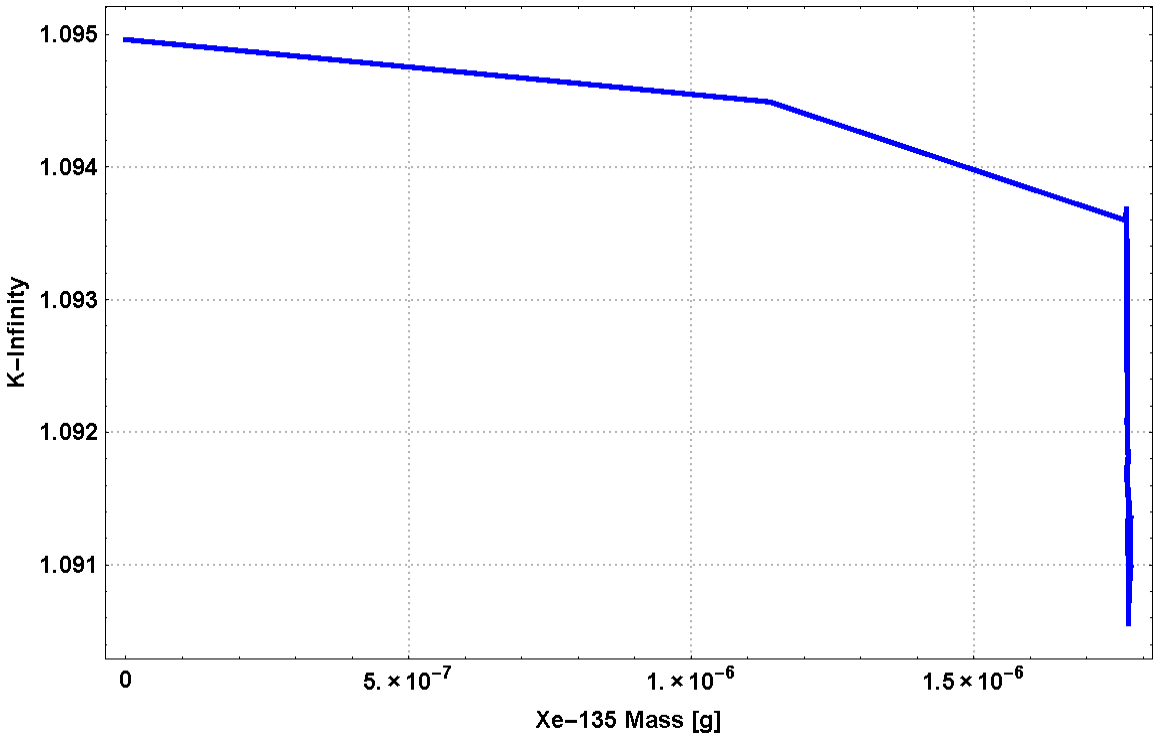

Figure 3.3: MCNP calculated k_∞ behavior based on Xe-135 poison concentration.

Burnup behavior based on fission product analysis is a top forensic priority. This interest is due to the different analysis methods that can be utilized to determine fuel burnup and content (e.g. gamma spectrometry, mass spectrometry etc). Fission product ratios/signatures can reveal key features of reactor fuel and power history. The relatively low burnup of this reactor makes forensics challenging due to the sluggish in-growth of fission products. For example, Europium-154 does not start presenting itself until approximately 514 days into the burnup and the quantity is around 0.8 ng total in the fuel slug. Figure 3.4 below shows the Eu-154/Cs-137 ratio versus burnup. The relationship is fairly linear after 514 days until the last burn step but no information related to burnup is gained previous to 514 days ascribed to the extremely low burn rate. The sharp incline at

the beginning of burnup is indicative of a low amount of burn steps which under-represents the behavior of the isotopes. Figure 3.5 shows a relationship between the ratio Ru-106/Ba-138 and purity of plutonium content. The graph was fitted with a polynomial function with a reported R-squared value of 0.9962.

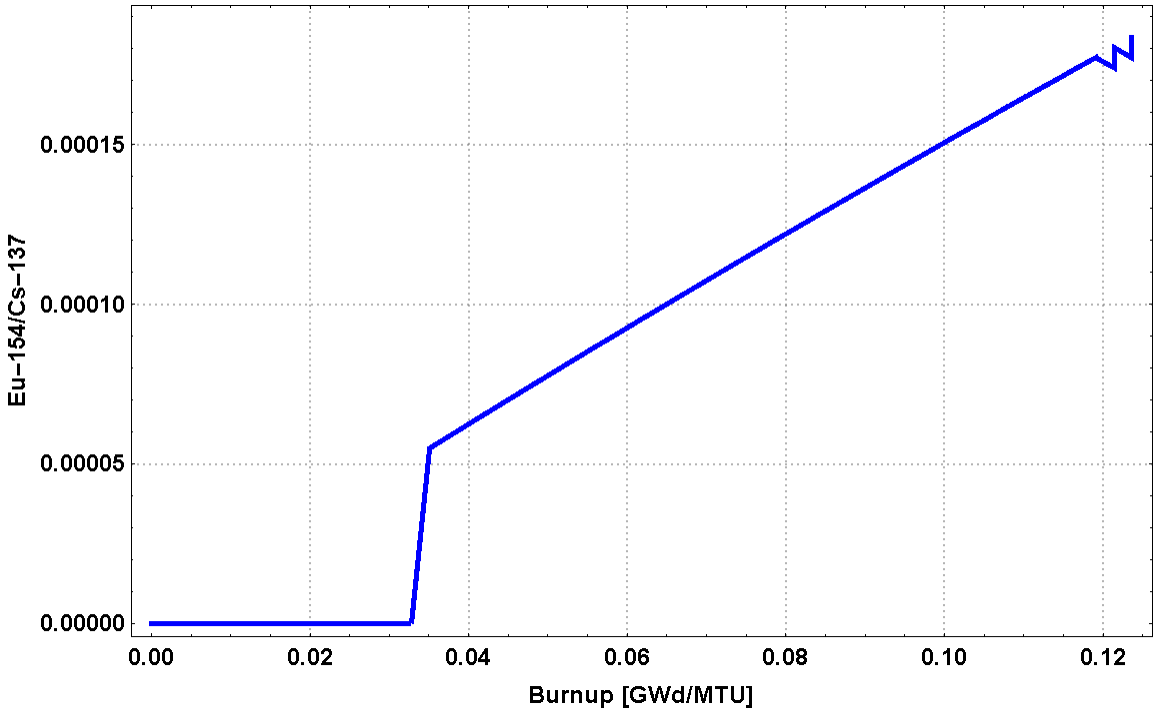

Figure 3.4: Europium-154/Cs-137 MCNP calculated ratio related to fuel burnup.

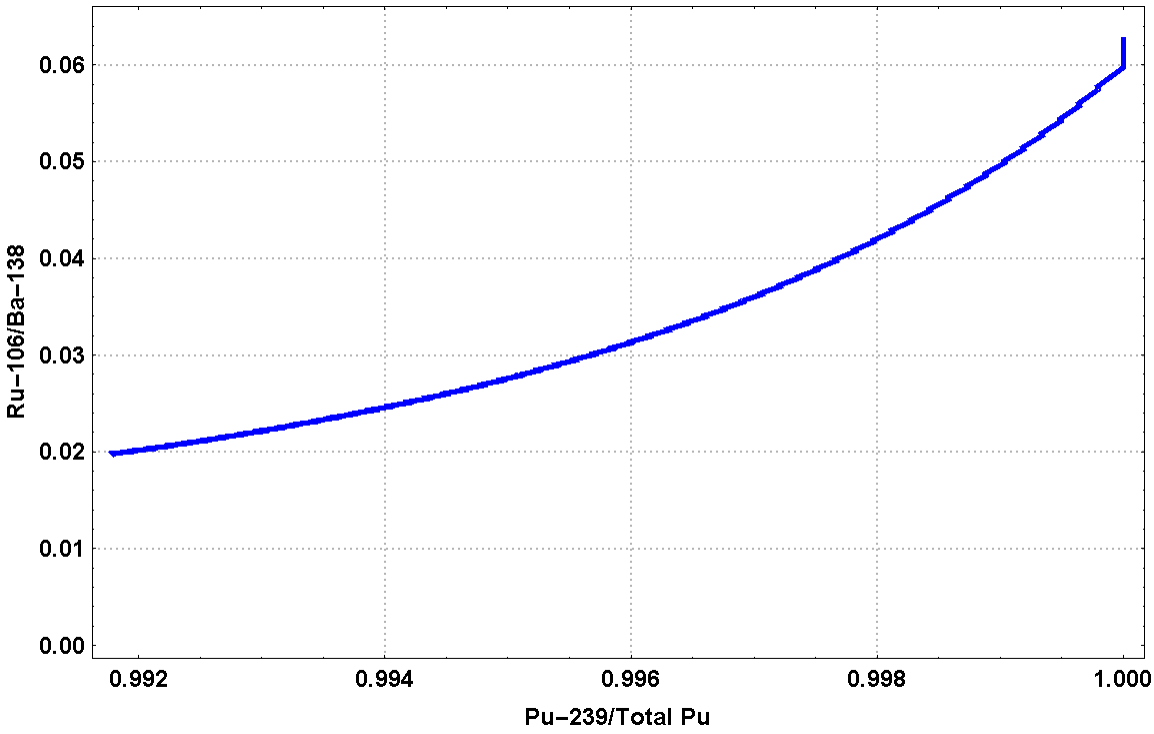

Figure 3.5: MCNP reported Ru-106/Ba-138 ratio related to purity of plutonium fitted with a 2nd degree polynomial. (First and second data points removed due to zero values)

The ratio Zirconium-94/Cs-137 was examined and shown to have a linear relationship after initial reactor start-up. Zirconium-94 and Cs-137 are good burnup indicators due to their low absorption cross sections and high U-235 thermal fission yields. Zirconium-94 is a stable isotope which does not affect the ratio when cool steps are present but the Cs-137 causes small fluctuations in the ratio due to the ~ 2 day cooling periods. This relationship is shown in Figure 3.6.

Heavy mass isotopics (Plutonium, Uranium, Neptunium etc.) are of value to the forensic community for mainly provenance determinations. One ratio that is a good gauge of plutonium purity is Ba-138/Total Barium attributed to the cumulative yield. This ratio with respect to burnup has a linear relationship with a reported R-squared value

of 0.9994 and is shown in Figure 3.7. These fission products are stable, and show no fluctuations due to cooling periods which is why they are good indicators of plutonium purity. If cooling times/periods are of interest, this ratio would not serve as an adequate gauge because of fission product stability.

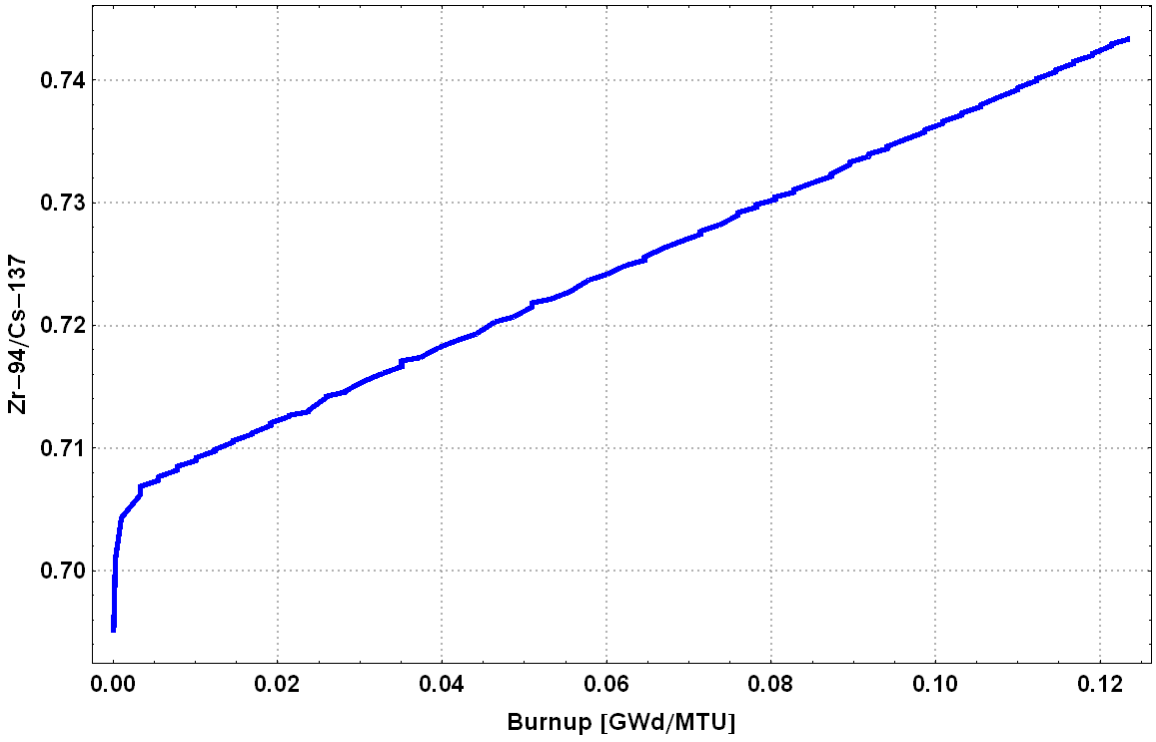

Figure 3.6: MCNP calculated Zr-94/Cs-137 ratio related to low-burnup.

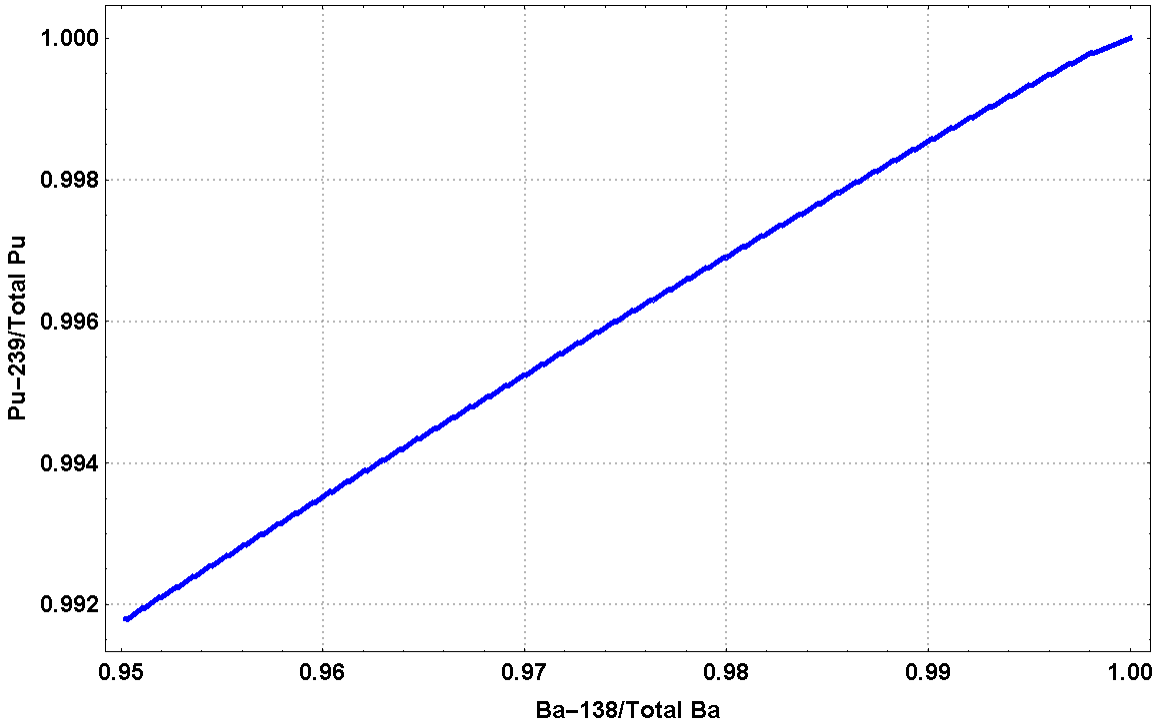

Figure 3.7: Ba-138/Total Barium content related to purity of plutonium.

Table 3.5: Pu-239/Pu-240 mass at discharge from reactor

Unit Cell Description [% carbon content]	**Pu-239 mass in fuel slug at 1822 days [g]**	**Pu-240 mass in fuel slug at 1822 days [g]**
0.00	1.357E-01	1.096E-03
0.12	1.355E-01	1.108E-03

Table 3.5 shows the plutonium content of the fuel slugs after 1822 days in the reactor. These two isotopes were of high-interest to the Manhattan Project attributable to weapon design. The low Pu-240 content of this reactor was a result from the extremely

low burnup of the reactor system. Interestingly, the Pu-240 content increases with higher carbon content.

Ascribed to the long cooling time between discharge from the reactor and potential isotopic analysis, Amercium-241 or Pu-241 concentrations can be obtained from mass spectrometry analysis. This heavy mass analysis and the subsequent concentration values can be related to cooling times of the fuel slug because of the half-lives of Americium-241 and Pu-241.

3.3 Scale Unit Cell Calculations

The Scale code package was developed by Oak Ridge National Laboratory for the U.S. Nuclear Regulatory Commission (NRC) with 89 computational modules presented to the user. A number of these physics codes were used in this research, including but not limited to: KENO-VI, TRITON, T-DEPL-2D and 3D, CSAS6. The modules mentioned used current nuclear data libraries for continuous-energy and multi-group neutronics calculations.[25]

Eigenvalue calculations used the CSAS6 module that was designed for enhanced criticality safety analysis using KENO-VI geometry input. This package was designed for automated cross-section processing for the KENO-VI Monte Carlo code (continuous energy) to determine the effective eigenvalue of the specified problem.

3.3.1 Scale Eigenvalue Calculation

As with the previous unit cell calculations, the carbon content was varied with the Scale eigenvalue calculations. The module used for the calculation was the CSAS6 which

was designed for enhanced criticality safety using the ENDF/B-VI 238 group cross-section library. This module uses KENO-VI geometry input (combinatorial) and uses continuous energy to determine the eigenvalue of the chosen problem. As with the MCNP eigenvalue calculation, each unit cell ran 10,000 particles and 1000 cycles with 500 initial cycles skipped, calculation results can be found in Table 3.3 below. Fluxes within the fuel and moderator regions were examined and can be found in the Table 3.6 below. The same thermal, epithermal and fast energy bin values were used as the above MCNP analysis.

Table 3.6: Unit cell eigenvalue calculation results with varying carbon content.

Unit Cell Description (carbon content [%])	**k_∞ value (at 95% confidence level)**	**Average neutron lethargy causing fission [MeV]**	**Average mean free path in fuel [cm]**
0.0	1.10016 ± 0.00030	1.80097E-01 ± 1.44021E-04	9.44254E-01 ± 2.11645E-05
0.12	1.09977 ± 0.00029	1.77014E-01 ± 1.45282E-04	9.44273E-01 ± 2.01313E-05
0.23	1.10039 ± 0.00027	1.73725E-01 ± 1.42350E-04	9.44277E-01 ± 2.06029E-05

The eigenvalue calculation for the unit cell containing no carbon calculated a k_∞ value of **1.10068 ± 0.00048.** Equal fuel volumes were used between MCNP and Scale KENO-VI Monte Carlo calculations along with the same number of cycles, particles and generations skipped. The "average" carbon content of natural uranium metal of that time period gave an eigenvalue of **1.09977 ± 0.00029.** This drop in the k_∞ value was expected

due to the displacement of the fissile atoms within the fuel elements. Essentially the addition of carbon atoms within the fuel element added more moderation to the unit cell system which in turn softened the energy of the neutron spectrum. This softening in the neutron spectrum can also have an adverse effect on neutron energies being at the key resonance regions of the fissile elements within the fuel. The eigenvalue calculation of the maximum amount of carbon (0.23%) of that era reported **1.10039 ± 0.00027**. The closeness of the k_{∞} values was expected on a small unit cell scale.

3.3.2 Scale Burnup

Burnup within the Scale code package was completed using the TRITON control module. This computer code is a multipurpose package used for transport, depletion, sensitivity and uncertainty analysis. For the purposes of this study, TRITON was used for 3D configuration but can also be used for multi-group transport calculations of 1D and 2D configurations as well. Along with these calculations, the ORIGEN depletion module was used for the isotopic concentrations within the fuel slug. The T6-DEPL option was selected for this study which uses burnup-dependent cross-section preparation and 3D Monte Carlo transport calculations. In addition, TRITON uses a predictor-corrected approach to process the depletion scheme. The cross-section and transport calculations are based on the anticipated isotope concentrations at the midpoint of a depletion subinterval. The ORIGEN depletion calculations are then performed over the first half of a subinterval or the full subinterval. ORIGEN completes the depletion calculations over smaller time steps/intervals which are automatically decided by the TRITON module. It is also noteworthy, after the last depletion step TRITON employs the OPUS module to generate the time-dependent concentrations of the nuclides of interest. Although 3D

calculations are desired within the forensics communities, future studies should examine 2D calculations and the effect on the desired ratios within an assembly.

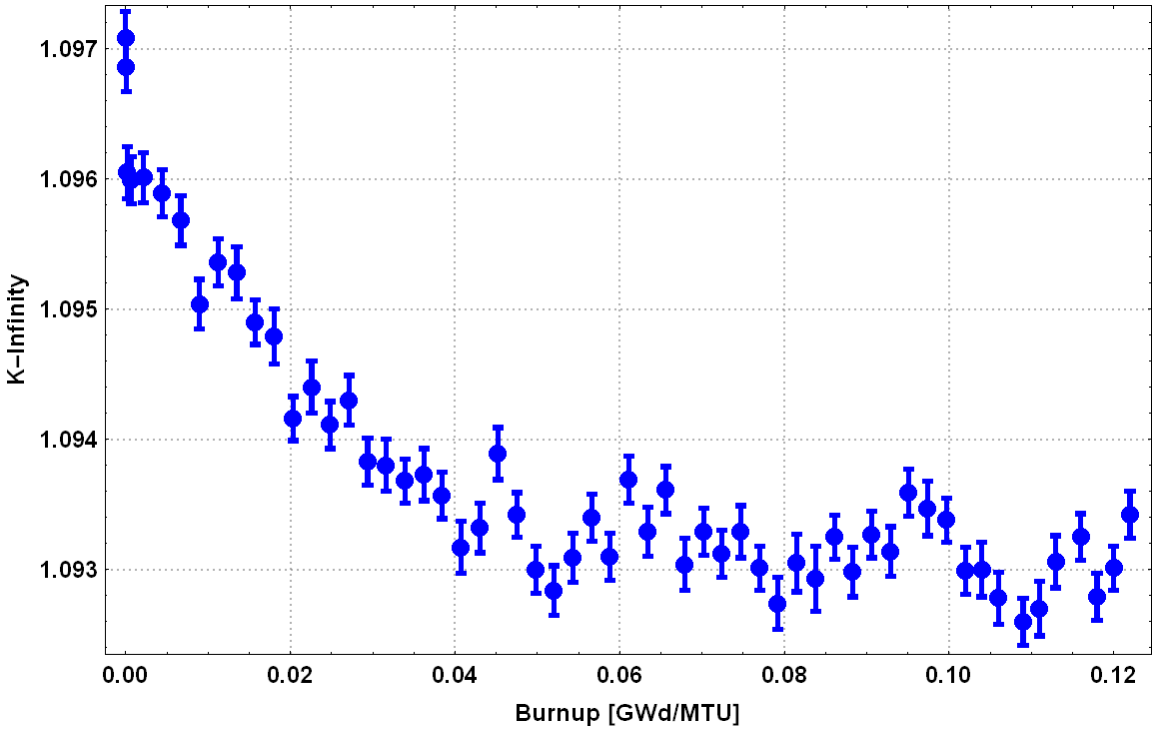

Figure 3.8: Scale reported k∞ behavior with respect to burnup.

The k_∞ behavior within the unit cell with respect to burnup is shown in Figure 3.8 above. The oscillatory behavior of the k_∞ value is explained by the cooling steps input into the depletion module. Also, the raw k_∞ data has less granularity due to the TRITON determined time interval length being significantly shorter than the actual amount of burn steps.

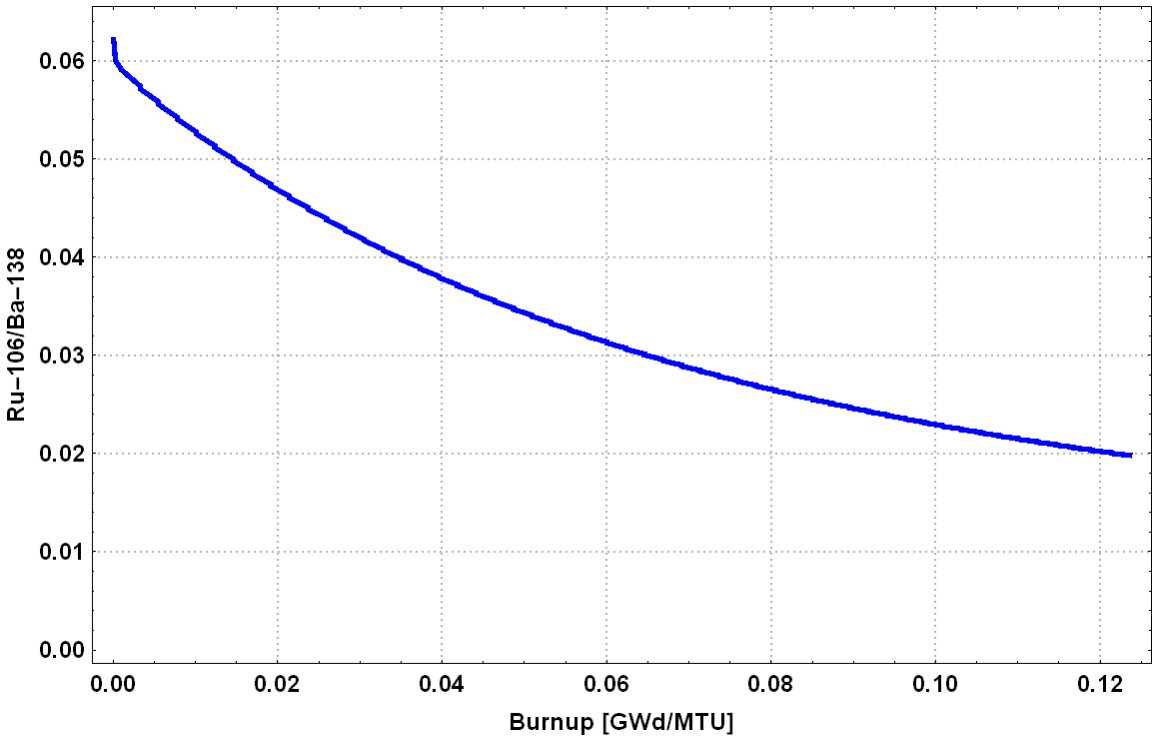

Figure 3.9: Ru-106/Ba-138 relationship with respect to burnup.

As shown above in Figure 3.9, the Ru-106/Ba-138 ratio has a logarithmic relationship to the burnup within the unit cell. Ba-138 is a naturally occuring isotope and Ru-106 has a half-life of around 373 days. Nondestructive and destructive analysis can be performed on a fuel slug/pin promptly after removal from the reactor core. As mentioned previously, the Ba-138 radioisotope is a good measure of total overall fissions across each different fuel due to the closeness of the cumulative yield values. When paired with Ru-106, this ratio shows the plutonium fissions declining as burnup progresses.

In Figure 3.10 below, the Ba-138 (stable) concentration is plotted with respect to the unit cell slug burnup with a perfect linear relationship. This concentration could be determined at any point in time after discharge from the core by destructive analysis

methods. This isotope is a good indicator of overall fissions within the natural uranium slug.

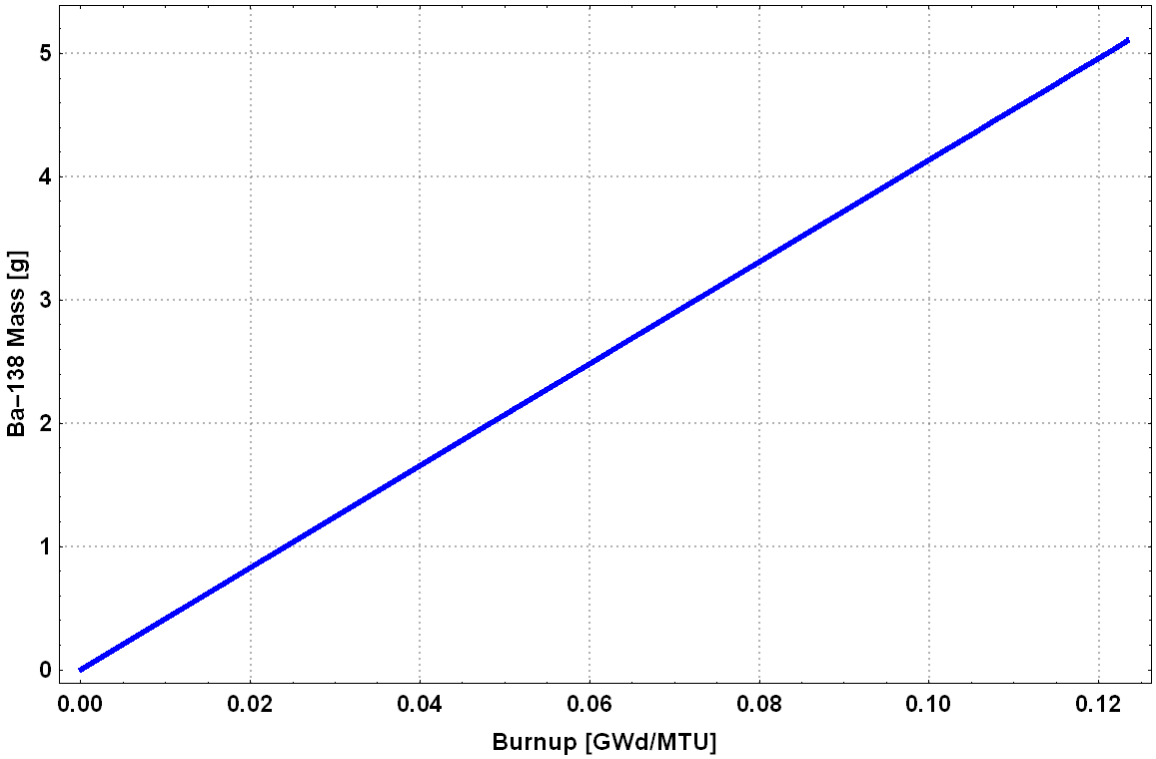

Figure 3.10: Ba-138 concentration with respect to burnup.

Also shown below in Figure 3.11, is the Ru-106 concentration with respect to burnup. This concentration is relevant to forensics due to the difference in fission yields between Pu-239 and U-235. The fission yield of Ru-106 is 11 times higher in Pu-239 than the fission yield from U-235. Aquiring a gamma ray spectrum of this isotope will indicate the ratio of Pu-239 fissions to total fissions. Total fissions can be calculated by using an isotope with near identical fission yields from Pu-239 and U-235. A good example of this would be acquiring a gamma spectrum from Cs-137.[10] This graph also indicates Pu-239 fissions are increasing as burnup progresses.

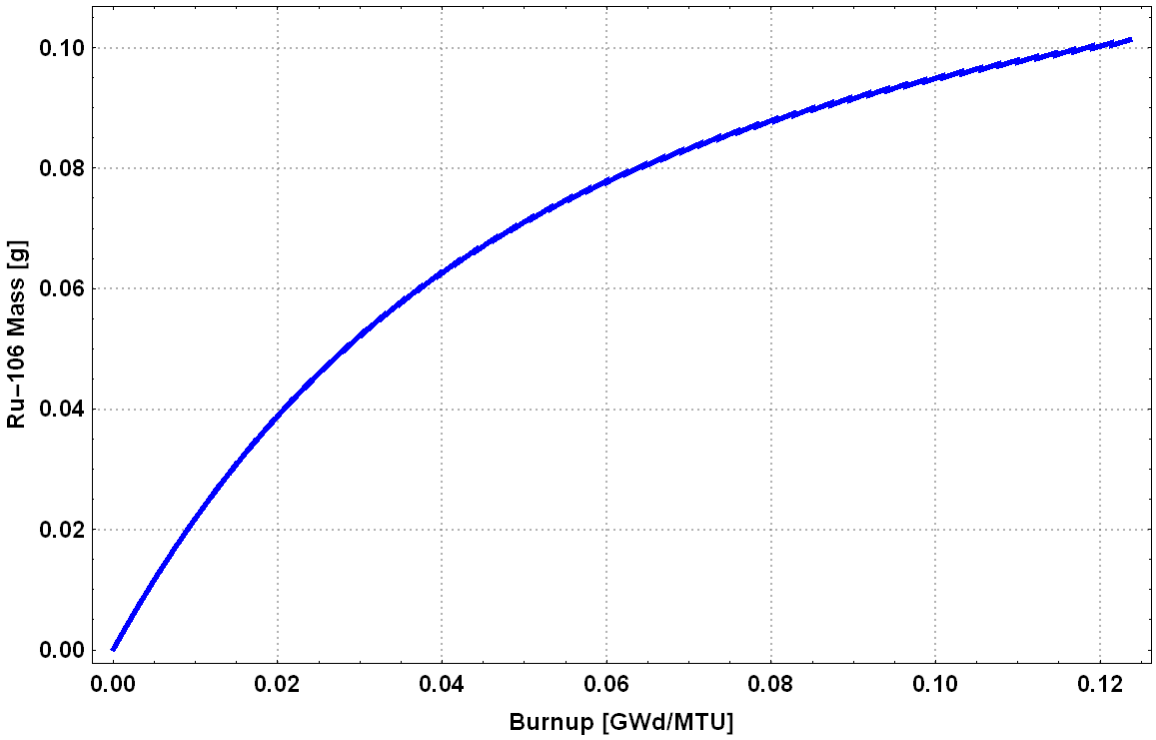

Figure 3.11: Ru-106 mass content with respect to burnup.

As shown below in Figure 3.12, the Zirconium-94 and Cs-137 ratio provides a good indicator of burnup due to the linear relationship. This is owed to the long half-life of Cs-137 (~30 years) and the high fission yield of the two isotopes. The position of these two isotopes on the fission yield curves of Pu-239 and U-235 could also indicate total number of fissions within the fuel slug with passive methods while the reactor was operational. Prompt gamma spectrometry following the removal of the fuel slug with respect to the Cs-137 (Ba-137m emission) could be used to determine the total number of fissions within the slug at discharge.

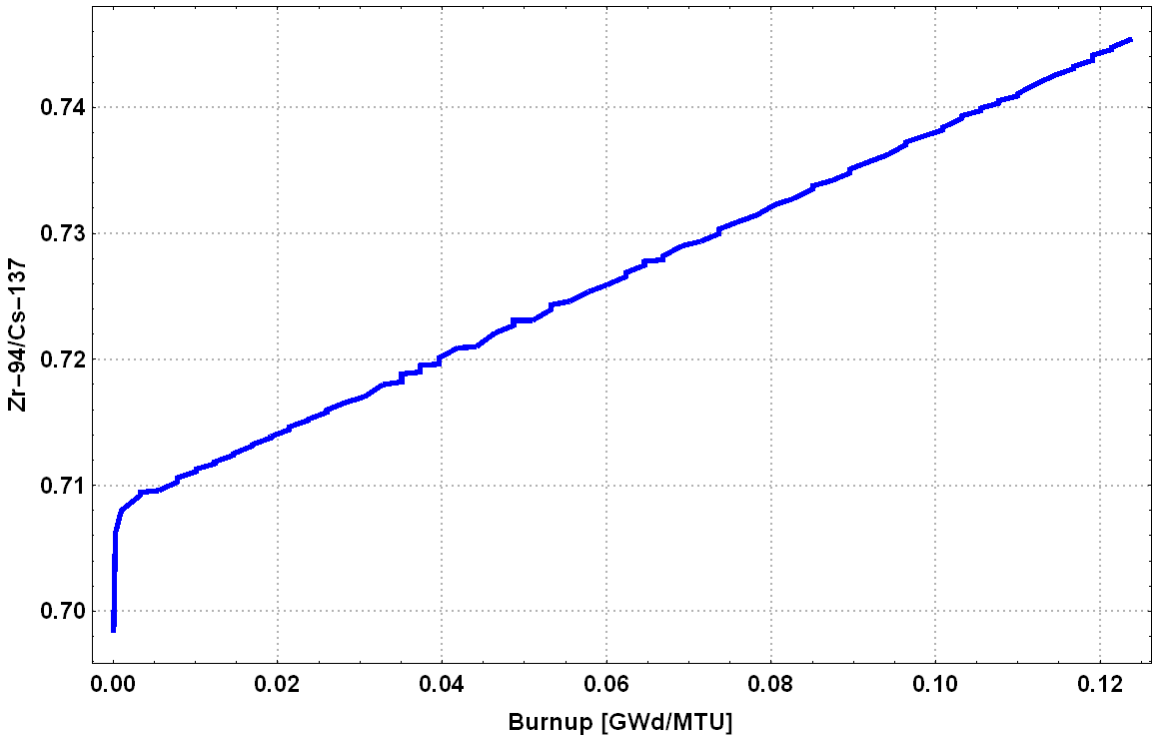

Figure 3.12: Zr-94/Cs-137 ratio related to burnup.

As discussed in the previous sections, the plutonium isotopics and isotope ratios can be used for reactor type determination, through exploiting the differences in magnitude of the neutron spectrum that was used to create the Pu within the slug or fuel pin. Shown below in Figure 3.13 is the relationship of the neutron spectrum seen within the X-10 unit cell.

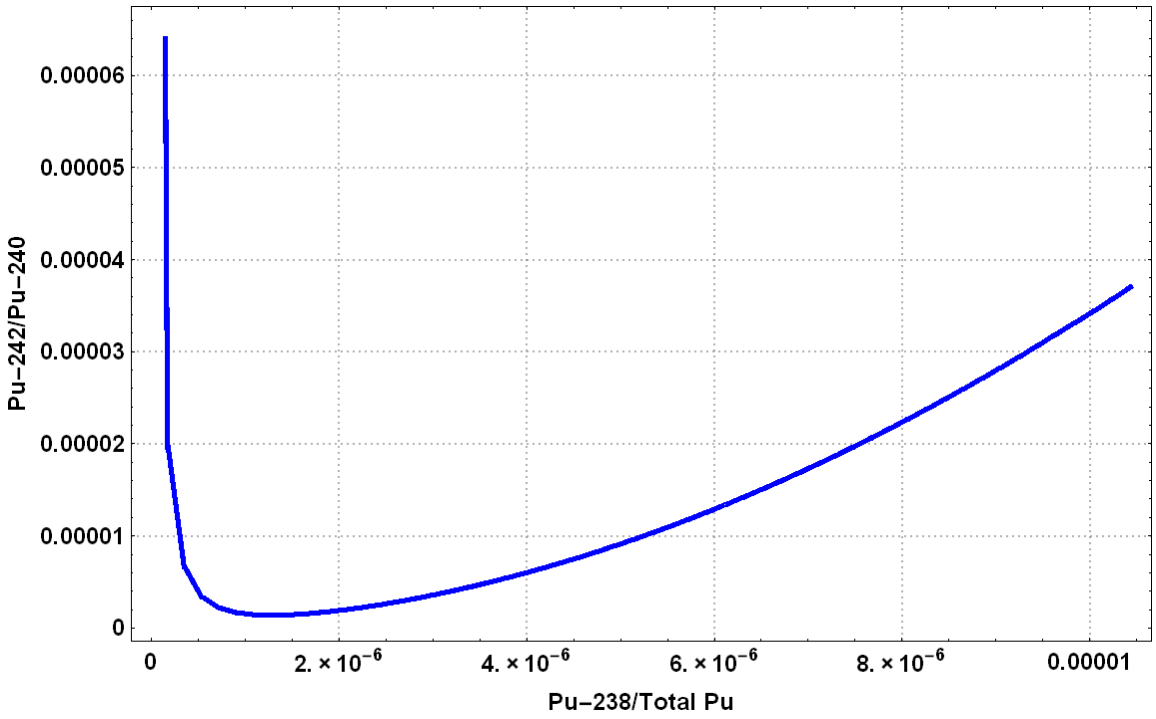

Figure 3.13: Neutron spectrum correlation with Plutonium isotopics at steady-state operation.

The erratic behavior of the graph is attributed to the startup of the reactor and the Pu-239 being created but not yet burned (fissioned). Shown in Figure 3.14 below is the behavior after 179 days of reactor operation. The spectrum behavior has a power correlation when observing the Pu-238/Total Pu ratio. If mass spectrometric methods are employed the type of reactor that created the plutonium could easily be determined by the magnitude of the Pu-242/Pu-240 ratio or the Pu-238/Total Pu ratio. The extremely low burnup of this fuel slug and the spectrum measurements will certainly be different when compared to era production reactors (e.g. Hanford, NRX, and Calder Hall type).

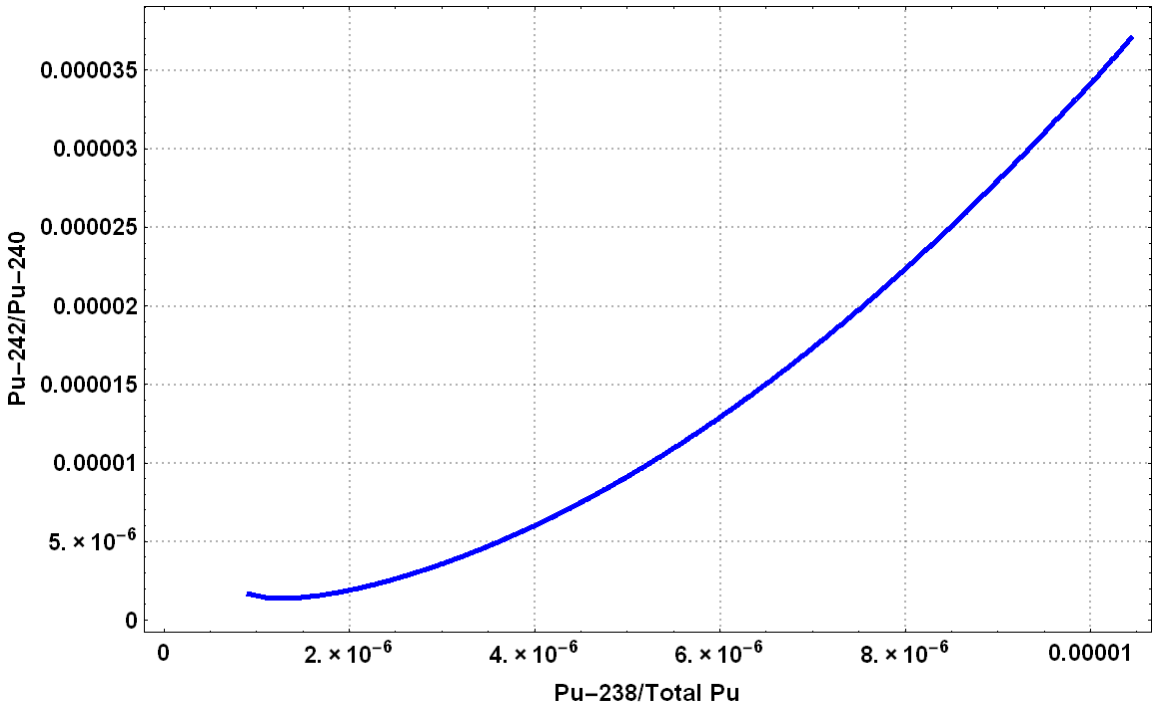

Figure 3.14: Neutron spectrum correlation with Plutonium isotopics after 179 days of reactor operation.

Xenon ratios can be attributed to different fission events such as normal reactor operation versus a reactor incident or nuclear explosion (prompt events). As shown below in Figure 3.15, the Xenon-135/Xenon-133 ratio remains throughout the burnup of the fuel slug. This low ratio (when compared to a nuclear explosion) is attributed to the extremely low burn of the fuel slug. Also noteworthy, Xe-133 has similar cumulative fission yields from Pu-239 and U-235 (~7%). This information can be leveraged in determining the total number of fissions from reactor operation or a prompt nuclear incident. More discussion of Xenon isotopics is found in previous sections.

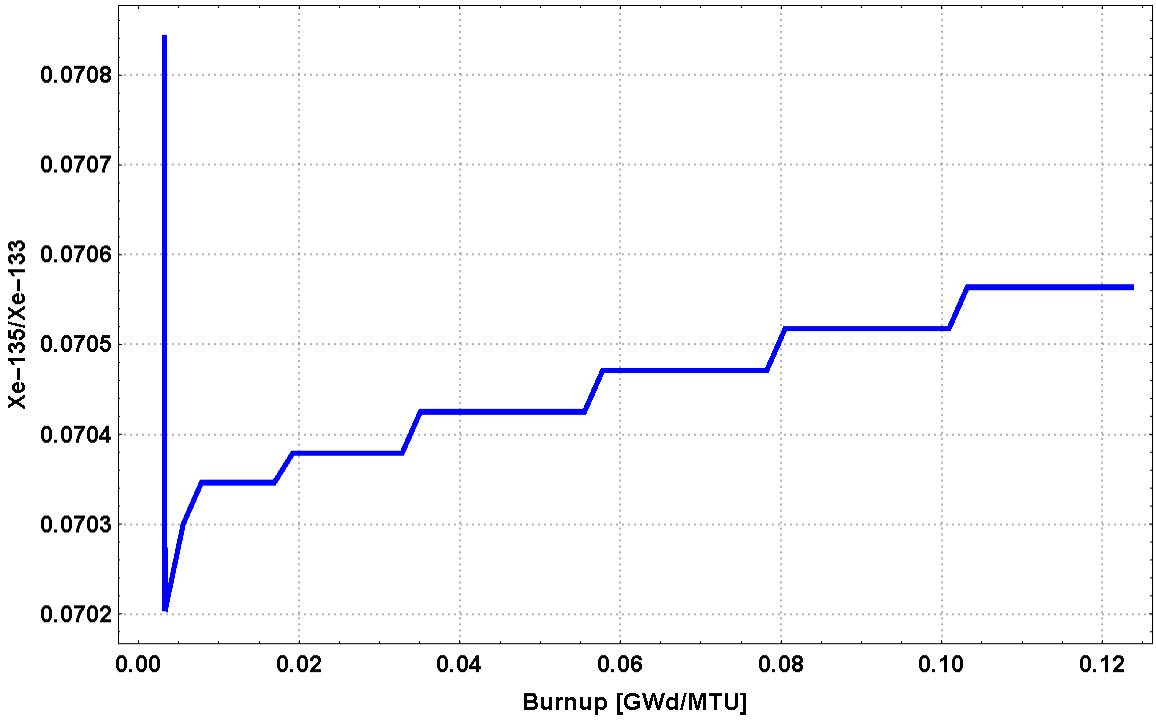

Figure 3.15: Xe-135/Xe-133 mass ratio with respect to burnup.

3.4 PENTRAN Unit Cell Calculations

The Parallel Environment Neutral-Particle TRANsport (PENTRAN) 3-D deterministic (S_N) code system developed by Sjoden and Haghighat was used for the next comparative study of unit cell eigenvalues and burnup. This code system allows the user to fully decompose the angle, energy and spatial components in a parallel computer environment for a given problem. It also gives the user the option of forward or adjoint calculations using discrete ordinates simulations. The discrete ordinates approximation of the transport equation discretizes the energy, angle and space variables into a finite amount of angles, energy groups, and space (spatial grids) over the entire user defined phase space. Cross-sections were derived and collapsed from the ENDF/B-VI 238 group library using Scale's T-NEWT module.

3.4.1 PENTRAN Eigenvalue Calculation

For the basis of the PENTRAN eigenvalue calculation, carbon content was not varied (average value used). Homogenization of the previously defined unit cell was also examined. The angular ordinates and symmetric quadrature sets were also varied greatly to demonstrate the physical behavior of the neutrons within the system and the effect on a given solution. The angular dependent scattering cross-section (P_N) is expanded using spherical harmonics and the Legendre Addition Theorem and the level-symmetric quadrature approximations (associated weights, i.e. S_N) are applied to the integral term of the Boltzmann transport equation. Eigenvalue solutions are given as the result from an iterative solution and the actual solving of the Boltzmann transport equation. Descriptions of a source iteration method and the Boltzmann transport equations along with further discussion of P_N approximation and S_N quadrature sets can be found in the PENTRAN user manual shown in the reference section of this report.[17] The eigenvalue results are shown below in Table 3.7.

Table 3.7: Unit cell eigenvalue calculations varying P_N order and S_N quadrature.

Unit Cell Description (3group), P_N order, S_N quadrature	Iterative Eigenvalue	Transport Solution Eigenvalue
3, 32	1.105995 ± 0.000107	1.111508 ± 0.0044786
3, 16	1.095991 ± 0.000001	1.096772 ± 0.00064119
3, 6	1.095491 ± 0.000000	1.095971 ± 0.0004022
3, 8	1.094599 ± 0.000001	1.095210 ± 0.0005122
5, 8	1.091555 ± 0.000010	1.093674 ± 0.0017649

5, 12	1.083289 ± 0.000023	1.089099 ± 0.0049205
5, 6	1.093736 ± 0.000003	1.094607 ± 0.00071512
2, 12	1.064229 ± 0.000054	1.080521 ± 0.014169

From examination of the eigenvalue calculations which varied P_N order and S_N quadrature, the eigenvalue calculation was affected greater by varying the P_N order rather than the S_N quadrature. This lower quadrature requirement is possibly caused by the high scatter nature of the graphite within the unit cell and the large volume ratio it holds in this problem. The high scatter associated with the graphite allows for a low S_N order to be used due to the scatter being captured across fine mesh boundaries by larger angles. Doubling the S_N quadrature from S_{16} to S_{32} showed a significant jump in eigenvalue but tracking all those angles in a unit cell calculation is computationally expensive.

Homogenization of the unit cell was also completed using PENTRAN. At first, homogenization of the entire unit cell volume was attempted but too little fuel volume and an overwhelming amount of graphite made the main reaction in the system scattering rather than absorption in the fuel elements. A smaller subsection of the unit cell was homogenized (at channel boundaries) which minimized the amount of graphite (scattering material) in the homogenized fuel section of the unit cell. Table 3.7 shows the results of these computations. Figure 3.16 shows a schematic of the X-10 homogenized unit cell. The red region is homogenized with air, cladding, fuel and graphite. The yellow region is pure graphite.

Table 3.8: Homogenized unit cell calculations varying S_N quadrature

Unit Cell Description (3group), P_N order, S_N quadrature	**Iterative Eigenvalue**	**Transport Solution Eigenvalue**
3, 16	1.093874 ± 0.000009	1.093008 ± 0.00072889
3, 6	1.091238 ± 0.000016	1.091340 ± 0.000091
3,8	1.091439 ± 0.000010	1.091395 ± 0.000033

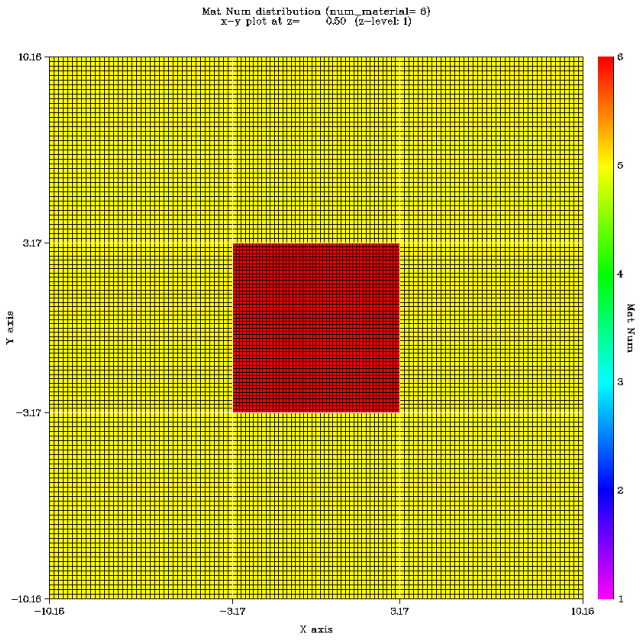

Figure 3.16: PENTRAN homogenized unit cell.

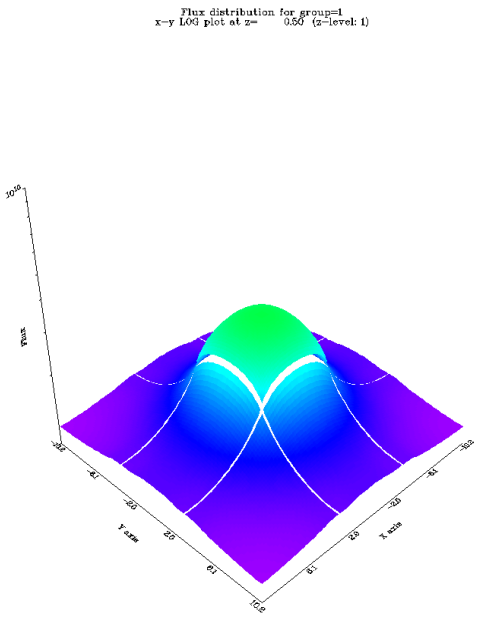

Figure 3.17: PENTRAN 3D fast flux (Group 1) plot

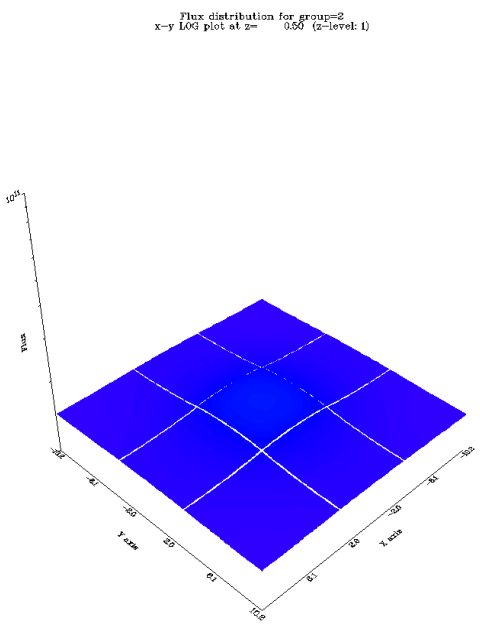

Figure 3.18: PENTRAN 3D epithermal flux (Group 2) plot

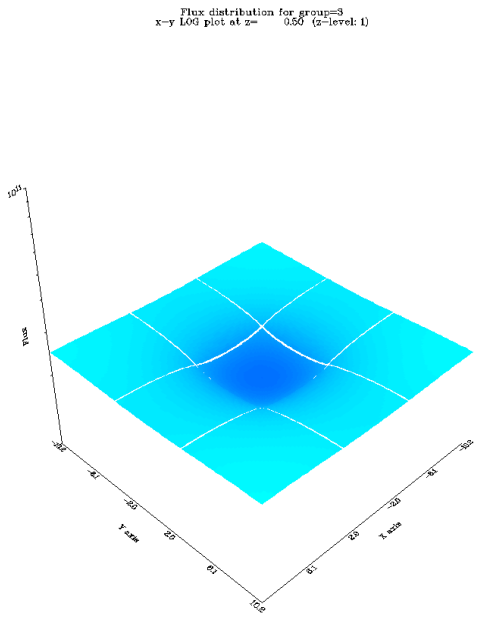

Figure 3.19: PENTRAN 3D thermal flux (Group 3) plot

Shown above in Figures 3.17-19 are the 3D plots associated with the flux in the X-10 homogenized unit cell. The fast flux is mainly confined to the middle coarse mesh, which is expected due to the fissile material being restricted to this entire coarse mesh. Figure 3.17 shows the epithermal flux which is considerably lower magnitude within the middle coarse mesh. The high thermal flux is predominantly confined to the perimeter coarse meshes, which is also expected due to the moderation of the neutrons from the fast energy fissions contained in the fuel element.

Again, varying the S_N order of the system did not significantly change the eigenvalue answer. This behavior is also due to the scattering nature of the now "fuel volume" which is homogenized with the high scatter graphite moderator along with the natural uranium fuel. The percent difference between the S_{16} and S_6 calculation was 0.2413% while the percent difference between the S_6 and S_8 was 0.0184%. The relative

low error between the S_{16} and S_6 calculation puts in perspective choosing a less computationally expensive eigenvalue problem depending on the purpose and application of the calculation.

PENTRAN Group dependent flux distribution intensity maps of the P_3-S_{16} unit cell are pictured below (Figures 3.20, 3.21, and 3.22) in ascending order of group. Minimal ray effect was seen in all group flux distributions. Figure 3.20 shows the fast flux distribution map and indicates the fast neutron flux being the highest in the fuel region which is expected due to the location of fission and subsequent release of fast neutrons. The fast flux also falls off rapidly showing the moderation power of the graphite, where neutrons are scattered out of fast energies in a short relative distance.

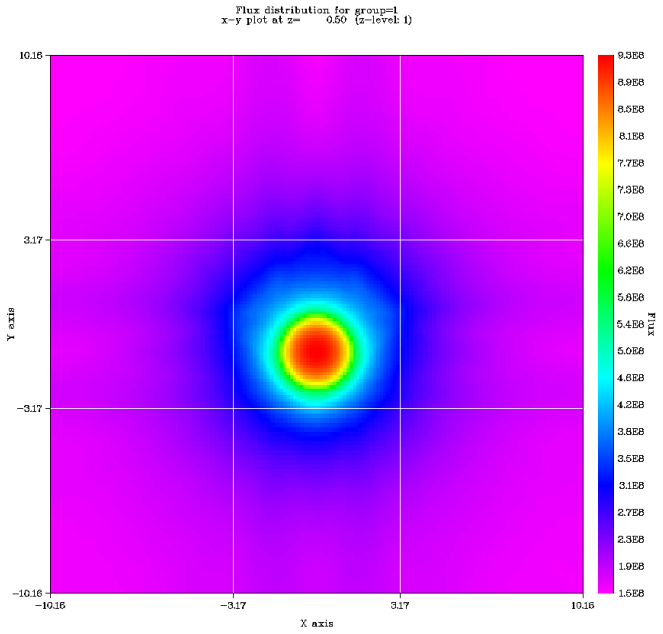

Figure 3.20: Group 1 (fast) flux distribution intensity of unit cell.

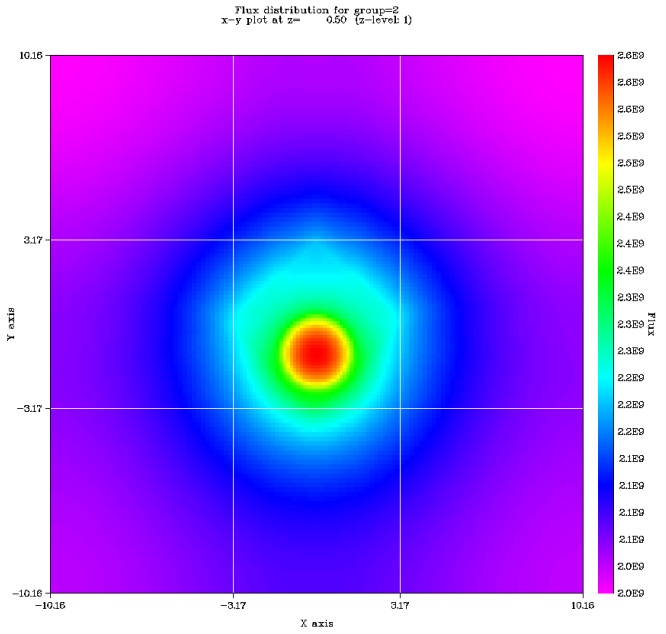

Figure 3.21: PENTRAN group 2 (epithermal) flux distribution.

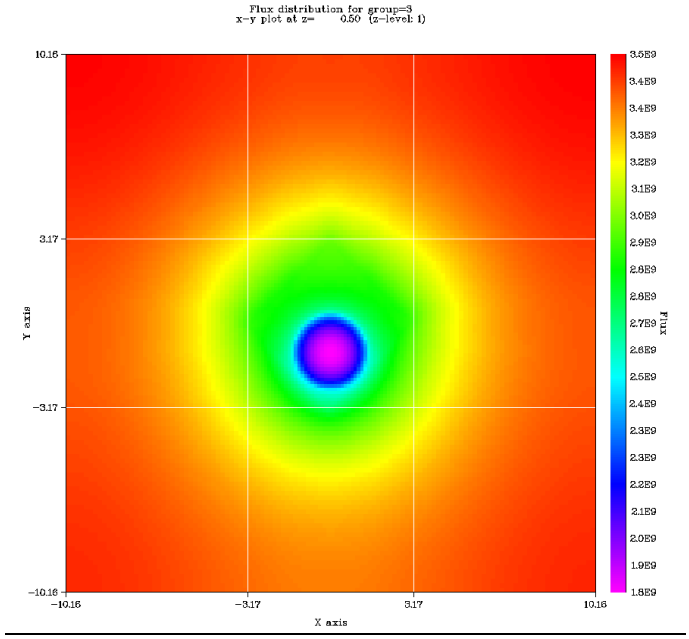

Figure 3.22: PENTRAN group 3 (thermal) flux distribution.

The epithermal flux is also the highest within the fuel region and falls off drastically outside of the fuel channel. It seems to reach a minimum at the corners of the unit cell which is expected due to the proximity to the fuel. The thermal flux in the system is highest on the perimeter of the unit cell. This flux locality behaves as expected due to the nature of the graphite and the design of the reactor. The high thermal flux on the perimeter demonstrates the purpose of a thermal reactor which is to thermalize neutrons to cause fission within the fuel and to breed Pu-239 for weapons purposes.

3.4.2 PENBURN/PENTRAN Burnup

PENBURN is a deterministic transport depletion solver. Depletion is solved using the linear chain method and burnup is calculated by direct solution of the Bateman equations. This type of solution is direct which yields exponentially short computation time. For further explanation of the linear chain method and computation logic please see the PENBURN manual referenced at the end of this study.[18]

Shown in Figure 3.23 are the averaged k_∞ values with respect to burnup. The k_∞ values are averaged across the last 4 outer iterations after the convergence criteria are met.

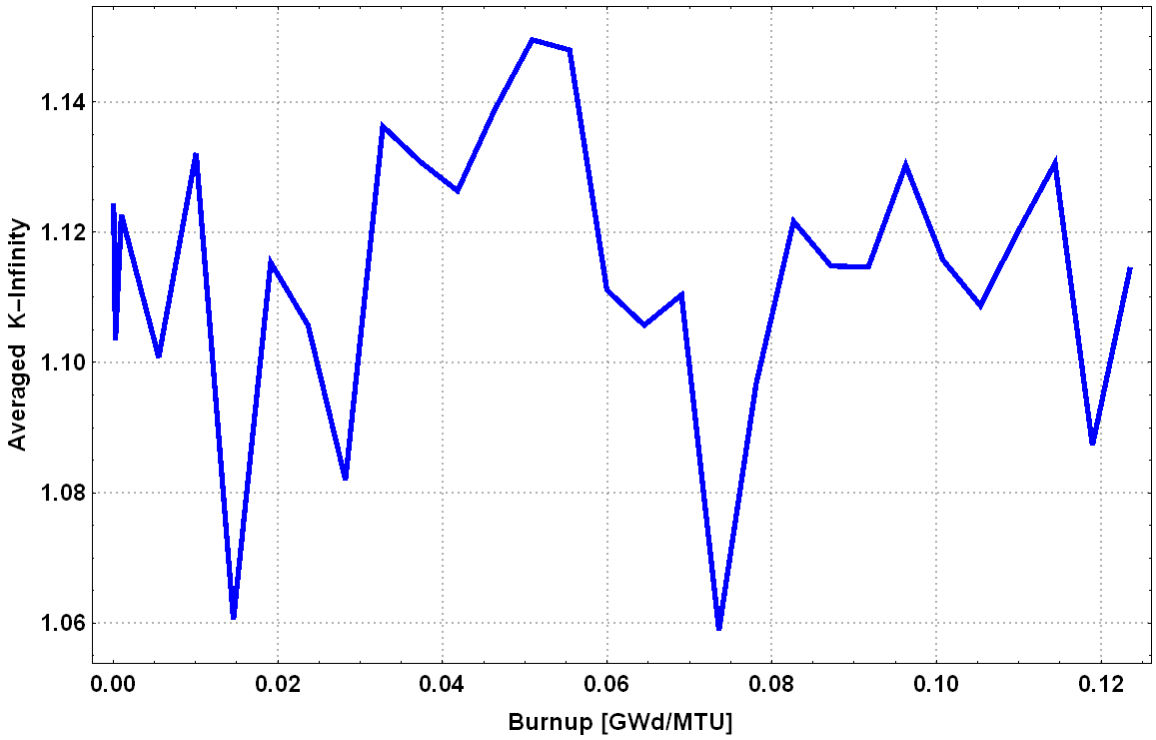

Figure 3.23: Averaged k_∞ values with respect to burnup the increase in k_∞ attributed to Pu-239 production.

The k_∞ behavior across the burnup of the unit cell oscillates between eigenvalues of approximately 1.06 to 1.14. Examining one of the common neutron poisons in reactor burnup could provide an explanation into the oscillatory performance of the k_∞ value.

Xenon-135 has an enormous neutron capture cross-section and is the cause for drops in reactivity within a reactor core. Shown below, the mass of Xe-135 across burnup stays fairly constant with exception to the beginning and end of life in the burnup cycle.

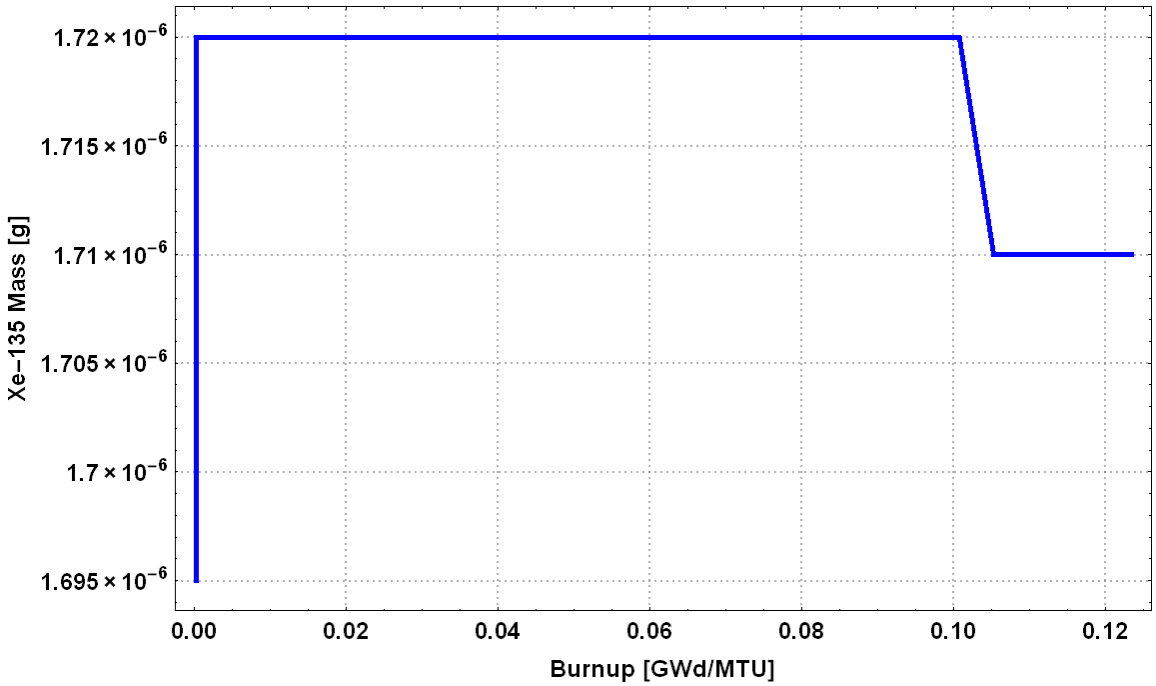

Figure 3.24: Xe-135 mass across burnup of fuel slug.

Total fissions within the fuel slug can be quantified by the amount of Ba-138 and also Ba-137 (stable fission products) that is produced across the irradiation within the reactor. In Figure 3.26, Ba-137 production is plotted in reference to burnup.

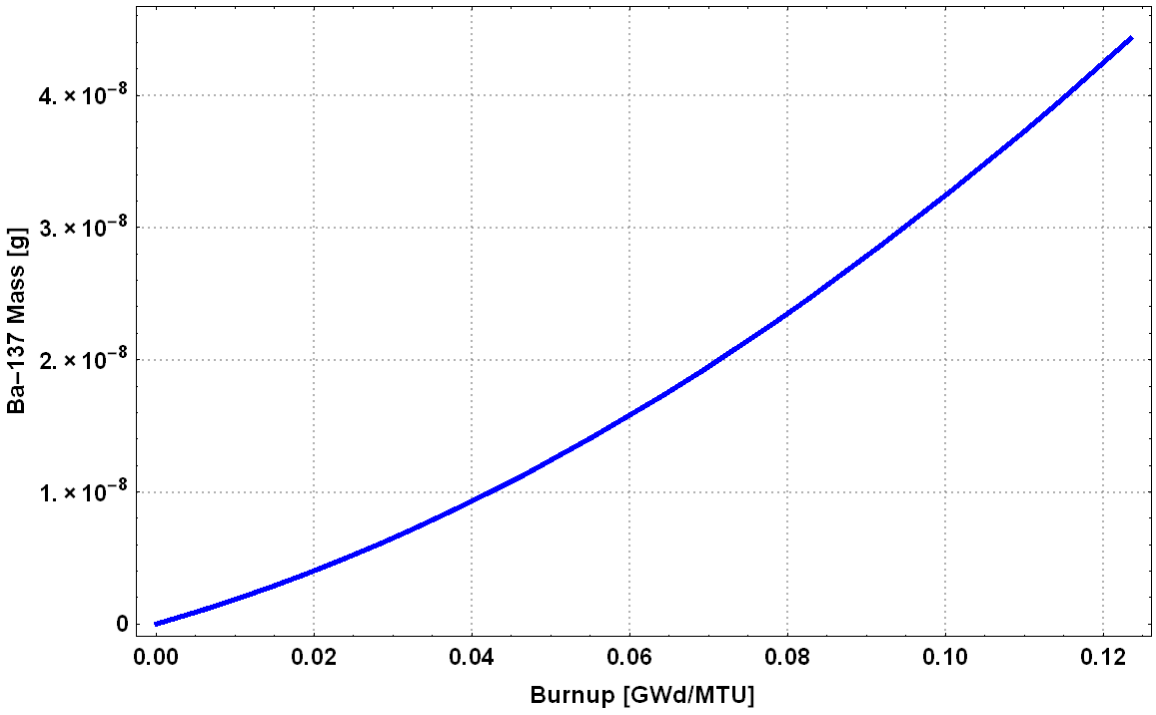

Figure 3.25: Ba-137 mass ingrowth in reference to burnup.

Showing Ba-137 rather than Ba-138 is to illustrate the similarities between the two stable isotopes. The fission yields between the two isotopes are high (around 6% between U-235 and Pu-239) which makes this a prime candidate for total fissions between the two fuel types. Cs-137 is the parent of Ba-137 which causes the plot to mimic exponential ingrowth because of the decay of the parent.

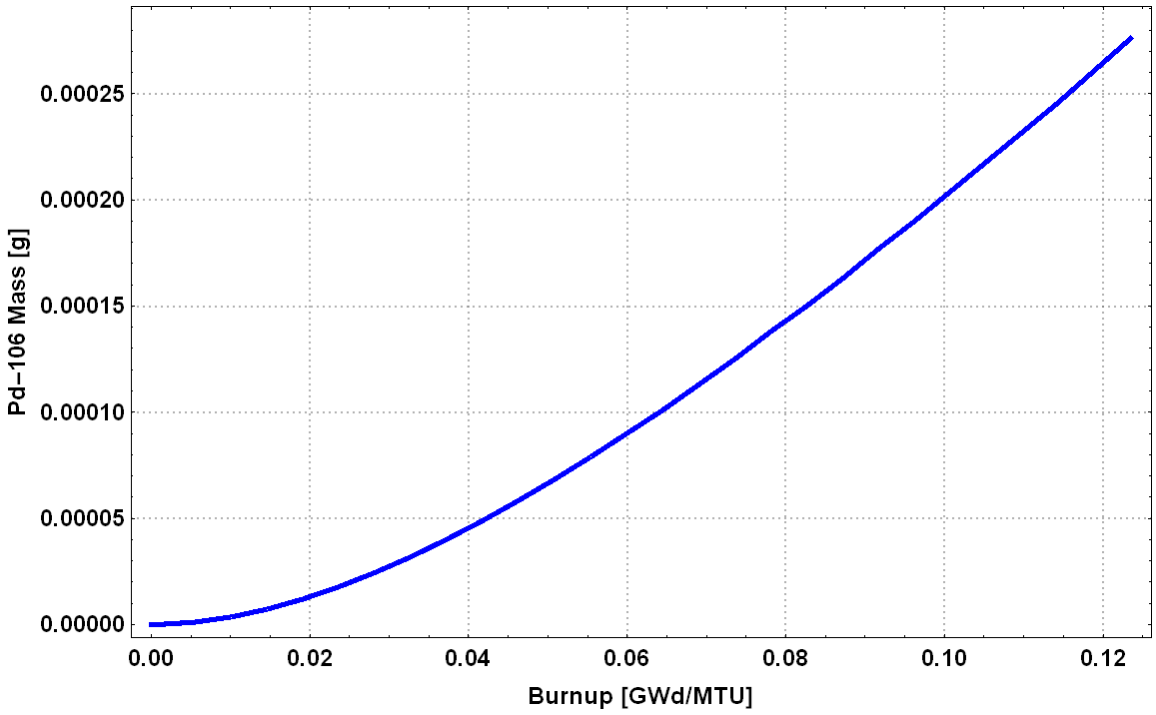

Figure 3.26: Pd-106 mass associated with burnup.

As highlighted in chapter 2, Pd-106 has a cumulative yield in Pu-239 that is approximately 11 times higher than U-235. The high yield in Pu-239 and the difference between the U-235 cumulative yields makes this a prime candidate for the total number of Pu-239 fissions within the system. Shown above in Figure 3.26 is the Pd-106 mass growth as a function of burnup. The shape of the growth is expected as at the beginning of life of reactor operation the Pu-239 is burned in but contributes very little to the overall fissions within the system.

Even higher of a difference between fuel types, is Ag-107. Pu-239 has approximately 23 times higher cumulative yield of Ag-107 when compared to U-235. The isotope is stable and can be characterized with destructive analysis such as mass spectrometry. This higher difference between fuel types makes this an even better

candidate for total Pu-239 fissions. Shown below in Figure 3.27 is the Ag-107 mass with burnup progression.

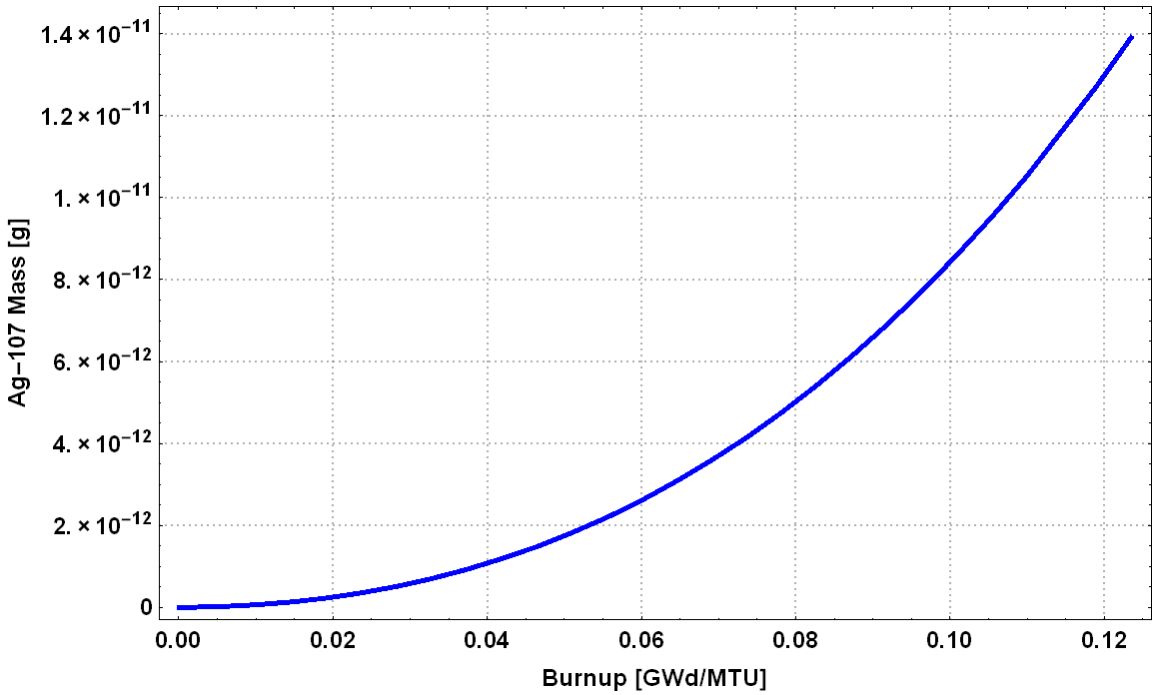

Figure 3.28: Ag-107 mass ingrowth with respect to unit cell burnup.

The Pu-239 fission behavior is more pronounced with this isotope attributable to the radical difference between cumulative yields. This stable isotope is a pristine indicator of Pu-239 fissions within the system.

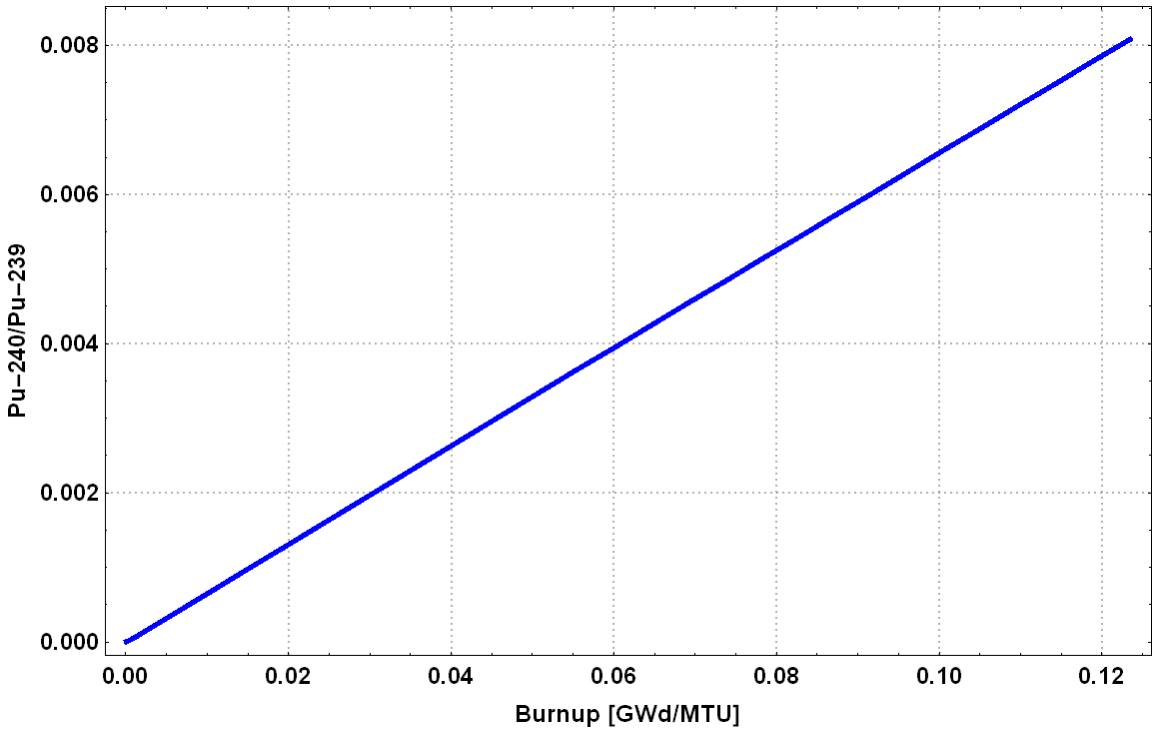

Figure 3.28: Pu-240/Pu-239 ratio with respect to burnup.

Shown above in Figure 3.28, is the Pu-240 to Pu-239 ratio with reference to burnup. PENBURN predicts the Pu-240 content reaches approximately 0.8% after the 5 year burnup. This is an important ratio in reference to weapon design and correspondingly when the fuel slugs need to be removed from the reactor so the Pu-240 content does not reach over 7%. Comparison of this ratio between deterministic and Monte Carlo codes is found in the next section.

3.5 Comparison and Impact of Unit Cell Solutions

The purpose of this chapter is to compare and contrast results from the previous 3 codes ran on the X-10 unit cell. This analysis should provide a forensic measure for calculations resulting from each of these code systems. The MCNP and Scale

calculations both used Monte Carlo (MC) neutron transport while PENTRAN employs deterministic transport. Also, PENTRAN and Scale use multi-group (MG) cross-sections derived from ENDF/B-VI libraries and MCNP uses continuous energy (CE) cross-sections. A 3-group collapse of the cross-sections was performed for PENTRAN unit cell eigenvalue calculation and burnup. While these codes completed the same calculations (i.e. eigenvalue and depletion), there were differences among the code platforms.

3.5.1 Comparison of Eigenvalue Calculations

To best illustrate the similarities and differences between the eigenvalue results of the unit cell, the below table (Table 3.9) was created for each eigenvalue result. The eigenvalues reported below are for the 0.12% carbon content (average for this era). Also noteworthy, the PENTRAN iterative eigenvalue result was used for the comparison.

Table 3.9: Eigenvalue calculation comparisons between code platforms.

Code Employed	Code Notes	Eigenvalue
MCNP	MC/CE	1.09489 ± 0.00016
Scale	MC/MG	1.09977 ± 0.00029
PENTRAN	$P_N = 3$, $S_N = 32$, MG	1.105995 ± 0.000107
PENTRAN	$P_N = 3$, $S_N = 16$, MG	1.095991 ± 0.000001
PENTRAN	$P_N = 3$, $S_N = 6$, MG	1.095491 ± 0.000000
PENTRAN	$P_N = 3$, $S_N = 8$, MG	1.094599 ± 0.000001
PENTRAN	$P_N = 5$, $S_N = 8$, MG	1.091555 ± 0.000010

PENTRAN	$P_N = 5$, $S_N = 12$, MG	1.083289 ± 0.000023
PENTRAN	$P_N = 5$, $S_N = 6$, MG	1.093736 ± 0.000003
PENTRAN	$P_N = 2$, $S_N = 12$, MG	1.064229 ± 0.000054
PENTRAN	$P_N = 3$, $S_N = 16$, MG, Homogenized	1.093874 ± 0.000009
PENTRAN	$P_N = 3$, $S_N = 6$, MG, Homogenized	1.091238 ± 0.000016
PENTRAN	$P_N = 3$, $S_N = 8$, Homogenized	1.091439 ± 0.000010

PENTRAN entries dominate the table in order to determine the best result from the least amount of computational overhead. With respect to the PENTRAN (deterministic transport) homogenized unit cell, the resulting calculations between S_{16} and S_6 quadrature orders yielded a 0.24 percent difference. Computationally running an S_6 calculation requires less overhead and time without the sacrifice of accuracy. Comparing the MCNP eigenvalue result to the PENTRAN heterogenous calculation, the PENTRAN P_3 S_6/S_8 quadratures were the most accurate. With respect to the homogenized deterministic calculations, the P_3 S_{16} eigenvalue was the most accurate. This high quadrature and scattering moment is partially due to the amount of scattering material added to the fuel volume. The greatest effect on the eigenvalue with respect to deterministic calculations was the P_N order. A lower P_2 calculation was performed using an S_{12} quadrature set that yielded an eigenvalue of 1.064229. This value had a 2.8 percent difference when compared with the MCNP continuous energy eigenvalue calculation, but equaled a 3.3 percent difference when compared to Scale eigenvalue. Deterministically, for a heterogeneous calculation on a thermal neutron spectrum the P_N order required is 3 or

higher and the quadrature can be dropped down to S_6 for an accurate representation of the eigenvalue. For a homogenized unit cell, the P_N order is also required to remain high (3 or higher) along with the quadrature (S_{16}). This higher quadrature set is due to the uniform distribution of moderator with the fuel volume.

Comparison of the Monte Carlo transport codes revealed a 0.44 percent difference between the eigenvalue solutions. This difference is attributed to the treatment of the cross-sections in the problem. Scale used the 238 group cross-sections while MCNP uses continuous energy. The problems both tracked and ran the same amount of particles and number of cycles.

3.5.2 Comparison of Burnup/Depletion Calculations between Monte Carlo Transport Codes

Due to the proliferation concerns of special nuclear material, accuracy is required for computational forensic analysis. This section highlights the differences and similarities across the different neutron transport codes.

Plutonium produced within the fuel slug/elements is a great benchmark for the transport code analysis. Figure 3.29 documents the results of the total mass of Pu-239 produced with respect to burnup between the two Monte Carlo transport codes. The main difference between the two codes is the cross-section processing.

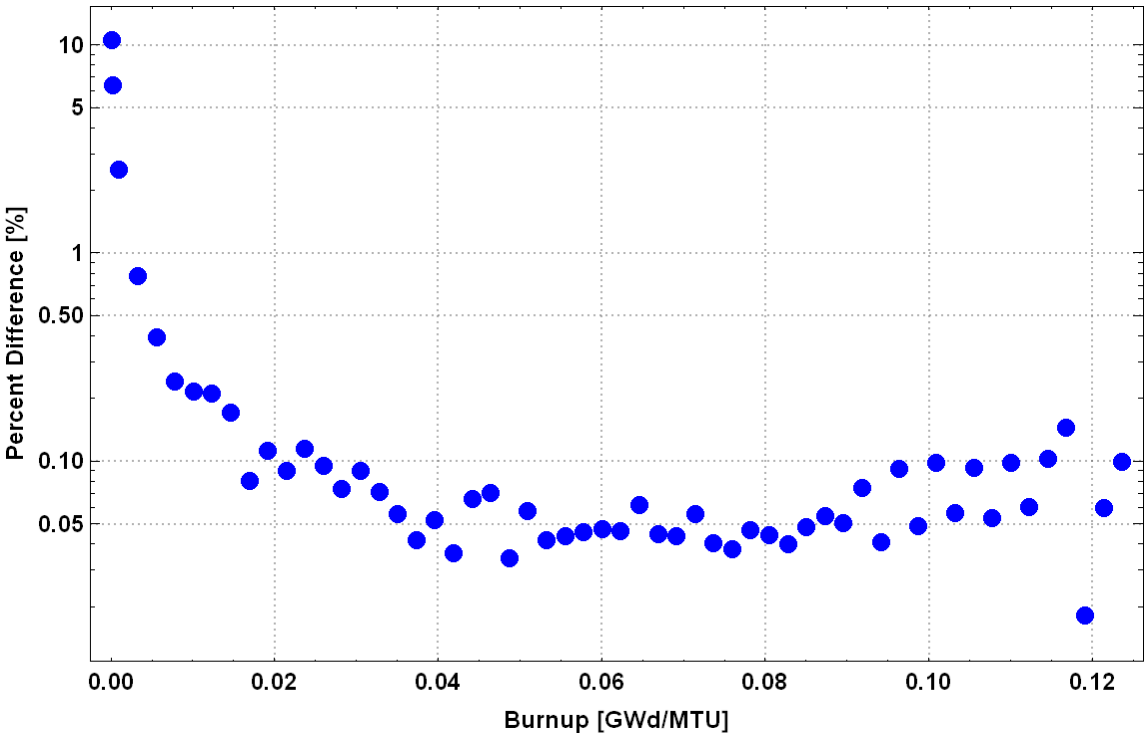

Figure 3.29: Pu-239 mass percent difference between Monte Carlo transport codes (Scale & MCNP).

As shown above, the largest percent difference between the Scale and MNCP code systems were at the beginning of the burnup. The error then dips down to under 1% rather quickly, and oscillates around 0.1%. Cross-section processing differences between the two codes affects the outcome very little after the initial power time period.

Another way to highlight the codes ability for performing depletion is to ratio one of the major fissile constituents to the total mass of the isotopes with the same atomic number. In this case, the Pu-239 plus Pu-241 mass content to total plutonium content was ratioed in order to highlight the differences of depletion calculations with higher mass plutonium species.

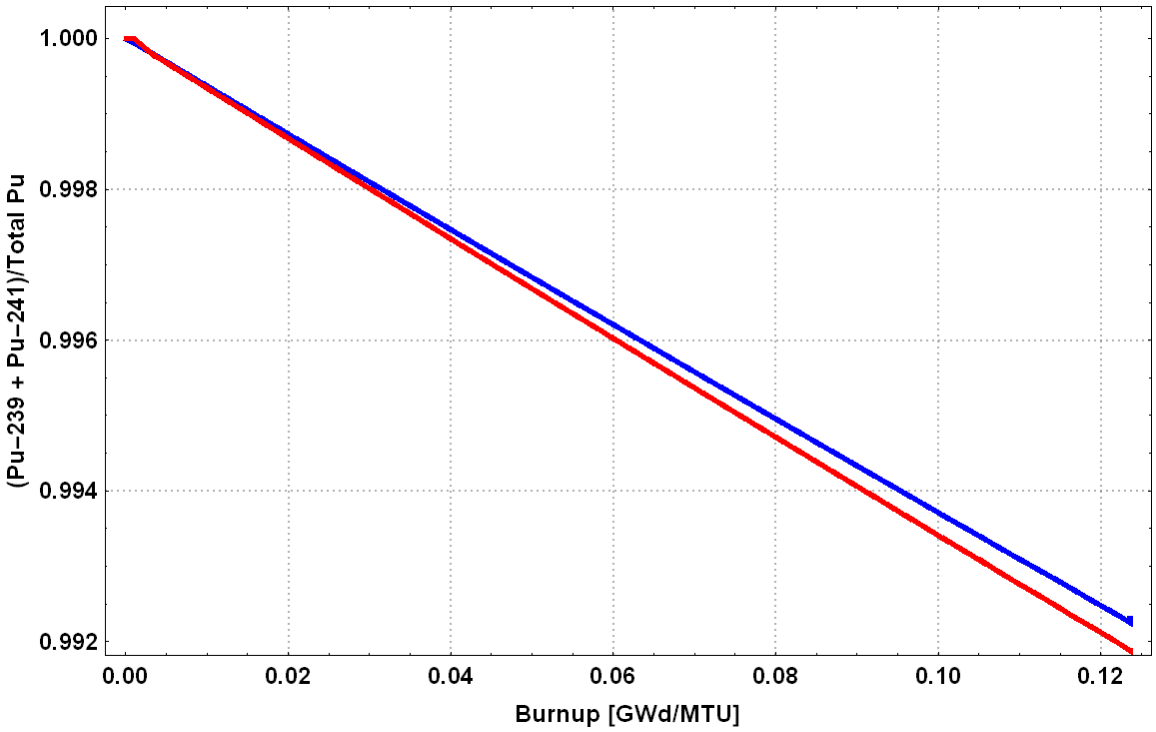

Figure 3.30: Pu-239 + Pu-241 to total plutonium content by mass with respect to burnup. Scale KENO code results are shown in blue and MCNP results are shown in red.

As seen above, at early burnup the Pu-239 + Pu-241/total plutonium ratio is nearly identical across each Monte Carlo code. As burnup progresses and more transmutations are occurring the two code calculations diverge. This divergence is most likely due to the cross-section processing between the two codes. From a nonproliferation perspective, the overestimation of the purity of fissile isotopes produced is far less damaging than underestimating the purity.

For comparison of burnup levels, the NRX design reactor has a higher burnup on the fuel elements. Shown below in figure 3.31 is the Pu-239 plus Pu-241 to total plutonium mass ratio with respect to burnup. The low burnup of the X-10 unit cell and the divergence at higher burnup values is concerning from a nonproliferation standpoint

and different reactor designs (shown below in figure 3.31). Higher burnup reactors are used for fast production of SNM which causes divergence of this ratio between the two Monte Carlo code systems. The percent difference between the final fissile plutonium ratios with respect to burnup shown below is only 0.42% and the percent difference between the two code systems with respect to total plutonium content produced is 0.02%.

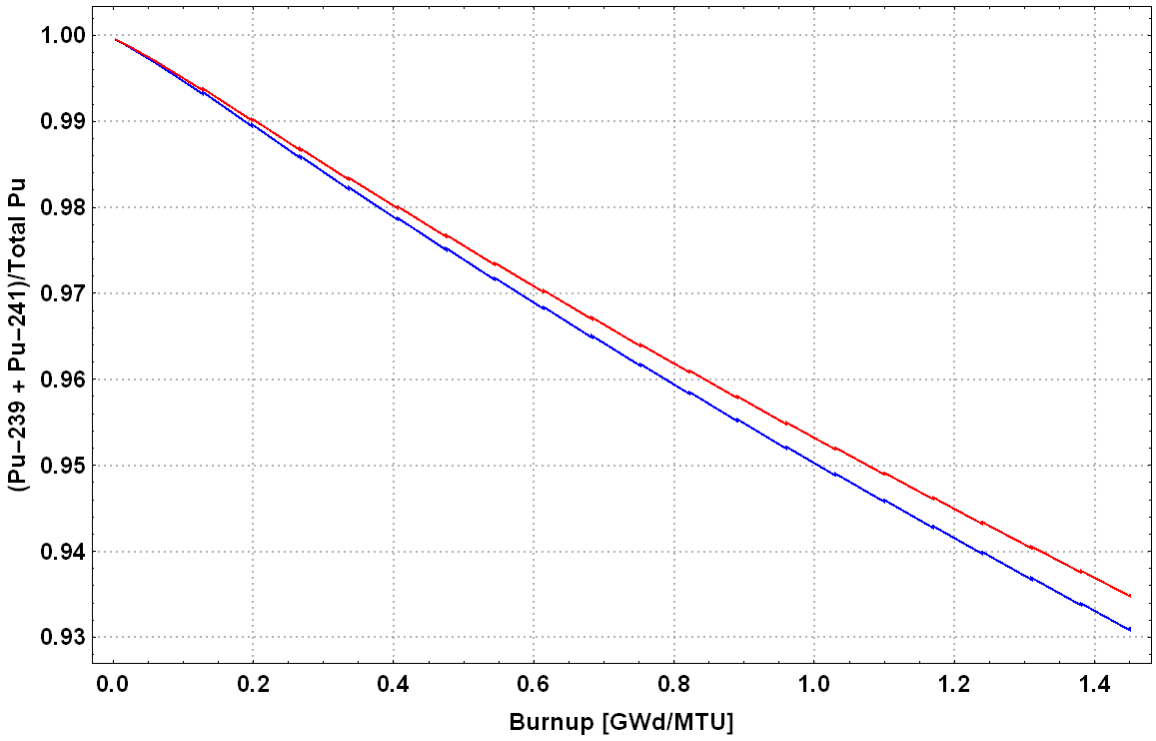

Figure 3.31: (Pu-239 + Pu-241)/Total Pu mass ratio of NRX design reactor with respect to burnup. Scale is shown in blue and MCNP is represented by red.

Over or under-estimating plutonium content within a reactor is ambiguous with respect to nonproliferation. Under-estimating plutonium content would obviously allow unaccountable material to be diverted without knowledge. While over estimating would send a false positive of material diversion when no actual material is missing. The percent differences between these values are small but this represents one pin within the

reactor so this error will be more pronounced across an entire assembly, especially with higher or lower burnup zones within the reactor. The percent difference between the two code systems in respect to amount of plutonium produced is small.

Total fissions within the unit cell using the Cs-137 content (grams and activity) is also a good indicator of burnup and code differences. Again both codes use Monte Carlo transport methods but differ in cross-section processing. This difference was highlighted in the previous Pu-239/total plutonium content. Shown below is the caesium-137 content with respect to burnup.

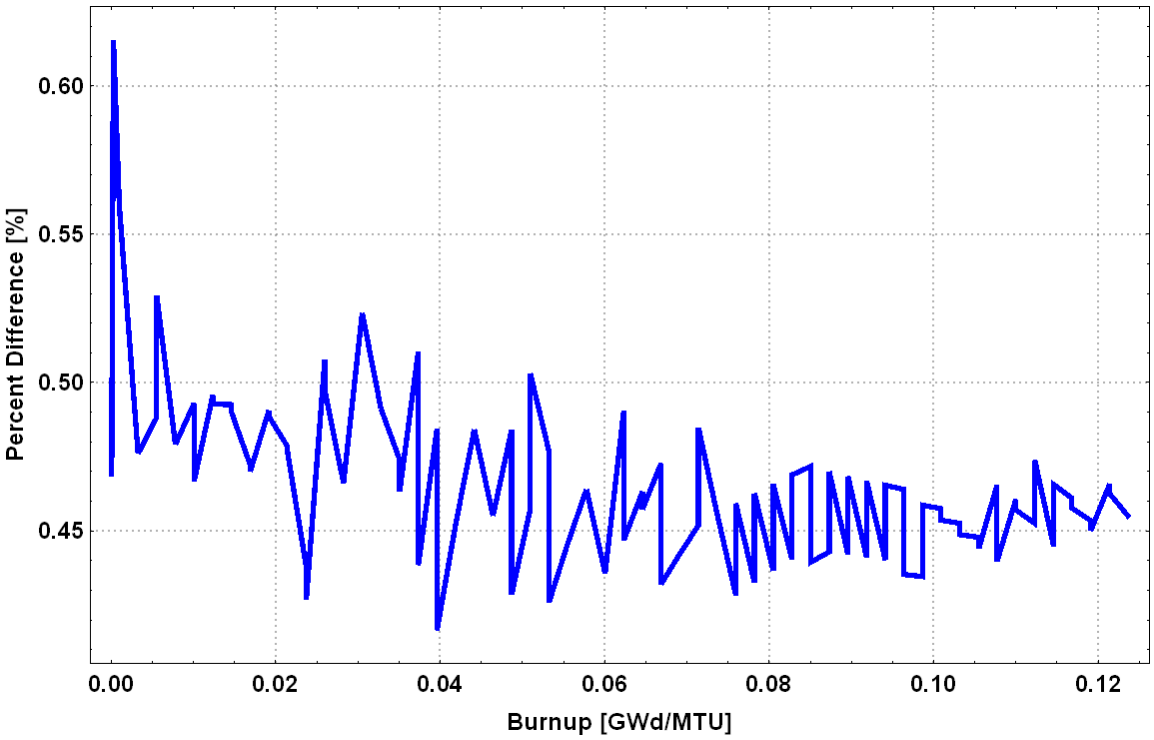

Figure 3.32: Percent difference of Cs-137 mass between Monte Carlo codes.

Above in figure 3.32, the Cs-137 mass difference between the two Monte Carlo transport codes is shown. Between the two codes, the greatest difference in masses was at the

beginning of the burnup. After the power period, the two codes converge to around 0.4%. This low percent difference corresponds to a very close calculation with respect to the total fissions within the unit cell (once the reactor reaches steady state operation) with more expected error on the front end of the burnup.

Shown below in Figure 3.33, is the Ru-106 mass amount with respect to burnup for the two Monte Carlo codes. Again, the beginning of the burnup the masses are almost identical between the two code systems, but towards the end of the burnup the values start to diverge.

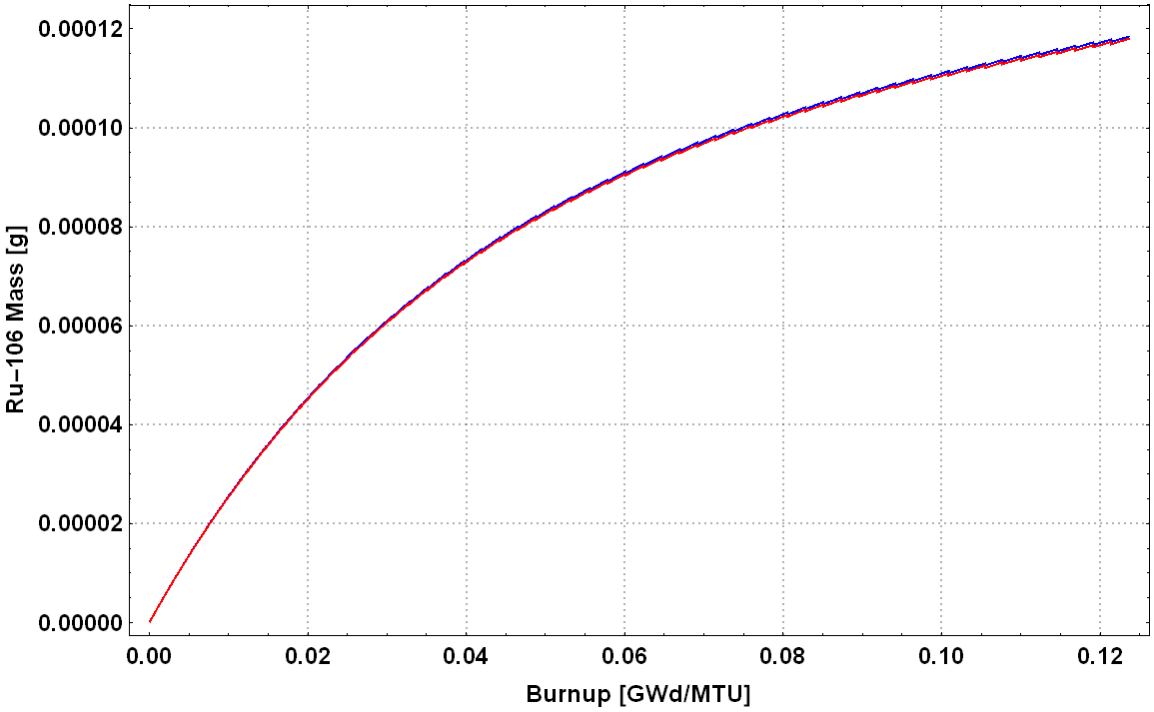

Figure 3.33: Ru-106 mass content with respect to burnup. Scale is shown in blue and MCNP is shown in red.

This ruthenium content demonstrates the amount of Pu-239 fissions within the fuel slug. The code systems simulate plutonium content grow-in similarly according to the Ru-106

content. Further studies are required on higher burnup production reactors such as a Hanford-B or NRX design fission product tracking capabilities. The higher burnup could cause these values to diverge more dramatically.

Shown below in Figure 3.34 is the Ba-138/Total Ba ratio with respect to burnup. Scale is shown in blue and MCNP is shown in red. The ratio is almost identical after the first four burn steps where MCNP predicts the ratio to be 1.0 (corresponds to all barium being in the form of Ba-138) while Scale predicts the ratio to be lower. This initial divergence shows the importance of having a finer granularity at the beginning of fuel burnup but this behavior is expected before the reactor reaches a steady-state operation.

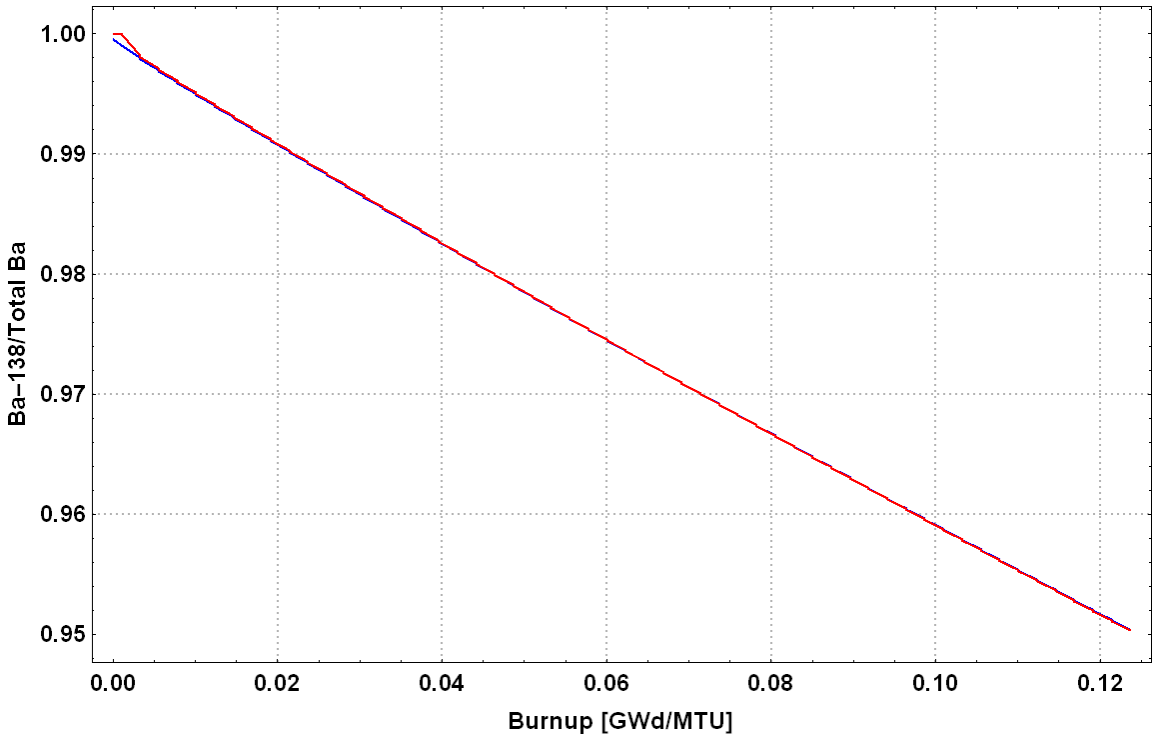

Figure 3.34: Ba-138/Total Ba ratio with respect to burnup. MCNP is shown in red and Scale is shown in blue.

The above relationship shows the two Monte Carlo calculations with respect to total fissions within the fuel slug are nearly identical.

3.5.3 Comparison of Burnup/Depletion Calculations between Monte Carlo and Deterministic Transport Codes

Differences between Monte Carlo transport code systems were highlighted in the previous section. For this study, the Scale code system will be compared to the deterministic transport code PENTRAN/PENBURN. This is due to the overestimation of plutonium purity Scale provided which is ideal from a nonproliferation standpoint. Fission product predictions between the two Monte Carlo codes were in very close proximity to one another. It is notable, that cross-sections used for PENBURN and Scale were derived from ENDF/B-VI libraries.

A good metric of burnup comparisons is the total Pu-239 mass produced after the burnup of the fuel slug. Shown below in Figure 3.35 is the total mass of Pu-239 with respect to burnup.

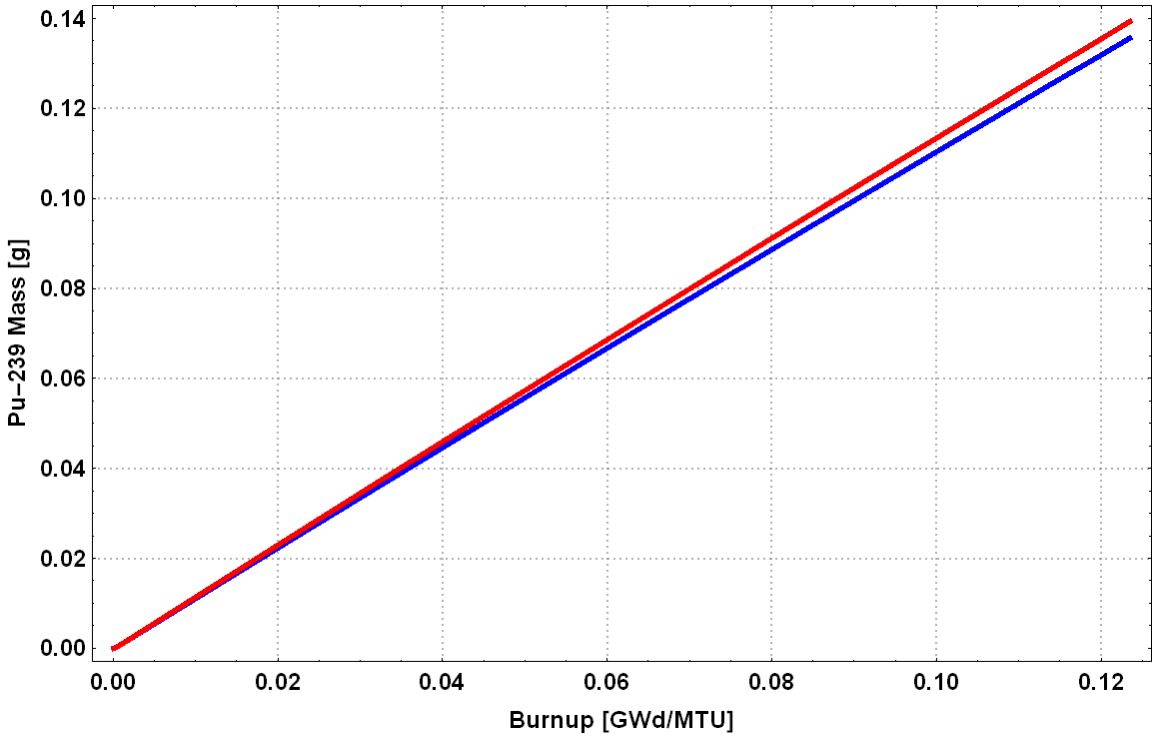

Figure 3.35: Total mass of Pu-239 after complete burnup. PENBURN is shown in red and Scale is represented by blue.

The above plot indicates the deterministic code predicts a higher production mass of Pu-239 than the Scale Monte Carlo code. At the end of life (last burn step), the percent difference in Pu-239 production is 2.68%. This percent difference highlights the dissimilarities in the calculations and the sensitivity to the methods employed.

Rather than examining the production of one fissile isotope, the higher mass Pu-241 is another good metric for burnup comparisons between deterministic and Monte Carlo transport codes. The below figure demonstrates this relationship.

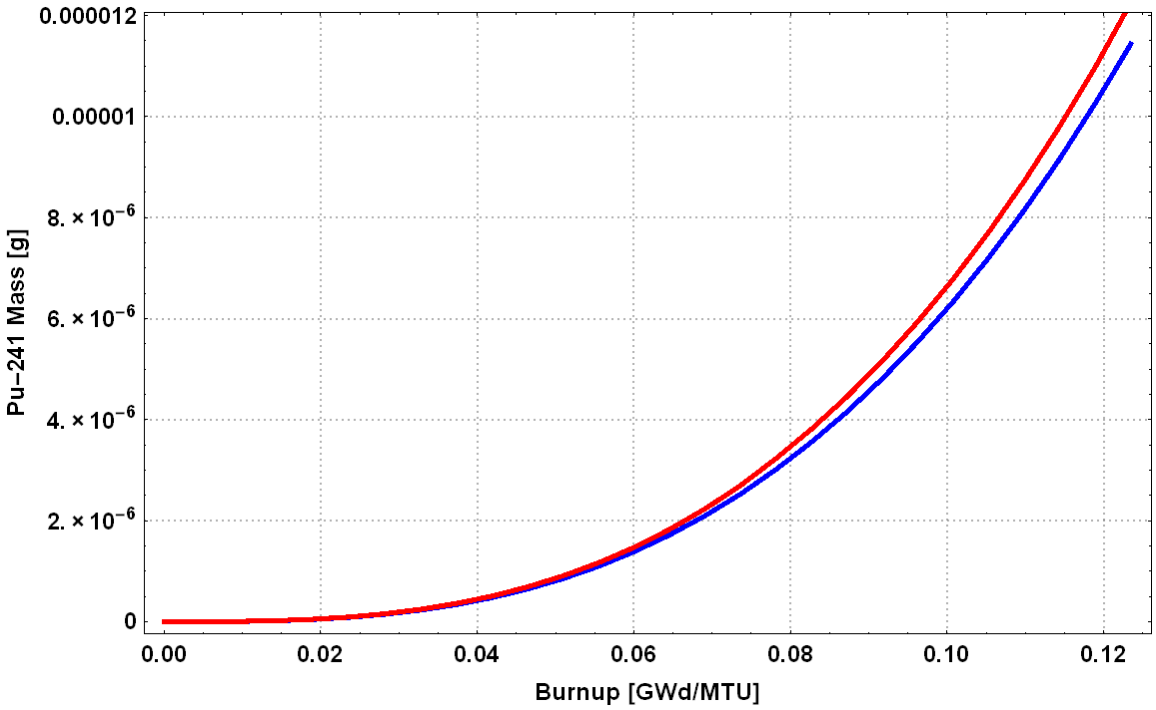

Figure 3.36: Pu-241 mass appreciable to burnup. PENBURN represented by red and Scale represented by blue.

The above plot shows the two codes were fairly consistent in early life of the reactor but start to diverge as burnup increases. Pu-241 content after the last burn step showed a 6.87% difference between deterministic and Monte Carlo transport codes. This high percent difference in fissile isotope production is concerning due to the small nature of the unit cell burnup problem. Some of this difference is also attributable to the difference in heavy metal mass between the two problems. Deterministic transport discretizes the spatial components which can lead to over or under representation of the volume of heavy metal. In this situation, a very fine meshing of the unit cell was completed which resulted in a volume of 61.90086 cm^3. The scale volume was set at 62.29256 cm^3. This represents a 0.63079 percent difference between the volumes. This small amount of

difference between the volumes of the heavy metal would still leave the deterministic case with a slightly higher Pu-241 mass prediction.

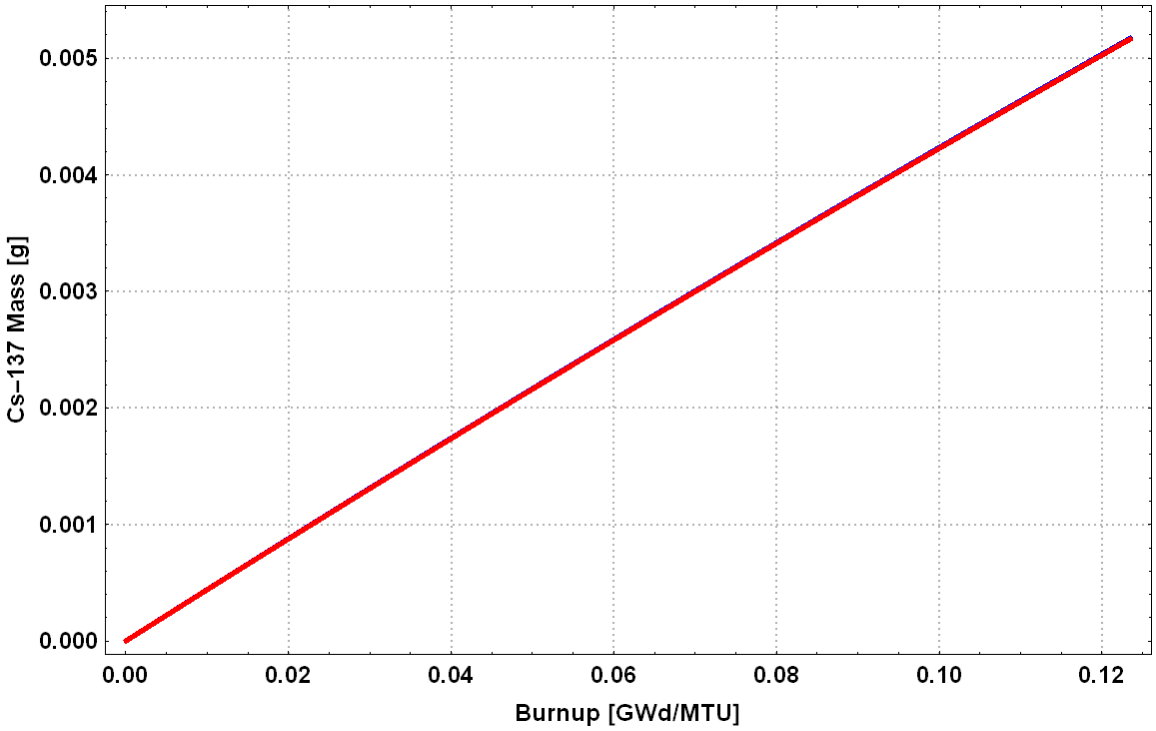

Figure 3.37: Cs-137 mass with respect to burnup. PENBURN is shown in red while Scale is shown in blue.

The above plot represents the Cs-137 mass ascribed to burnup. The two code systems have nearly identical Cs-137 mass content across burnup. This isotope is a good indicator of total fissions within the system and is shown to be consistent across differing transport methods.

Another fission product of interest is Ce-140. This radioisotope has a close cumulative yield across all isotopes of interest within a fuel slug.

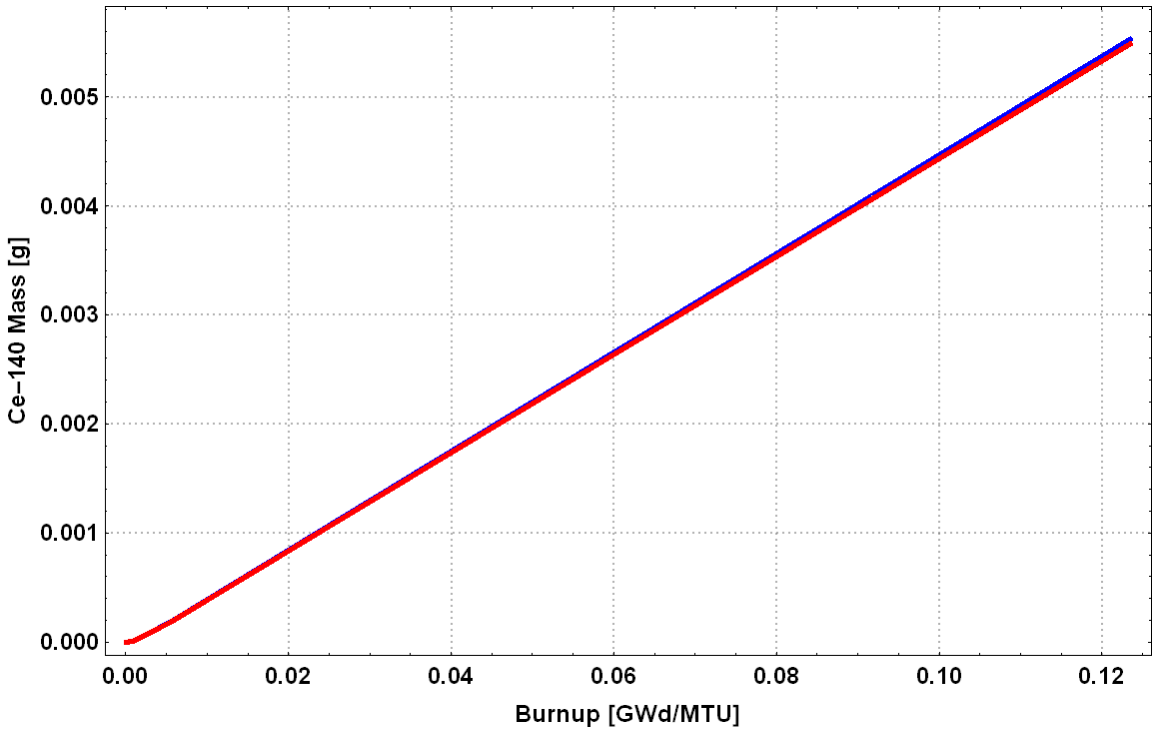

Figure 3.38: Ce-140 mass across burnup period. PENBURN is shown in red and Scale is shown in blue.

The values represented above are nearly identical across the period of burnup and represent total fissions within the system fairly well. Ce-140 is also a stable isotope and can be measured through destructive analysis at any point without loss of the isotope.

In conclusion of unit cell burnup comparisons, Monte Carlo codes performed very closely to one another apropos fission product predictions and actinide production and destruction but heavier isotope fissile production ratios diverged as the burnup progressed. It is noteworthy, that the two Monte Carlo codes yielded a 0.02% difference in total plutonium production with respect to the NRX design higher burnup model. The comparison between PENBURN and Scale code systems provided a glimpse into the differences between deterministic and Monte Carlo transport methods. Each of the codes

used cross-sections derived from the same libraries but differed on neutron transport methods. The Monte Carlo based code predicted Pu-239 content at the end of life to within 2.68% of the deterministic code while the Pu-241 mass content at the end of life was within 6.87%. Part of the difference in actinide masses can be credited to the difference in the spatially discretized heavy metal volume for the deterministic calculation and the static Monte Carlo volume. The lower reported masses of the actinides produced within the fuel slug by Monte Carlo transport should be investigated further.

CHAPTER 4

X-10 EIGHTH-CORE SIMULATION AND IMPACT ON FORENSIC ANALYSIS

Unit cell analyses have proven to be a good starting metric for full reactor core studies. The argument for completing unit cell analyses prior to full-reactor core examination is simply problem size. Beginning a forensic study by running lengthy full-core simulations is unreasonable due to lack of focus on specific markers or signatures. Targeting these signatures by running relatively hasty unit cell calculations is more reasonable before scaling up to actual problem size. Expanding to a full-reactor core simulation can also prove to be a slow process. Symmetry within a reactor-core can provide a shortcut to gaining full-core insight while running a problem that is truncated considerably. The X-10 reactor full-core analysis has been cut in half axially and by a quarter in x and y directions. This eighth core analysis is attributable to the symmetry by the fuel loading in the x, y and z-directions. Inspection of this eighth core simulation can also provide the flux/power distribution across the core. The power distribution could later be used in unit cell analysis by scaling the burnup slug by slug (if enough granularity is provided in the analysis).

4.1 Eighth-Core Parameters

As previously mentioned, full-core analysis are tedious, lengthy, and most importantly, unnecessary. Determining symmetry within a problem provides a means to

greatly reducing calculation times. X-10 reactor is symmetrical in x, y and z coordinates. For this reason, an eighth-core model was appropriate for modeling this reactor problem.

Full-core dimensions for X-10 are 24 feet in x and y and 24 feet 4 inches in z-direction. The eighth-core dimensions measure 12 feet in x and y and 12 feet 2 inches in the z-direction. Shown below in Figure 4.1 is the full-reactor core model and loading scheme for 1948.

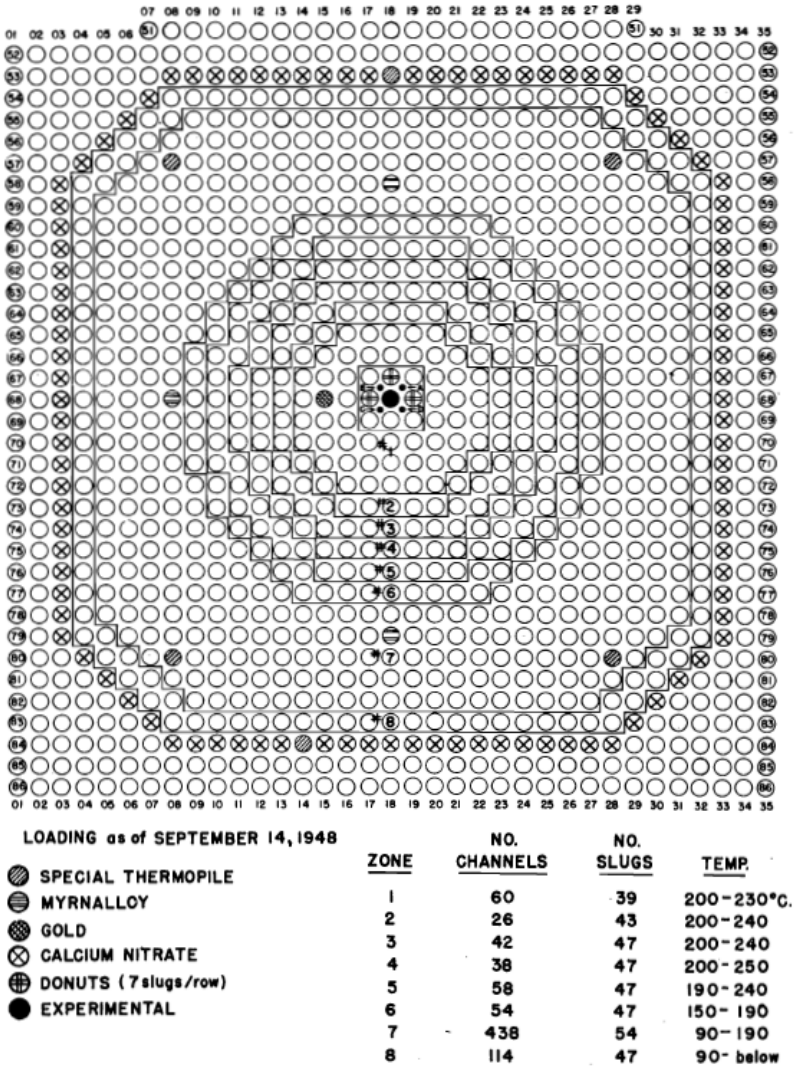

Figure 4.1: X-10 fuel slug loading scheme as of September 14, 1948.[19]

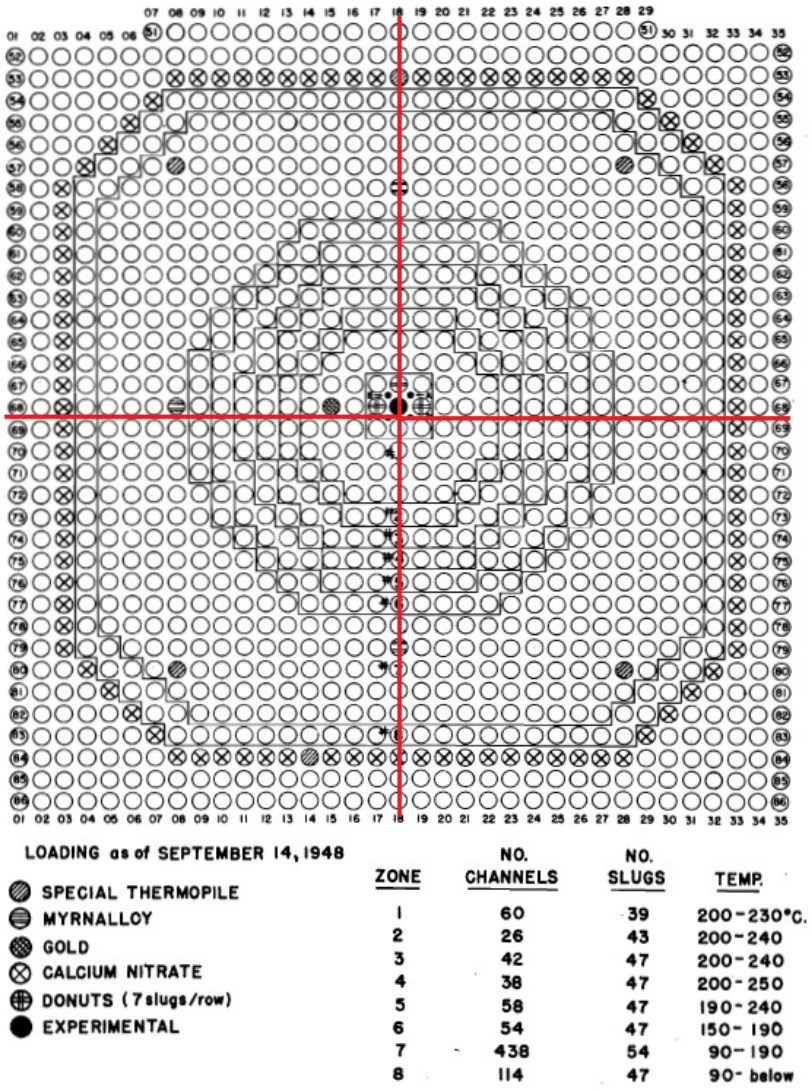

Figure 4.2: Division of X-10 reactor. Red line indicates true quarter-core slicing for total isotopics across zones.

Loading of the natural uranium fuel was completed by following the above 1948 loading scheme but cutting the calculated length of fuel in half axially. Also, temperature values were varied from zone to zone but not axially due to the small variation in temperature across the core and the outlet temperature of the air being slightly hotter than the inlet temperature. Modeling of the control-rods was also neglected due to the reactor sitting

barely above critical for the eighth-core eigenvalue calculation. The many experiment holes and shim rod penetrations into the graphite core was also ignored. For the depletion calculations, slugs near the periphery were burned in the reactor for a period of around 5 years. This length of time was used for all channels in the reactor, while in reality slugs were pushed through at differing times throughout the history of the reactor due to malfunctions in the aluminum jackets that surrounded the uranium metal and higher burnup near the middle of the core.

4.2 Scale Simulation

Scale's TRITON T6-DEPL module was used for the isotopic analysis along with KENO-VI geometry. KENO-VI module utilizes Monte Carlo neutron transport using 500 generations and 10,000 particles per generation were run (with 200 generations skipped). Boundary conditions were vacuum in the positive-x, negative-y and positive-z and mirror reflected for the negative-x, positive-y and negative-z directions. The analyzed channels in the core are shown in Figure 4.3 below. These channels were selected due to the location in the core. The fuel within the channels were then sliced by 10.32 cm to represent one slug of natural uranium and to highlight the isotopics at different locations in the interior of the core. The quarter-core figure below shows the channels that were analyzed in more depth (axial evolution of flux and isotopics). This section mainly highlights major plutonium isotopics across each zone (1-8).

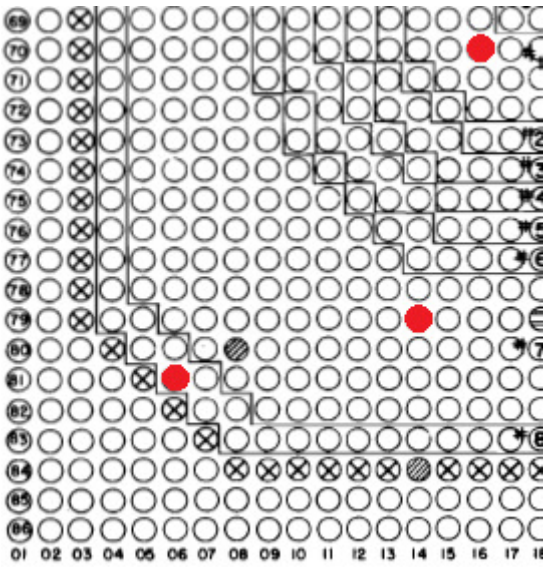

Figure 4.3: Quarter slice of X-10 reactor with highlighted channel simulations.

4.2.1 Scale Eigenvalue Calculation

For the eighth-core eigenvalue calculation 10,000 particles were started in each unit across the core and 500 generations were completed with 200 initial skipped. Shown below in Figure 4.4 is the average k-effective by the number of generations run. This k-effective plot is at the very beginning of life of the reactor.

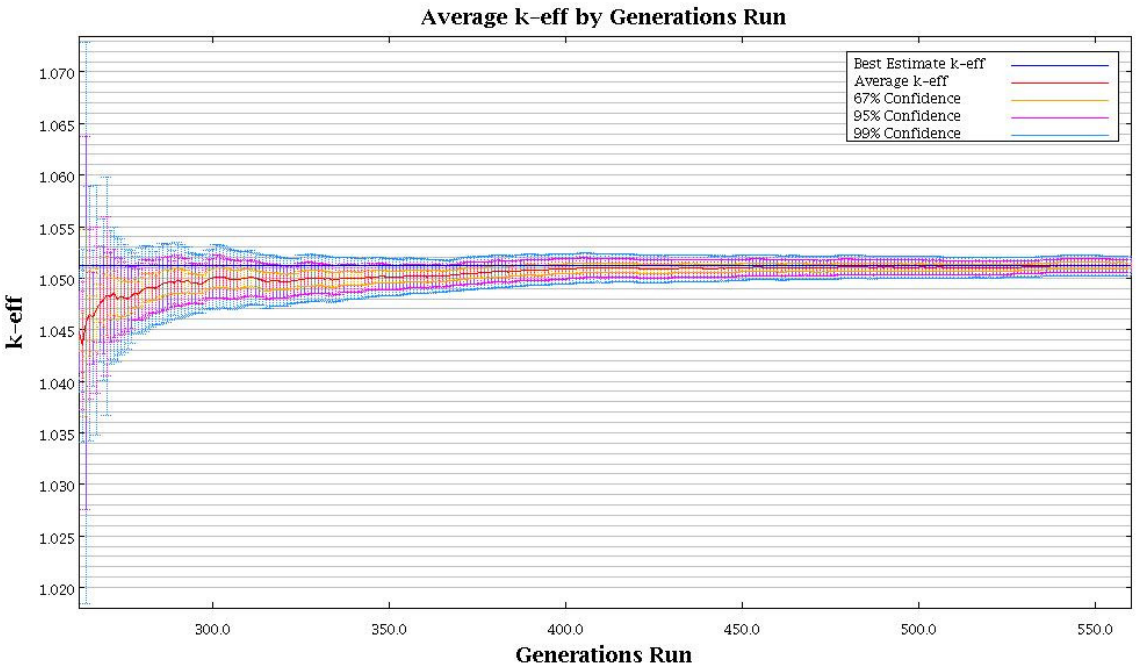

Figure 4.4: Average k-effective value by the number of generations run at the beginning of reactor operation.

Figure 4.5: Average k-effective value by the number of generations run at 380 days (steady state).

Figure 4.6: Average k-effective value by the number of generation run at end of reactor period.

The above k-effective plots (figures 4.4-6) demonstrate the behavior of the multiplication factor as burnup progresses. In Figure 4.4 the beginning of life for the reactor has an average k-effective value of 1.05126 ± 0.00030. Figure 4.5 shows the reactor multiplication factor after 380 days of operation which gives a value of 1.04813 ± 0.00030. While for the end of life for the reactor operational period, the multiplication value falls to 1.04798 ± 0.00028. The end of life for this reactor is considered around 5 years. This low percent difference (0.3125%) in the eigenvalue solution from the

beginning to the end of life demonstrates the extreme low burnup of the reactor and justifies burning the fuel for the entirety of the 5 years without shuffling.

4.2.2 Scale Flux/Power Distribution

Eighth-core calculations provide great data on operating conditions and how these conditions change over time. The flux distribution within the core plays a vital role in gathering isotopics across the fuel slugs. As the burnup increases the flux distribution changes as the core is breeding in other fissile isotopes and burning them away. The flux distribution also changes as fission fragment poisons are produced as these heavier isotopes fission. The three channels highlighted above in Figure 4.3 flux distributions are shown below in Figure 4.7.

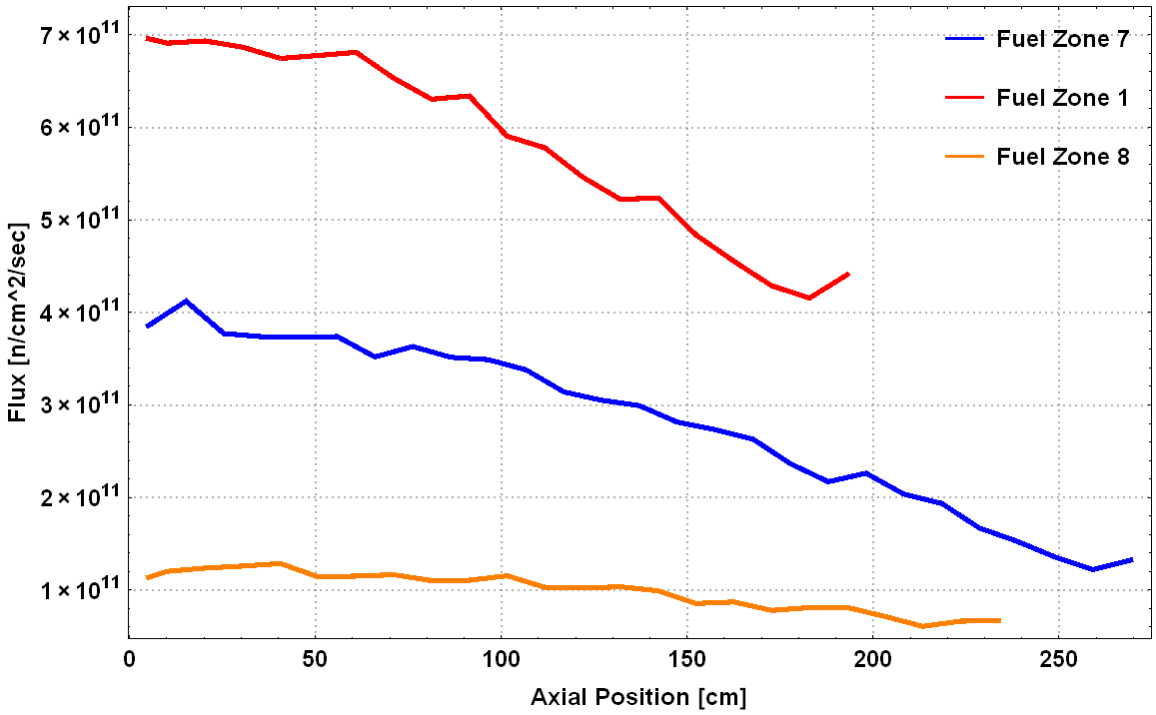

Figure 4.7: Flux distribution related to axial position at 3.5 MW.

Figure 4.7 shows typical flux behavior, each flux profile in the channel demonstrates a varying cosine function related to axial flux shape. The highest flux is in the center of the core and falls off compared to the outer fuel channel which has a flatter profile. This is due to the fuel loading of the modeled channels. Fuel loading in zones 1 and 2 are shorter axially with respect to fuel length compared to the outer channels. Shorter fuel length causes the buckling to be higher which causes the relative larger drop off in flux. The flatter flux profile on the outer channels will affect the isotopics with respect to burnup. Comparatively, a PWR's flux profile will drop many orders of magnitude while X-10's profile drops less than an order of magnitude. The relative flat flux profile across the core reveals the intention of the reactor which is meant for breeding purer plutonium for weapons use rather than for commercial power.

4.2.3 Scale Zone 7 Channel Burnup Analysis

The purpose of this section is to highlight the axial isotopic composition and characteristics of a specific channel. Focus on this channel will further aid benchmarking with respect to neutron transport codes if dissolution of slugs from this channel is accomplished (original intent of this study). The full inventory is decayed and presented in the output file of the Scale calculation. For the purpose of this study, isotopic characteristics are presented while the reactor was in operation. The burnup inventory was tracked on a per slug basis as total isotopics would be quantified with dissolution of the slug as a whole.

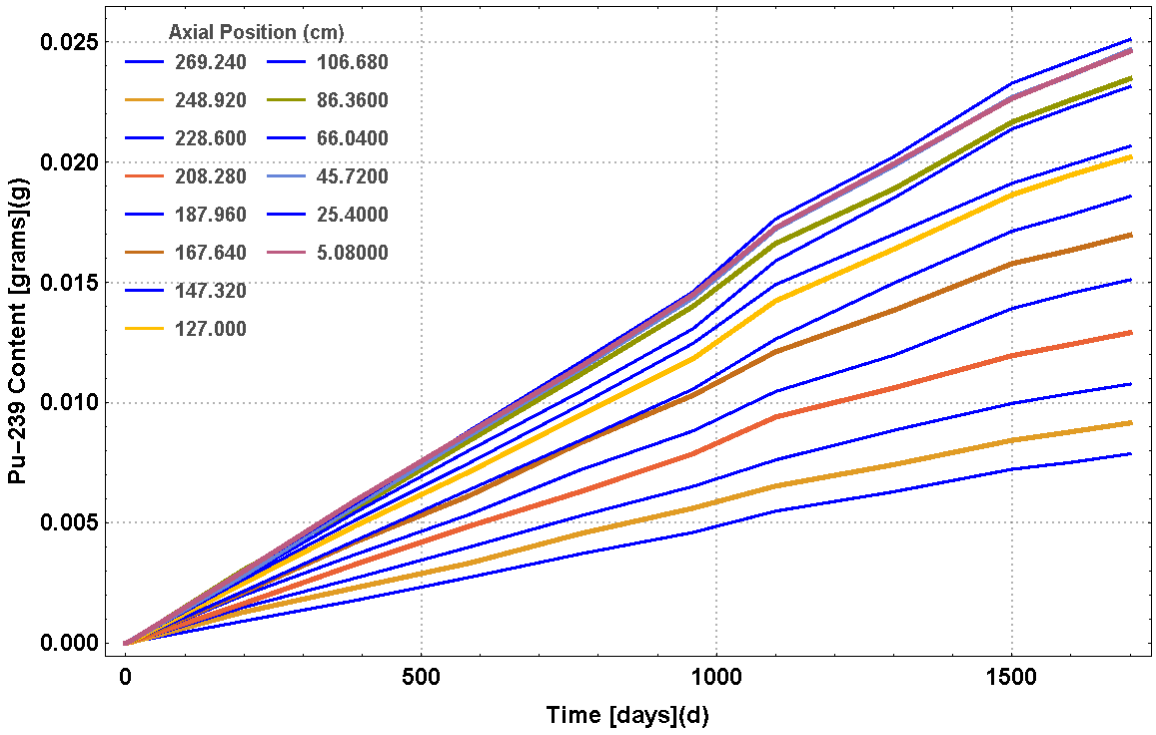

Figure 4.8: Pu-239 content in grams related to axial position from Scale 6.1 KENO/TRITON modules.

The above graph shows Pu-239 content with respect to axial position. It is noteworthy that these axial positions are the center of a respective slug. This also represents every other slug along the channel of interest as to not distort the presentation of the data. The slug at position 5.08 cm has a lower Pu-239 quantity when compared with the slug two positions away (outward). This change or higher plutonium quantity represents the peak power profile not being centered exactly at the middle of the reactor primarily caused by the uneven fuel loading of the pile. Plutonium production is more pronounced towards the center of the pile.

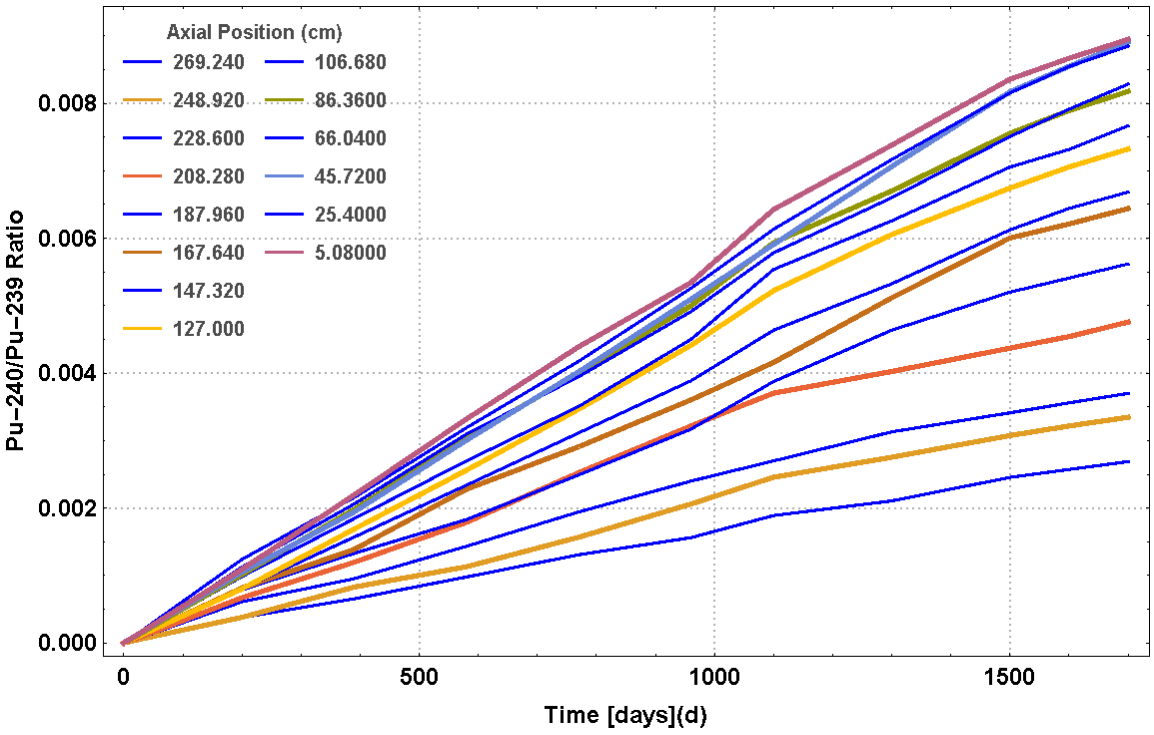

Figure 4.9: Pu-240/239 ratio related to axial position in channel of interest

Pu-240/239 ratio essentially is a metric of plutonium quality. The purity of plutonium is examined closer for 1000 days on and for the materials closer to the centerline of the reactor in Figure 4.10 below. The slug at position 25.40 centimeters from the centerline exhibits “normal” behavior until around 1400 days into the burnup cycle when the slug positioned at 45.72 centimeters becomes less pure. This behavior can be attributed to the oscillatory nature of the flux and burnup inventories.

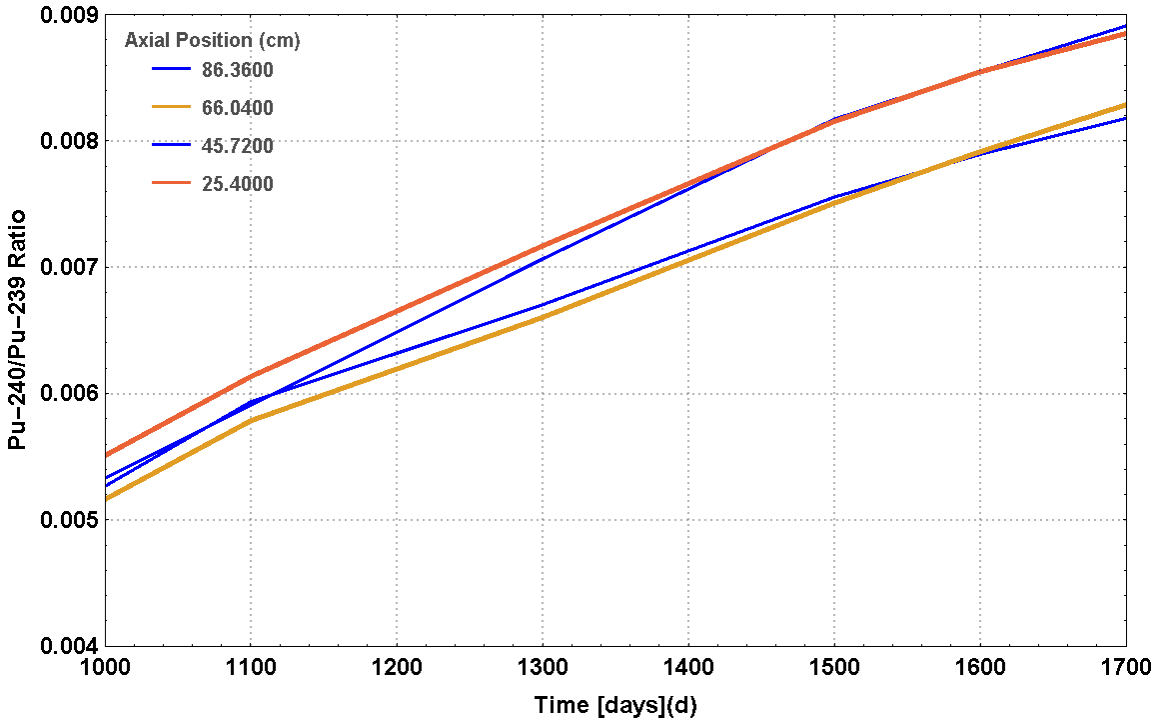

Figure 4.10: Pu-240/239 ratio for materials near centerline of reactor.

Examining the above change in purity of plutonium the slugs positioned at 86.36 and 45.72 cm axially are converged until approximately 1100 days where the two purities diverge. The slug positioned at 45.72 cm decreases in plutonium purity that eventually overtakes the slug positioned at 25.40 cm. Slugs positioned at 86.36 cm and 45.72 cm display odd behavior between approximately 390 days and 1100 days. The slug at 86.36

cm has lower plutonium purity between these times than the slug positioned at 45.72 cm. These two quantities diverge after the 1100 day mark and resemble normal axial behavior with respect to plutonium purity. This oscillatory behavior during this time period is a result of numeric rounding within the code system or the reactor system not reaching steady state behavior before 1100 days. This behavior can also be seen in Figure 4.11 as the materials start exhibiting expected neutronic behavior with plutonium purity.

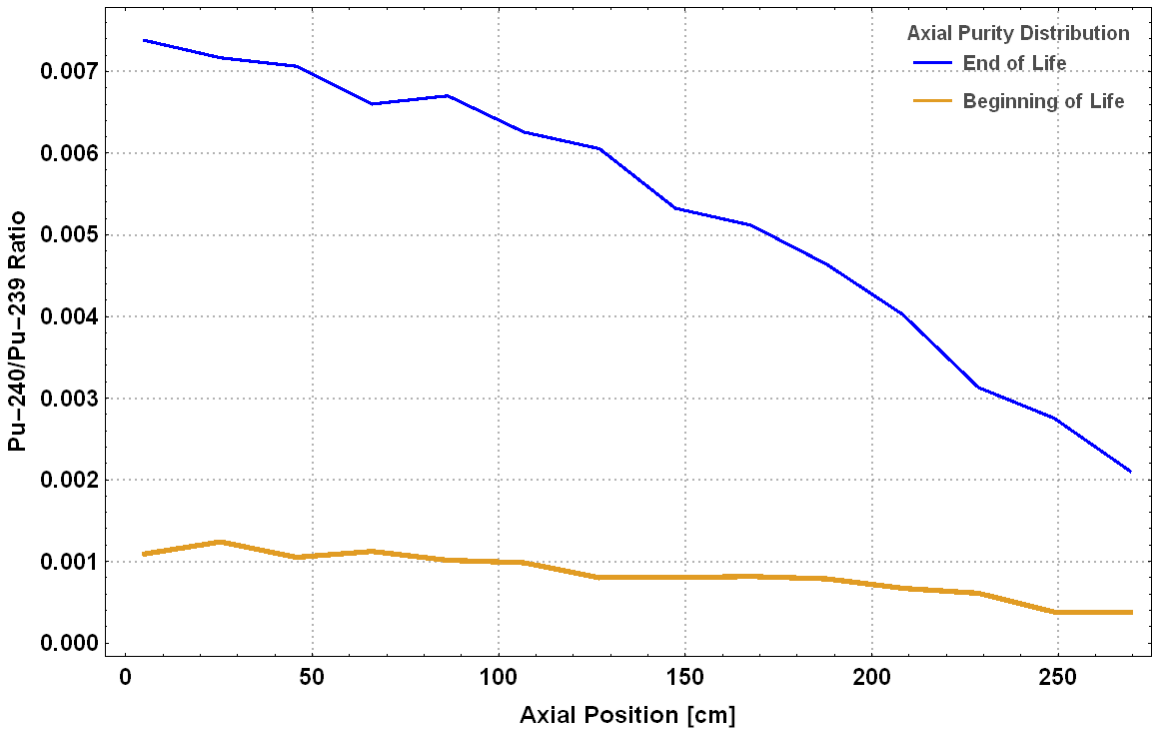

Figure 4.11: Axial Pu-240/Pu-239 ratio distribution.

Figure 4.11 displays the axial distribution of the plutonium purity at approximately 200 days and 1300 days. The beginning of life (BOL) plutonium purity is nearly constant while the end of life (EOL) distribution has a more drastic change. Although the EOL purity change is more severe than the BOL, the purity is still considered ivory grade

plutonium. For the centerline slug, the increase of the Pu-240/Pu-239 ratio is around 460% while the outermost slug ratio increases 576%.

X-10 is a low burnup reactor even by Manhattan Project era reactor standards. Using the 238 fine neutron energy group structure, group 204 represents the average neutron energy causing fission within the reactor. This average group number changes very little over the course of burnup. Group 204 has an energy range of 0.400 to 0.450 eV. This energy range represents a high absorption to fission ratio of the X-10 reactor and a softer spectrum comparatively.

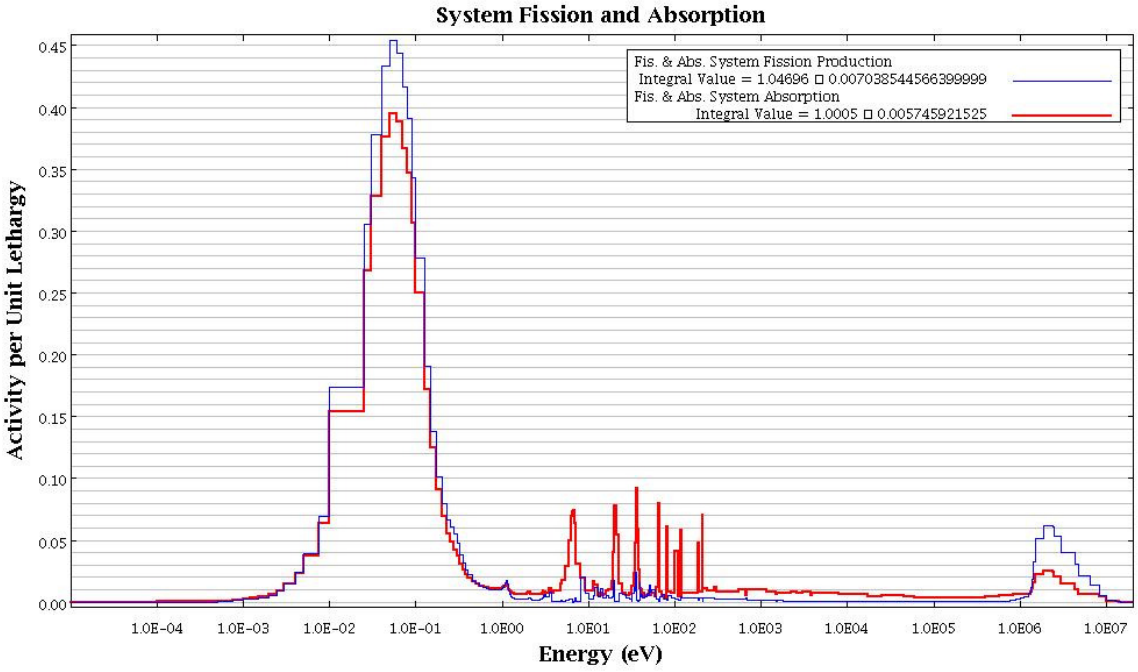

Figure 4.12: Neutron fission and absorption spectrum for system at steady state 1300 days.

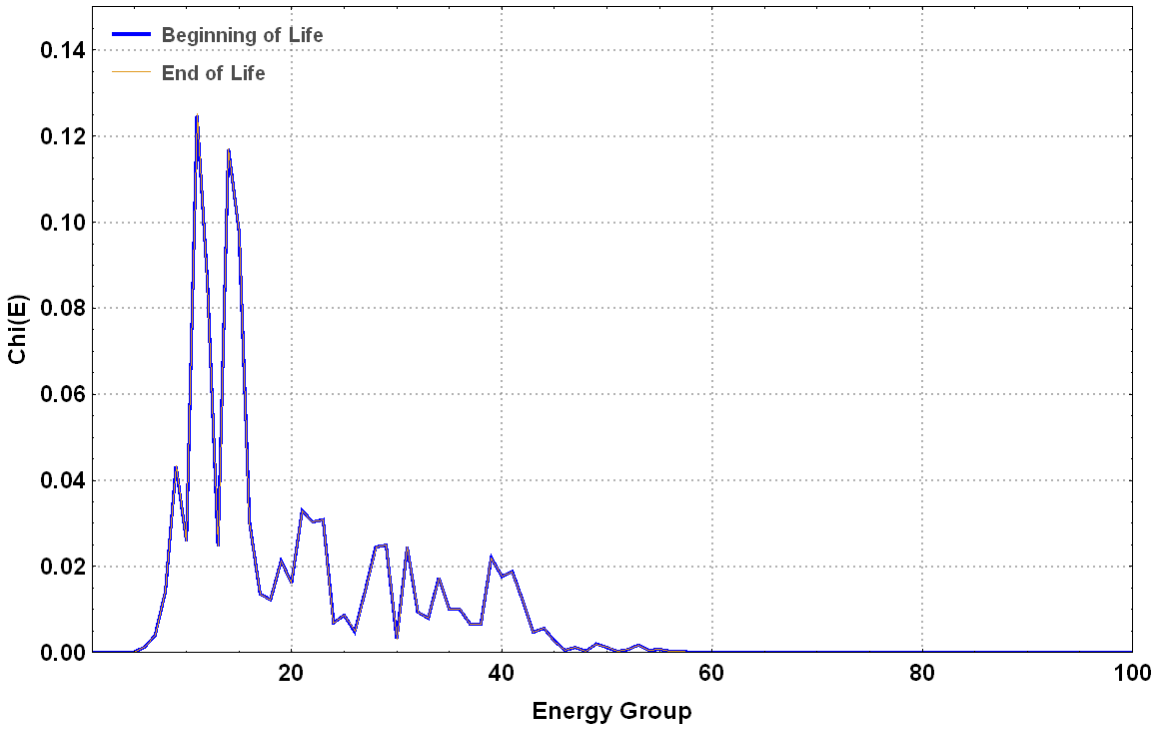

Figure 4.13: Chi distribution for X-10 reactor at BOL and EOL (238 neutron energy group structure used).

Correspondingly, the energy of the average lethargy causing fission within the reactor was 0.1755 eV. These low energy ranges of fission are due to the high capture to fission ratio of U-235 and Pu-239 between 0.1 and 1 eV.[5] Each neutron absorption between these energy ranges is highly likely to result in fission for U-235 and Pu-239. This prime energy range is illustrated in Figures 4.12 and 4.13. It is worth mentioning Figure 4.13 displays beginning and end of life for the reactor which there is almost no change in the Chi distribution.

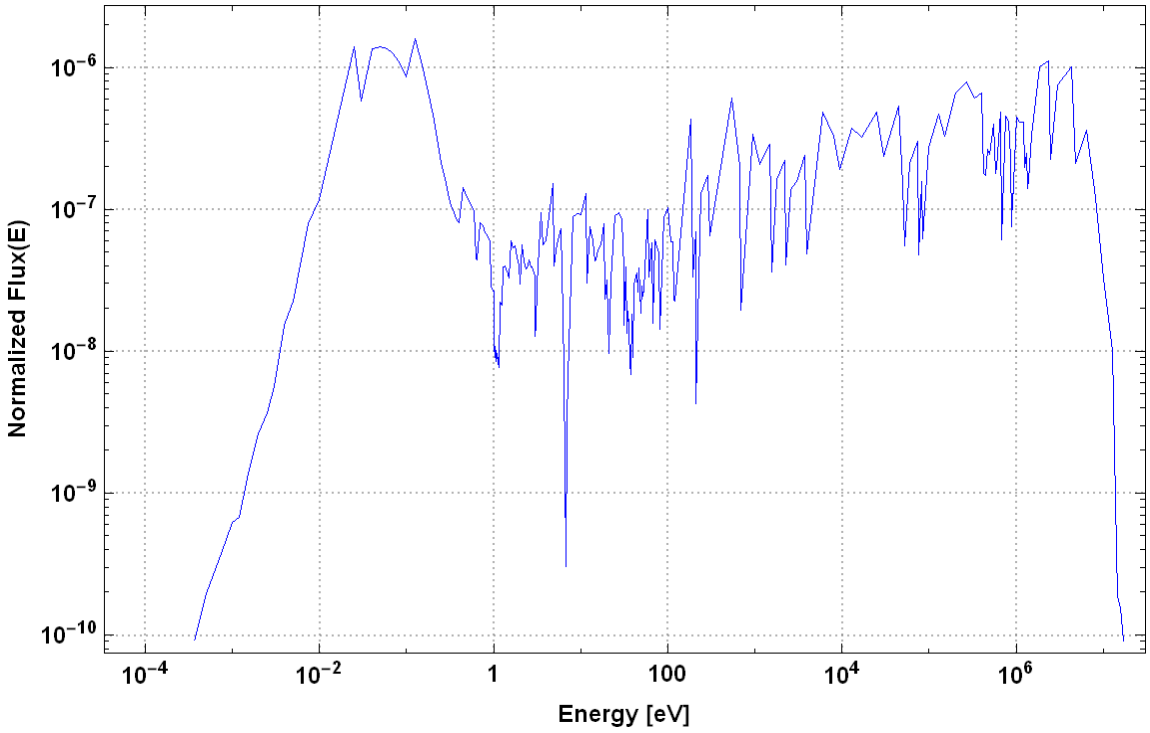

Figure 4.14: Normalized flux of neutron spectrum (log-log plot).

The normalized neutron spectrum shows an almost Maxwellian flux distribution in the thermal neutron energy range. Fast energy groups also show a higher flux but the relative errors in those groups are exceedingly high as with the lower thermal group fluxes (groups 234-238 have greater than a 10% standard deviation).

4.2.4 Scale Eighth-Core Nuclear Data Uncertainty

Newly added in Scale 6.2 beta-3 release, is the ability to perform uncertainty analysis on the nuclear data used for neutronics calculations. These uncertainties can be propagated through burnup calculations using the TRITON and KENO-VI modules. The Sampler module utilizes stochastic uncertainty rather than perturbation methods. Perturbation methods require forward and adjoint calculations to be completed. Sampler

randomly samples the nuclear data PDFs. This is completed for a set amount of "samples." The output distributions are then analyzed for the standard deviations of the responses. Currently, the inputs for the Scale sequences that can be sampled are: multi-group nuclear data, resonance self-shielding data, depletion data (fission product yields and decay data), and model parameters. For the purposes of this study, model parameter uncertainties were not analyzed. This study concentrated on nuclear cross-section and depletion data for the X-10 reactor fuel depletion analysis. Further reading on Scale Sampler module capabilities should be directed to citation at the end of this study.[20] The Sampler module was used to calculate uncertainty in each of the fuel zones found in the X-10 reactor.

Figure 4.15 shows a 2D depiction of the eighth-core modeled. This representation is a quarter slice of the actual reactor in the x and y axes. The quarter-core model is then divided in half due to the fuel length symmetry in the axial direction. Uncertainty analysis was completed on depletion calculations similar to the ones highlighted in previous sections. These uncertainties are calculated/propagated for the entire volume of fuel found in each section (zones 1-8).

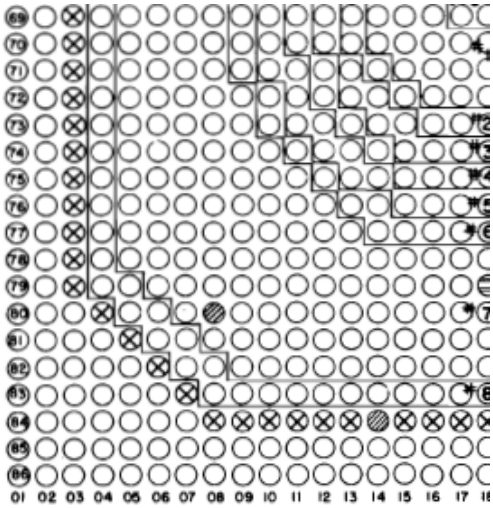

Figure 4.15: Eighth-core model depiction.

Uncertainty in plutonium isotopics has high importance in nuclear forensic or nonproliferation applications.

Most importantly or a high value metric of reactor operation, is total plutonium production. Each zone's plutonium production in the eighth-core model was added up to give total plutonium produced. The uncertainty was also propagated with the plutonium production. Figure 4.16 shows total plutonium production for the ~5 year time period (fuel was not burned constantly—there were 10 hour shutdown periods per week).

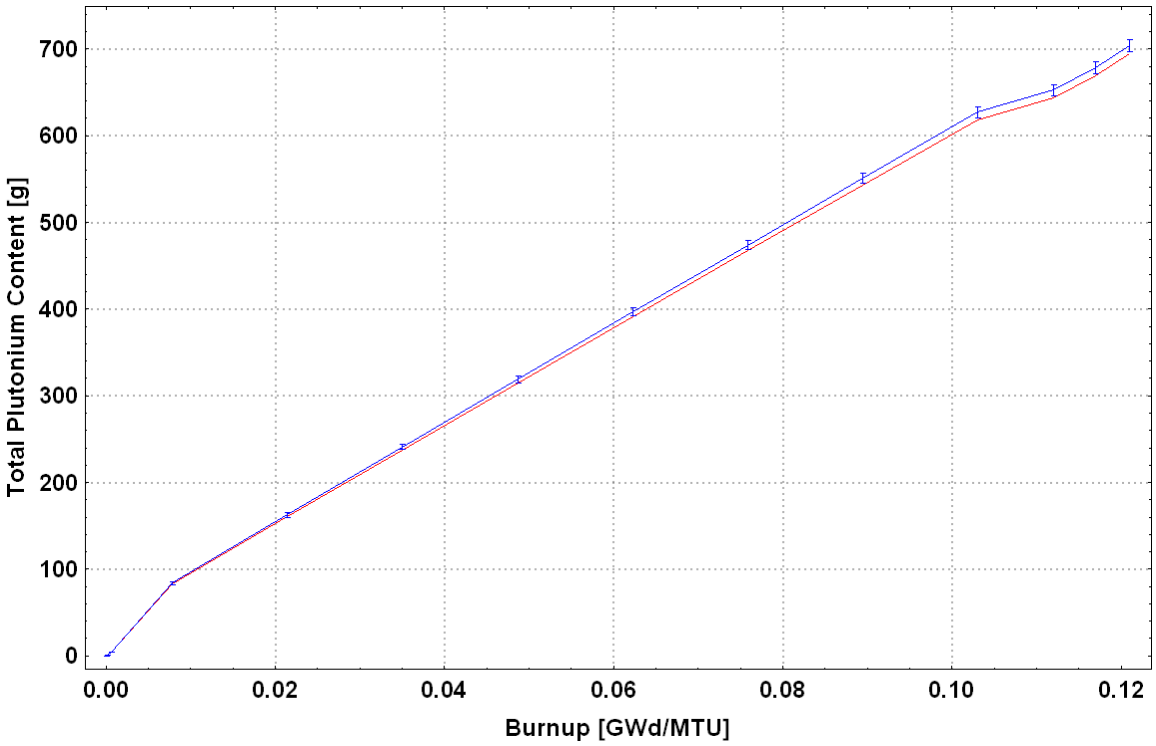

Figure 4.16: Eighth-core total Pu production with nuclear data uncertainty. Scale is shown in blue and MCNP in red.

Shown above is the total plutonium content added across the 8 fuel zones with propagated uncertainties at each burn step. The total eighth-core plutonium production across this burnup history is approximately 7.0340E+02 grams calculated by Scale and 6.9513E+02 calculated by MCNP. These calculated values by the MC codes represent a 1.18% difference. With the nuclear data uncertainty calculation performed by Scale and the flux uncertainty from MCNP these values are not statistically different. With uncertainty considered, this brings full-core production to around 5627.2 grams of plutonium (using Scale calculated value). An open-source quoted total plutonium amount produced between 1943 and 1945 was 326 grams.[21] If a two year burn period is examined the total plutonium production is around 2552.65 grams. Although the quoted

value was “around” 326 grams, the calculated amount was 2552.65 grams which represents if every slug in the reactor was processed and 100% was recovered. If the plutonium was just recovered from zones 1 and 2 (higher burnup zones), the total plutonium production was 405.6 grams across 2 years of burnup. In 1943, the primary means of plutonium separation was bismuth phosphate extraction process. The chemical recovery yield for this process is quoted at 90% which lowers the recovered plutonium from zones 1 and 2 to 365 grams. This amount is also assuming all material from reactor was processed and does not account for slug ruptures.

For potential future studies, only the plutonium isotopics will be reported but all isotopic inventories will be appended to the end of this thesis. Mass spectrometry analysis could be performed to gain “true” plutonium isotopics. One plutonium ratio that offers the opportunity for narrowing down which zone a slug was found in is the Pu-242/Pu-238 ratio.

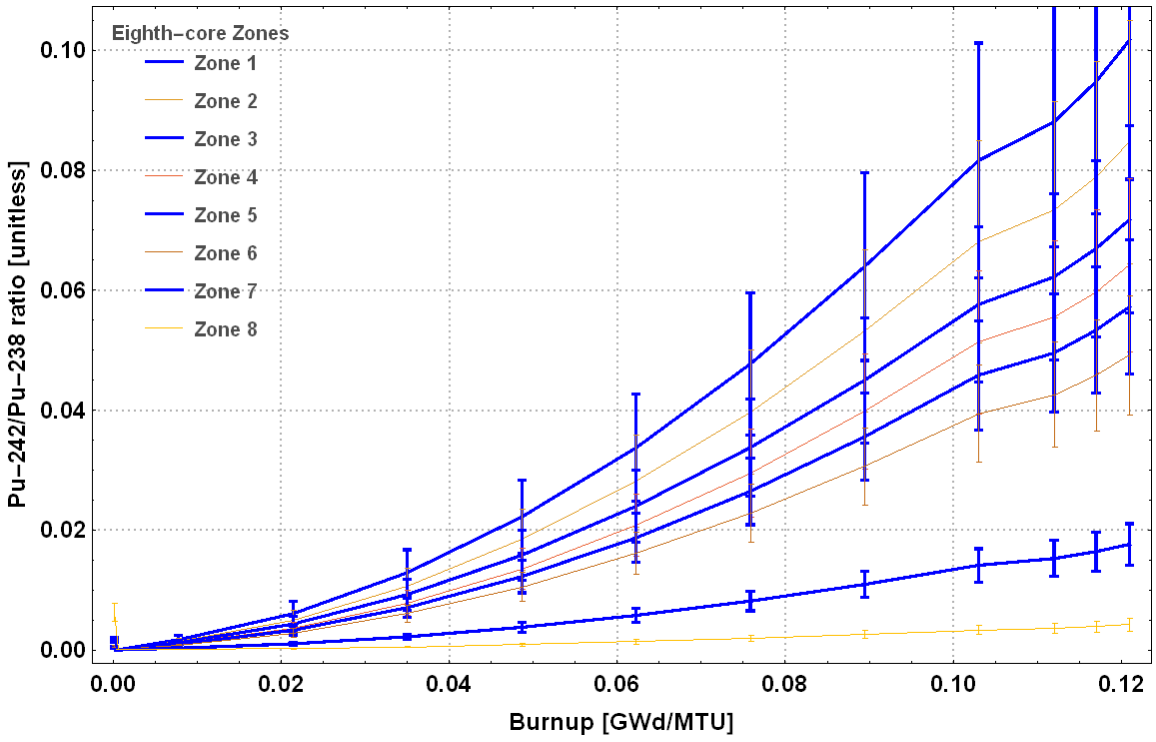

Figure 4.17: Eighth-core Pu-242/Pu-238 ratio according to zone with nuclear data uncertainty.

Figure 4.17 displays the Pu-242/Pu-238 ratio (by zone) evolution across burnup within the eighth-core model. The overlap in the one-sigma error bars for adjacent zones indicate the null hypothesis (ratios are the same value) in this case cannot be rejected. However, zones 7 and 8 are in fact statistically significant to a one-sigma confidence interval. If examined at steady state versus decayed to present day the distinction is clearer.

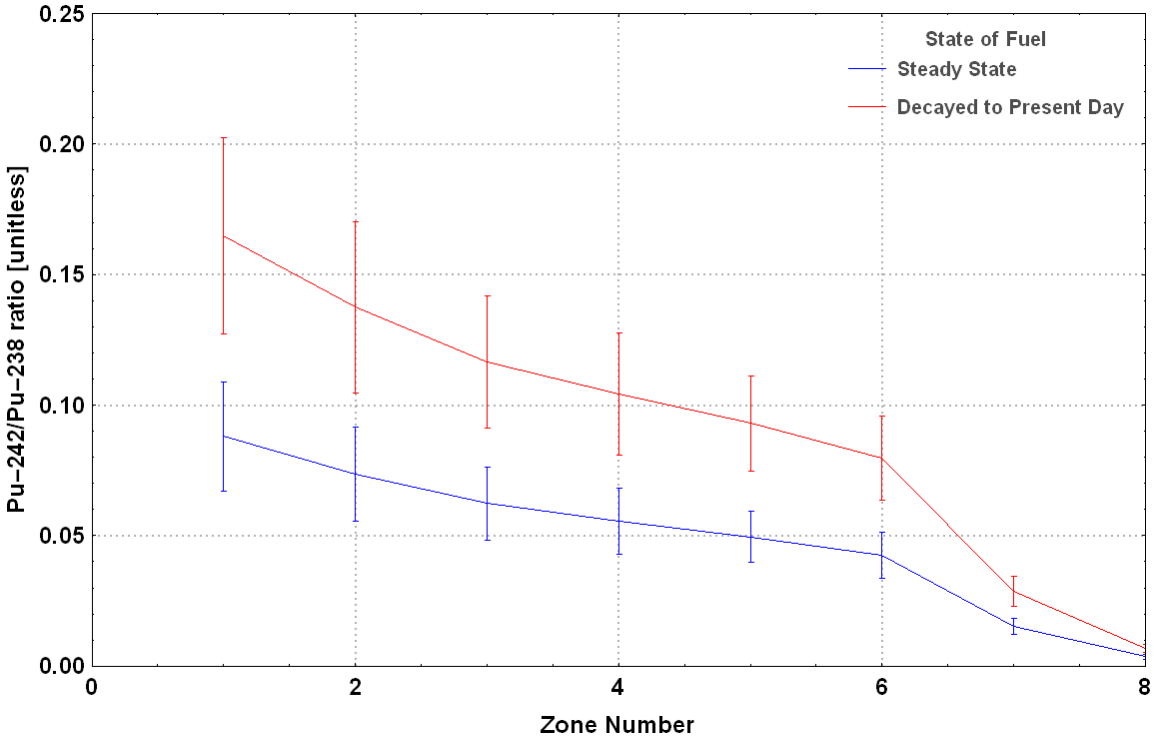

Figure 4.18: Eighth-core Pu-242/Pu-238 ratio related to zone with nuclear data uncertainty.

Figure 4.18 relates zone number and Pu-242/Pu-238 at steady state operation (~1300 days) and decayed to present day. The present day curve would be ideal for mass spectrometry analysis and gives high potential to narrowing down which zone a slug or interdicted material came from for the periphery zones (7 and 8) while the null hypothesis (ratio values are equal) for zones 1-6 cannot be rejected. The R-square fits on the two operation times gave values of 0.960. Linear fits for steady-state operation and decayed are:

y = 0.0964258 - 0.011091(x) and **y = 0.180325 - 0.0207181(x)**, respectively. This ratio offers mass spectrometry results to be optimized due to the higher difference in mass values (242 versus 238). The ratio is also considerably higher than the Pu-242/Pu-240

ratio which is indicative of neutron spectrum. Pu-242 and Pu-238 are both sensitive to neutron spectrum and enrichment, respectively.

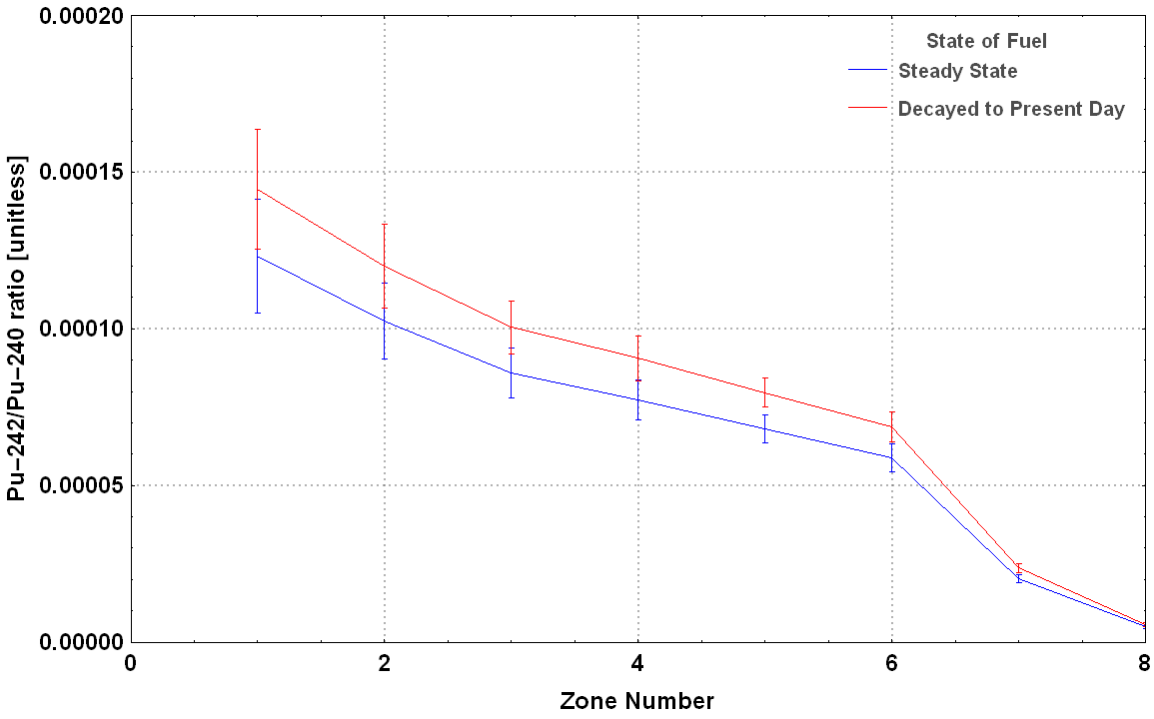

Figure 4.19: Eighth-core Pu-242/Pu-240 ratio related to zone with nuclear data uncertainty.

Comparatively, the Pu-242/Pu-240 ratio at steady state versus decayed to present day has no statistical significance (null hypothesis cannot be rejected) for any zone in the reactor except periphery zones 7 and 8. Only inner core vs. outer core fuel origination could be stated with a 68% confidence interval. This would be a good choice for mass spectrometry analysis if inner-core vs. outer-core origination was desired (from a computational standpoint) because the present day and decayed ratios are statistically similar to a one-sigma confidence. Actual measurements would potentially have lower error bars from counting statistics.

CHAPTER 5

FORENSIC ASSESSMENT OF X-10 SIMULATION RESULTS

Global concerns of non-sanctioned nuclear activities calls for the development and refinement of computational nuclear forensic intelligence (CNFI). Signature development and characterization of nuclear facilities is one important goal of CNFI due to restricted access to materials and inspectors. Characterizing reactors of the Manhattan Project era provides insight into these simplistic reactor designs that are extremely effective in breeding weapons grade plutonium. Providing newly developed uncertainty values in the nuclear data with respect to major actinide isotopics and fission products adds a unique perspective in material characterization and determining the intentions of a particular reactor design.

5.1 Outcomes Based on Assumed Operating Constraints

Full-core computational analysis can be unreasonable even with today's computational power. Time constraints and limited resources require sensible problem simplification, in this case, eighth-core analysis. One major assumption in eighth-core analysis is the symmetric division of the reactor. Previous to any eighth-core analysis, unit cell analysis should be completed as a preliminary step in reporting average isotopics and fluxes. Assumptions for unit cell analysis are more drastic but arguably an acceptable representation of the average flux and isotopics within the full-core. While representing boundary conditions as infinitely reflected seems extreme, the core of the reactor is a

repeated lattice structure. This repetition affords the argument of no net exchange of neutrons between the repeated unit cells. Therefore, unit cell analysis can give a quick answer as to isotopics and neutron spectrum.

Prior eighth-core analysis by Scale indicated an average group of fission of 204 (238 group ENDF/B-VII library for Scale 6.2-beta 3 data). The representative unit cell analysis by Scale also indicated an average group of fission of 204 with a significant drop in computation time. Another comparison is the energy of the average lethargy causing fission. Eighth-core analysis indicated 0.1755 eV while unit cell analysis calculated 0.1678 eV. Comparing the major plutonium isotopics of unit cell analysis vs. eighth-core also highlights the similarities and neutron spectrum "differences." Figure 5.1 is a plot of the Pu-240/Pu-239 ratio output from unit cell analysis and the overall eighth-core calculated value. The addition of nuclear data uncertainty from the Sampler module within the Scale code package adds another much needed metric for CNFI and nuclear reactor physics in general. In Figure 5.1, the one-sigma error bars shown do not overlap which indicate the null hypothesis (ratios are the same) can be rejected at a 68% confidence interval. Unit cell calculated Pu-240/Pu-239 value overestimates purity which is far less critical than underestimating. The percent difference at steady state operation and decayed to present day for the Pu-240/Pu-239 ratio is approximately 17%. This difference should be investigated further between higher burnup reactors of the time.

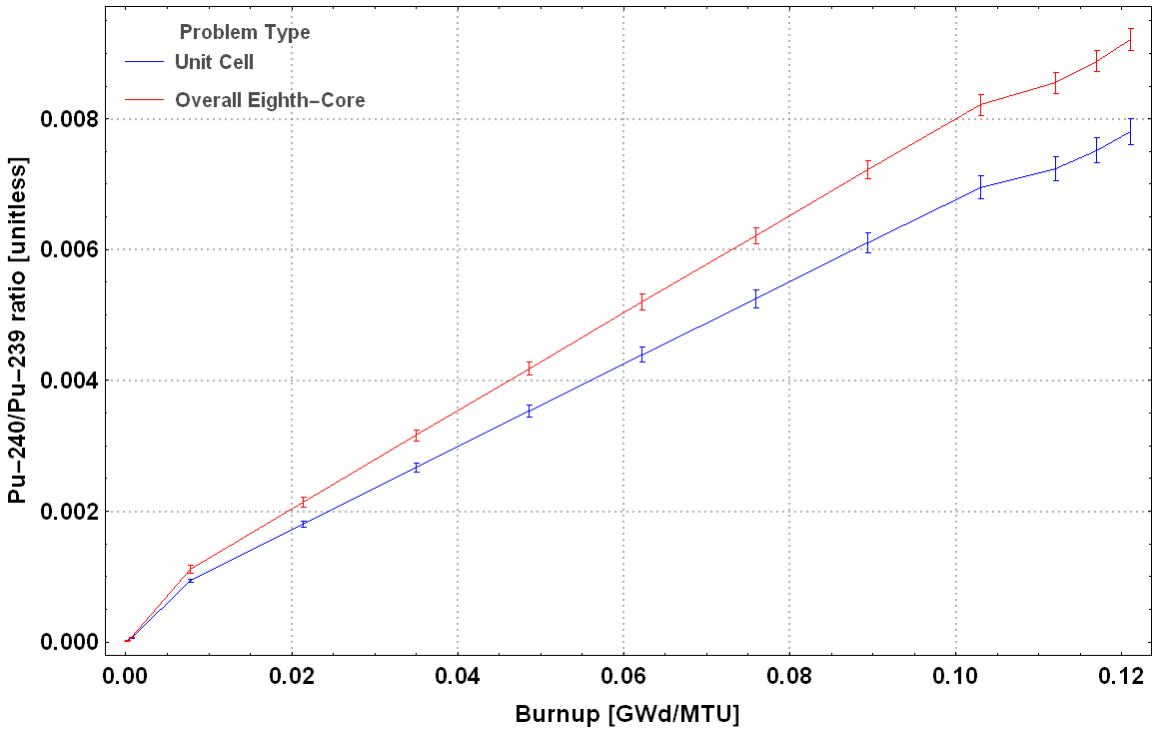

Figure 5.1: Plot of Pu-240/Pu-239 ratio in unit cell and overall eighth-core.

Clear statistical differences in nuclear forensics allows the scientist to determine what data sets can be exploited to highlight operating characteristics (intensions of reactor) and fuel isotopics used for attribution and ultimately deterrence.

Figure 4.7 in the previous chapter highlights the intention of the X-10 reactor. The flux drop axially and outward in the x and y direction of the reactor does not reach an order of magnitude difference. This behavior is a prime example of exploited forensic characteristics highlighting the true intention of the reactor which was to breed high purity weapons grade plutonium. The intelligently designed small change in flux profile in any direction within the reactor serves this purpose. Any larger change in flux profile

would change the isotopics of the fuel to hinder weapon design. The capture to fission ratio deviates from nearly one in the thermal range to lower values with hardening of the neutron spectrum.

5.2 Forensic Evaluation of Burnup Results

Neutronic simulations evaluated in this study highlight the similarities and subtle differences between transport methods and cross section processing. Monte Carlo transport completed with MCNP and Scale burnup results differed slightly if any. Figure 5.2 below illustrates the Pu-240/Pu-239 ratio with respect to burnup.

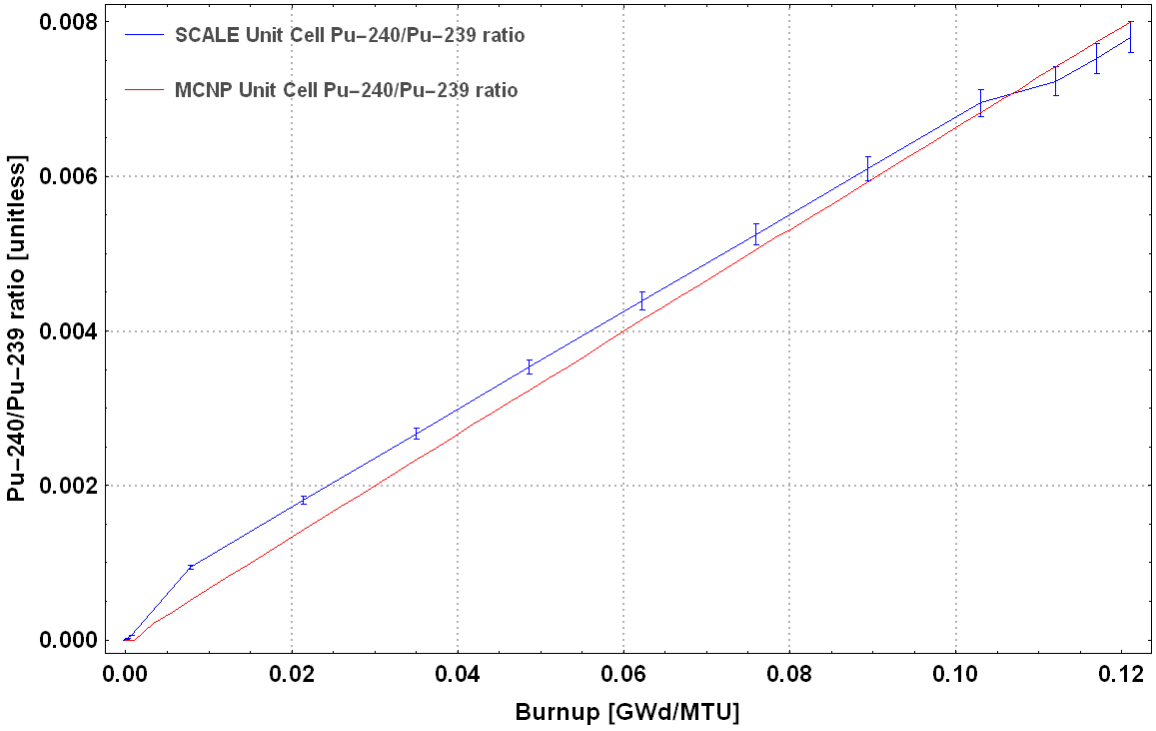

Figure 5.2: Pu-240/Pu-239 ratio progression with burnup using MC codes.

Scale's ability to calculate and propagate nuclear data uncertainty puts this graph into perspective. As the error increases with burnup (mainly attributable to Pu-240

uncertainty), the null hypothesis cannot be rejected due to the overlap of the one-sigma error bars. Therefore, the results between code systems and transport methods are not statistically significant in the unit cell case.

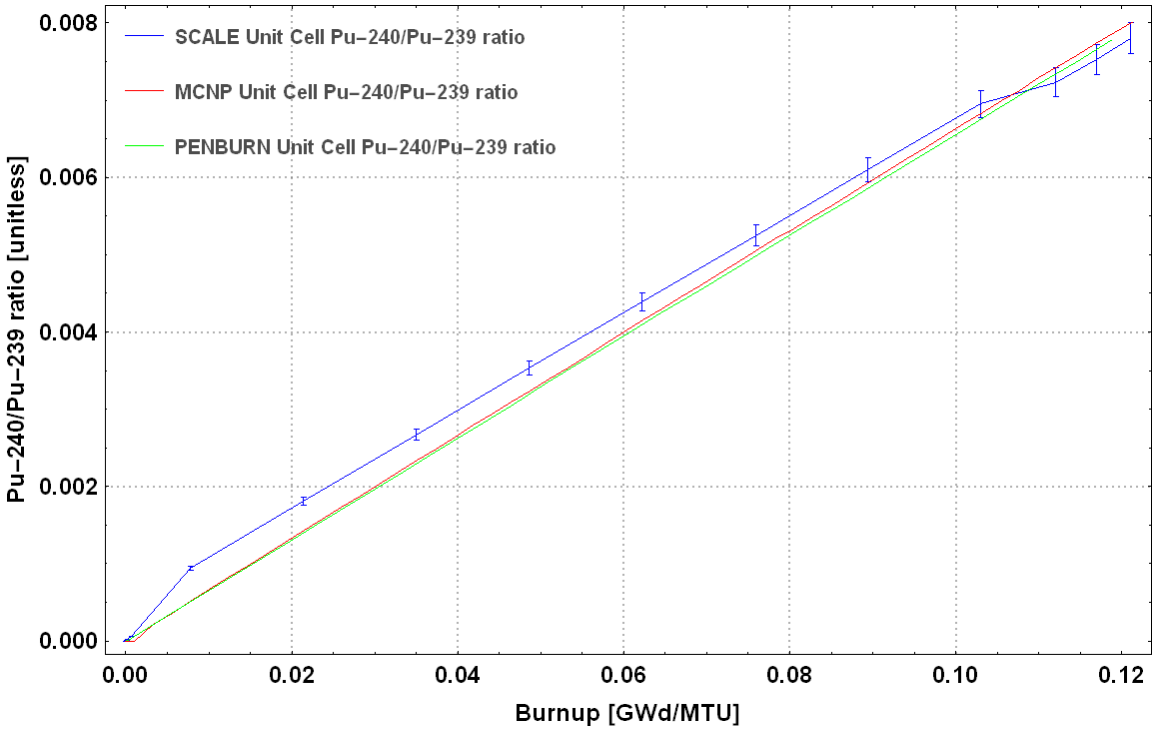

Figure 5.3: Pu-240/Pu-239 ratio comparison with discrete ordinates and MC codes.

In Figure 5.3 above, the three different code packages are plotted with respect to Pu-240/Pu-239 ratio. PENBURN and MCNP values align almost identically as burnup progresses. Scale and PENBURN use the same cross section values (ENDF/B-VI 238 group) and MCNP uses continuous energy cross sections. Again uncertainty in the nuclear data allows the researcher to state no statistical significance between the code systems. It is noteworthy the fissile material volumes were exact across the MC codes and PENTRAN's calculated material volume differed 0.64 %. The addition of flux uncertainty within the transport solution would make these uncertainty bars larger

solidifying the Pu-240/Pu-239 ratio being statistically insignificant across transport methods and code systems on a unit cell basis.

Past ORIGEN 2.2 calculations run on the X-10 fuel slugs state a total burnup after 5 years of 0.142 MWd/kg. This calculation did not take into account the mandatory 10 hour reactor period shutdowns per week, making the total burnup slightly higher. Burnup was completed on 7 of the X-10 slugs with a total Pu-239 gram amount of 1.129. This totals 0.1612 grams per slug produced in the reactor over the 5 years. Scale Pu-239 production value was calculated to be 0.1355 ± 0.00207 grams. These answers were statistically significant to the one-sigma confidence interval mainly because of the higher total burnup employed by BNL.[22]

Comparison of fission product inventory should be completed between transport codes. Figure 5.4 below shows Pd-106 predictive capabilities between all three transport codes with Scale including new nuclear data uncertainty option.

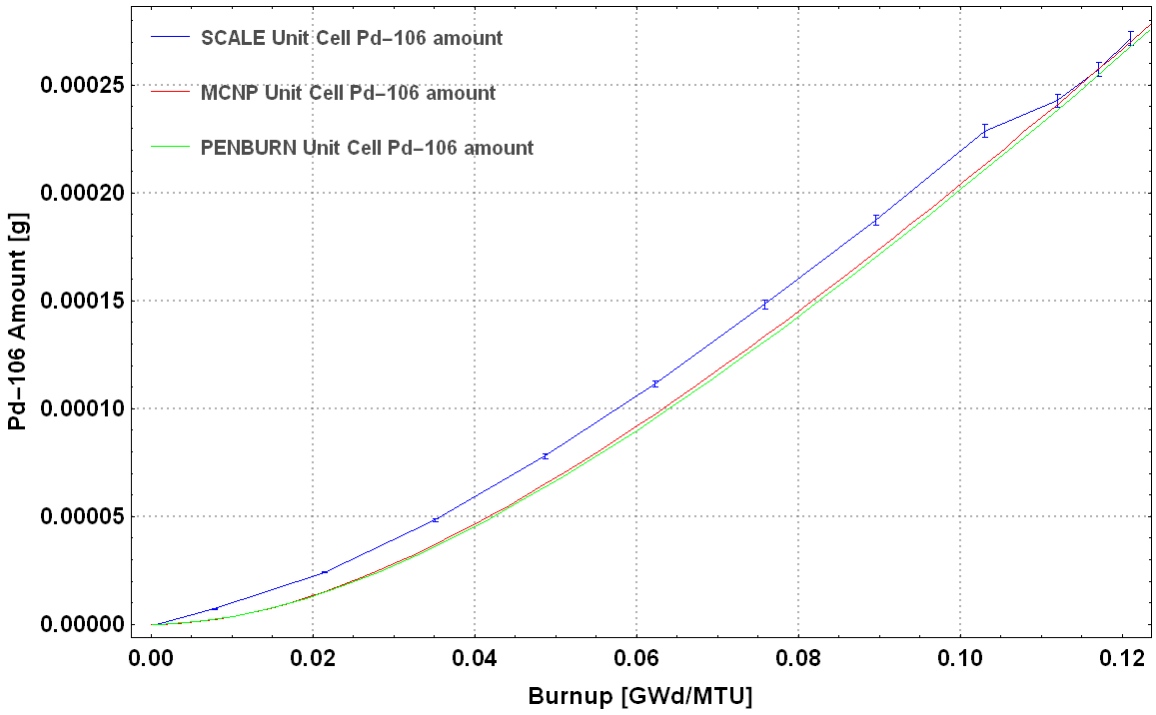

Figure 5.4: Pd-106 predictive capabilities of discrete ordinates and MC codes.

This above behavior demonstrates all codes capabilities of Pu-239 fissions and Pd-106 production. At the end of the burnup all values converge bringing the Pd-106 content within the unit cell indistinguishable between codes.

Minor plutonium isotopics test the predictive capabilities of the transport codes and are very good for comparing/contrasting depletion and burnup. This ultimate test is due to the more known and researched behavior of the major actinides versus the more unknown (relative to major actinides) characteristics of minor plutonium isotopes.

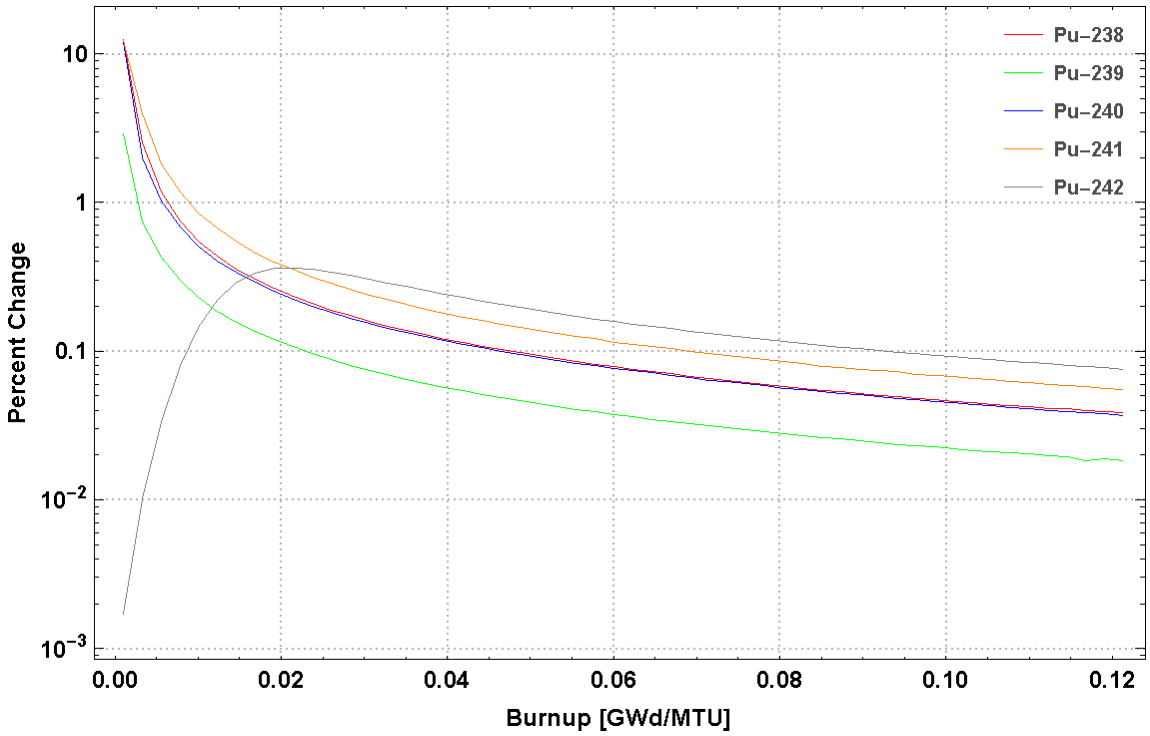

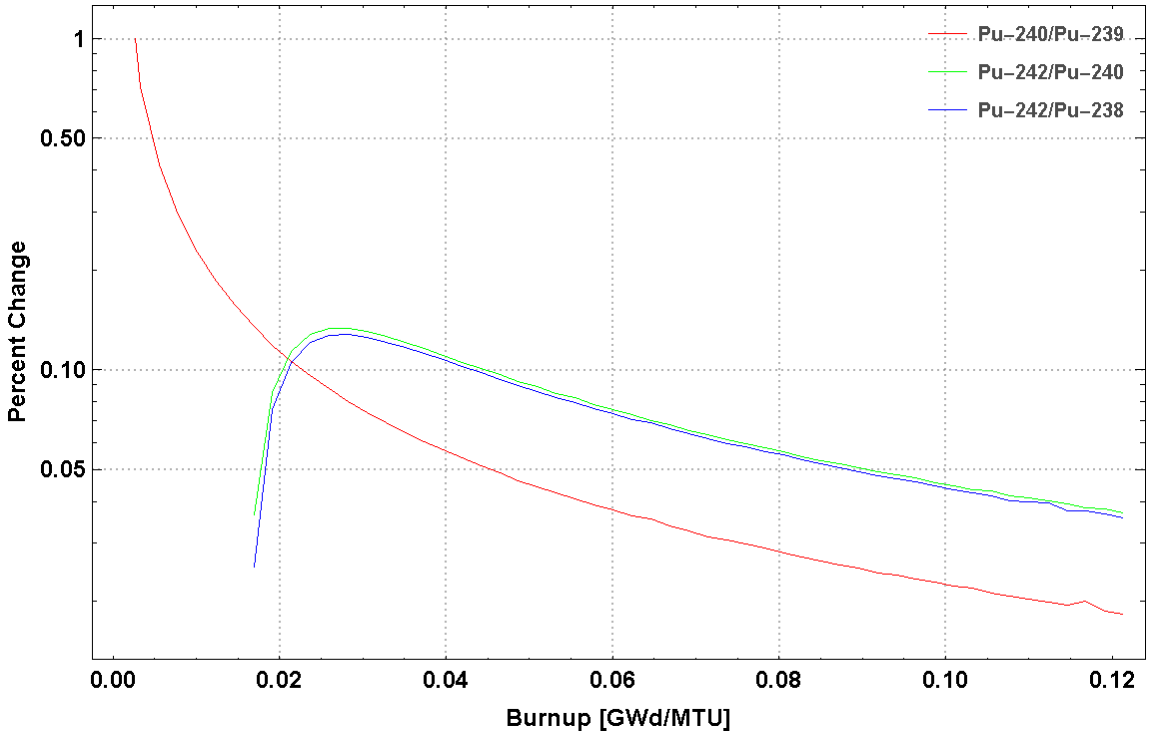

Figures 5.5-5.6: Percent change of Pu isotopics and major Pu ratios.

Figures 5.5 and 5.6 show the percent change from each burn step during steady state operation. The Pu isotopes change similarly from burn step 4 and beyond. All Pu isotopes have an increase in percent change between burn step 2 and 3. Pu-242 has the greatest percent change jumping almost 4 orders of magnitude. This change is most likely attributed to Pu-239 starting to burn within the reactor causing a slight shift in the neutron spectrum due to the higher effective energy released per fission (198.5 MeV) when compared to U-235 (192.9 MeV) and also the higher amount of neutrons released with the fission of a Pu-239 atom (2.874 vs. 2.432).[5]

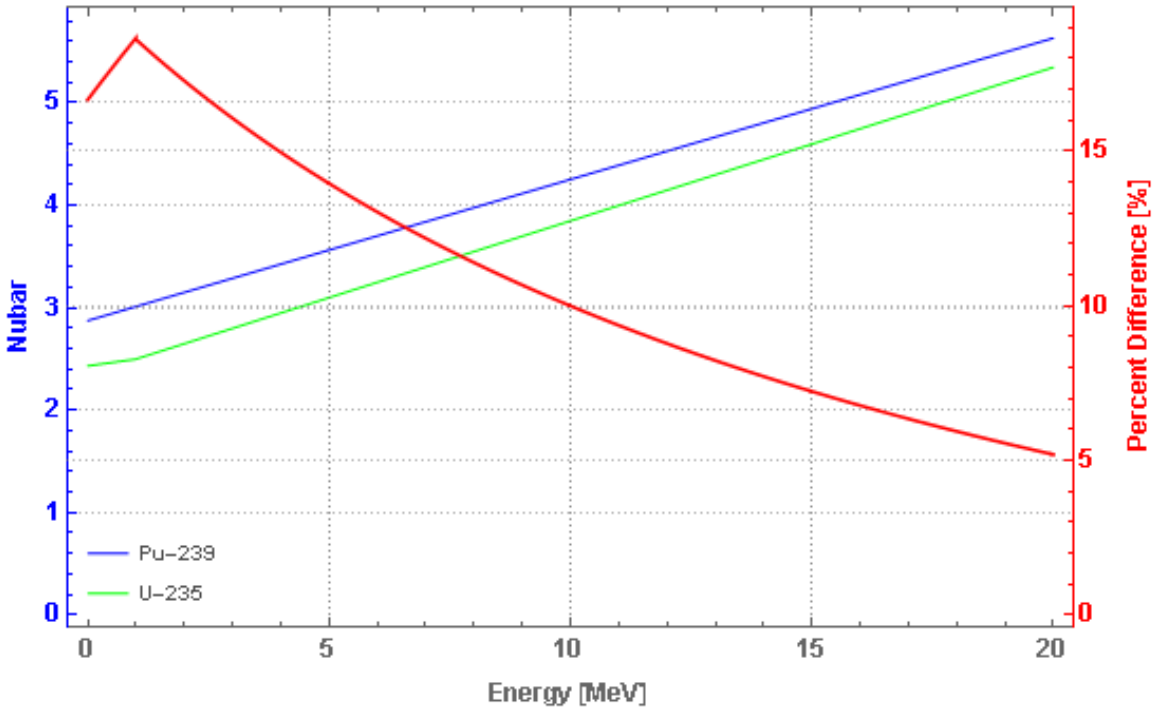

Figure 5.7: Pu-239, U-235 nubar and percent difference between nubar values.

Although most fissions occur at thermal energies, Figure 5.7 shows the overall trend of nubar values. The greater percent difference between Pu-239 and U-235 nubar values is at these lower energies. This behavior explains the sharp increase in Pu-242 percent

change with respect to burnup and also shows the sensitivity of Pu-242 with neutron spectrum.

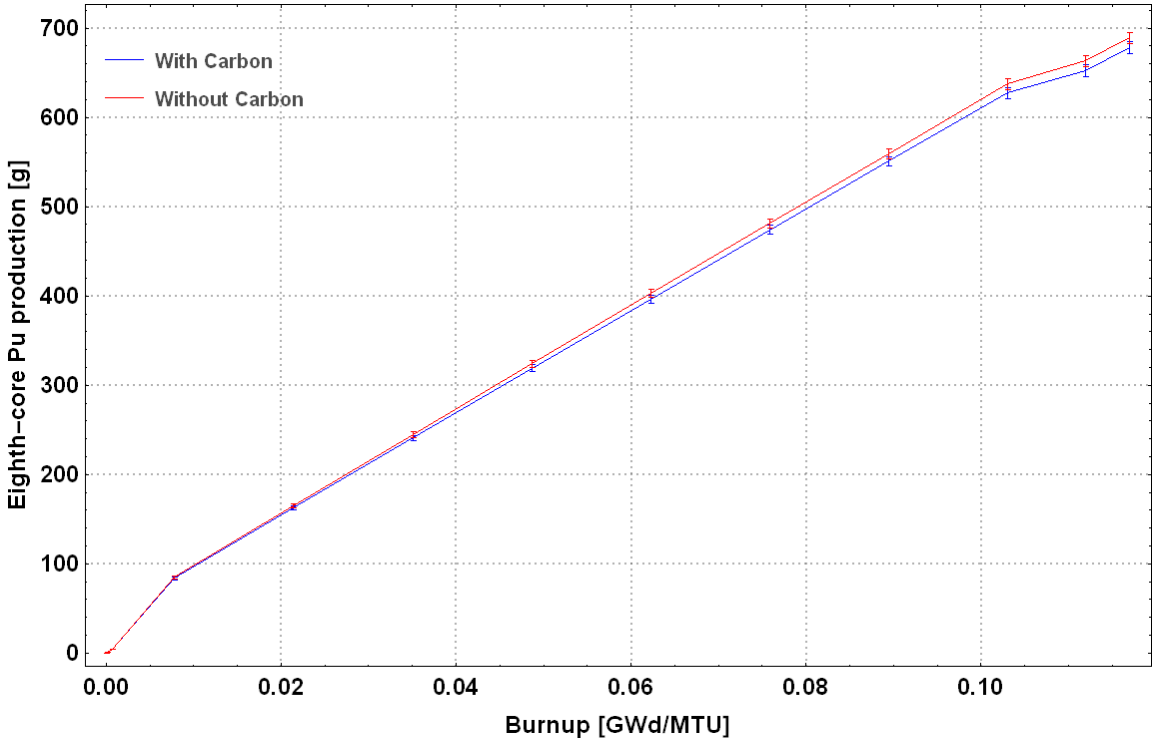

Figure 5.8: Eighth-core Pu production with and without carbon in fuel.

Above in Figure 5.8, eighth-core Pu production is displayed with and without carbon impurity in the fuel. With the nuclear data uncertainty, there is no statistical significance between the overall plutonium production. Overall the minor Pu isotopes varied the greatest between carbon and no carbon eighth-core calculations. Pu-238, Pu-241 and Pu-242 displayed a 3% difference between the average carbon content in natural uranium metal (0.12%) of the time and no carbon. Regarding zones within the reactor, the carbon content affected zones 1 and 2 the greatest with approximately a 4% difference in minor Pu isotope production. The difference in minor Pu production is due to the higher burnup within these zones and the added moderation in the fuel from the

carbon. Again, with error in the nuclear data these differences are not statistically different but these differences could intensify with higher burnup reactors and product statistically different results. This impurity affect needs to be investigated further with higher burnup production reactors and the potential gamma signatures from C-15.

5.3 Forensic Comparative Perspective of X-10 Signatures

Comparing these minor isotopes across codes is necessary for forensic evaluation but also comparing these minor Pu isotopes across reactor types highlights the differences in neutron spectrum and reactor intent. For comparison, a Westinghouse 17 x 17 assembly's Pu isotopics were calculated in ORIGEN-ARP with UO_2 enriched to 3.5% U-235.

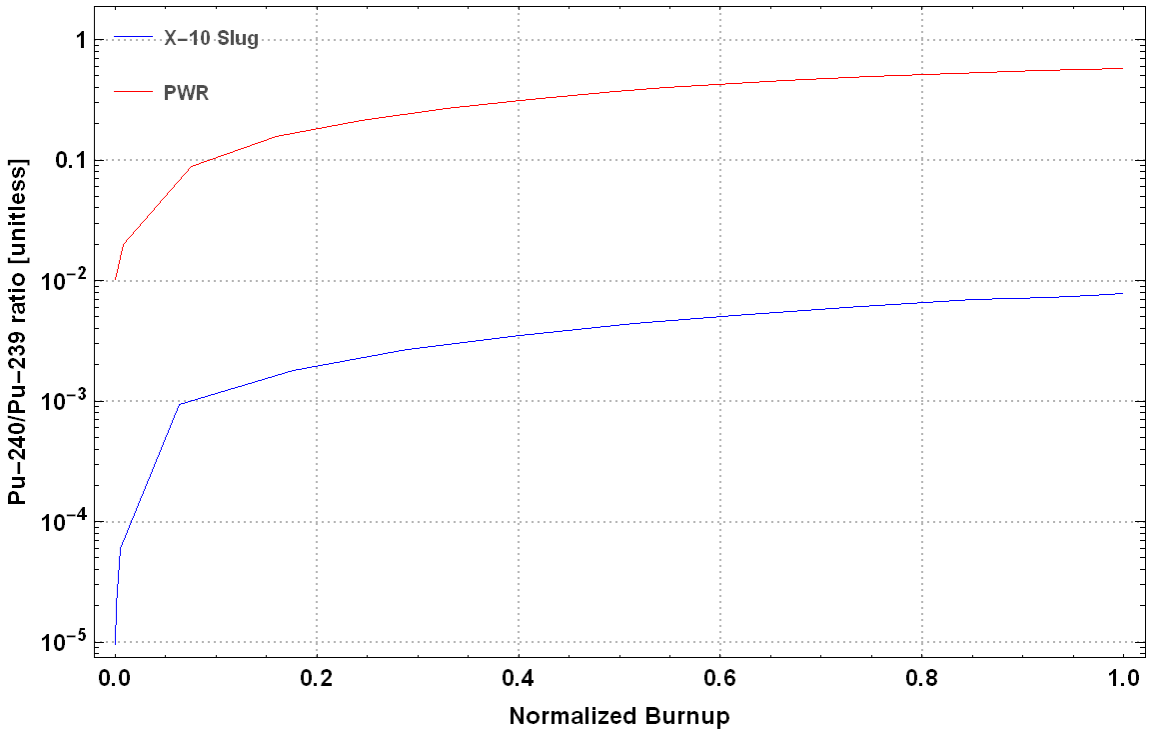

Figure 5.9: PWR Pu-240/Pu-239 ratio compared to X-10 reactor unit cell.

Figure 5.9 emphasizes the spectral differences in the reactor. Commercial power is not meant to produce pure Pu-239 for weapons uses while the early reactors of the Manhattan Project were solely used for weapons material production. The Pu-240/Pu-239 ratios between the two reactors differ by 2 orders of magnitude at steady state operation. The flat flux profile of the X-10 reactor is the cause of the extremely low Pu-240/Pu-239 ratio; while the scalar flux profile in a PWR will fall off approximately 4 to 6 orders of magnitude between the middle of the core and the pressure vessel.[23]

According to Mayer, Wallenius and Ray separating main reactor types using the Pu-242/Pu-240 vs. Pu-238/Total Pu data can be accomplished. Neutron spectrum inversely affects the Pu-242/Pu-240 ratio (the softer the spectrum the higher the ratio) while the Pu-238/Total Pu ratio is affected by initial enrichment.[1] The comparison of these two reactors offers extreme cases for this correlation.

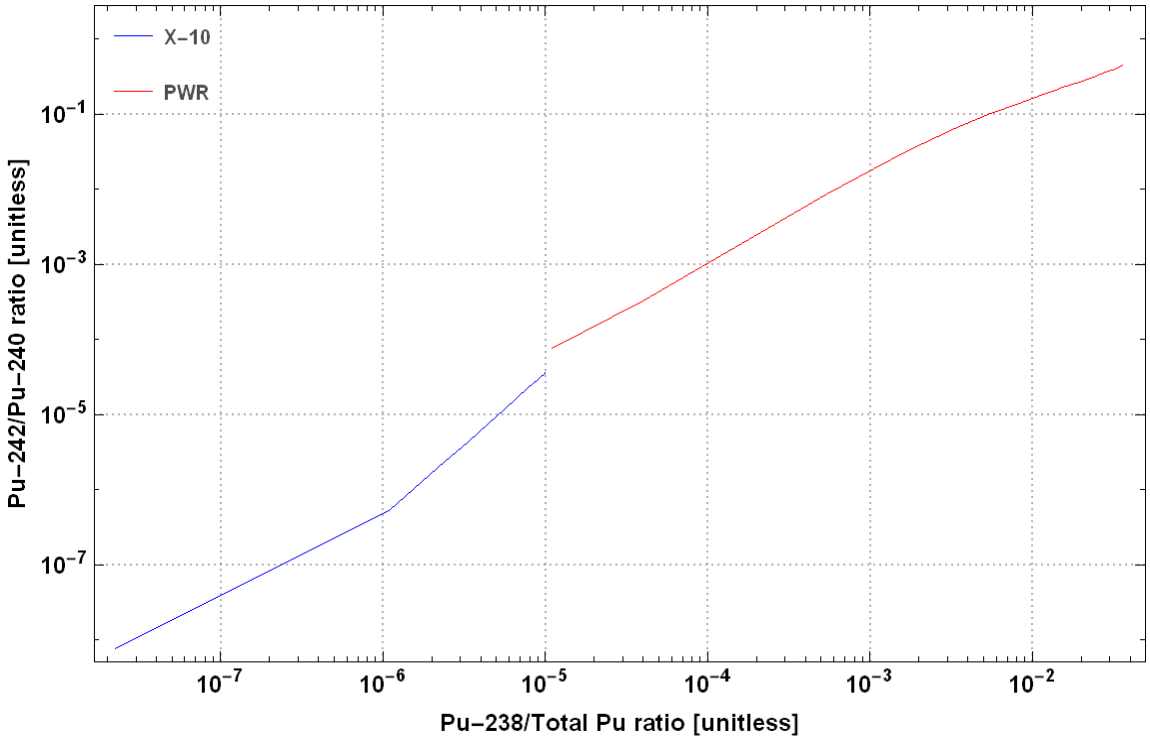

Figure 5.10: Reactor types comparison between PWR and X-10 isotopics.

Figure 5.10 illustrates the differences in neutron spectrum and enrichment. Examining the beginning of cycle and end of cycle for both reactors shows orders of magnitude difference in neutron spectrum and enrichment. Trends in the Pu-238/Total Pu meet expectations as the PWR begins with a higher enriched fuel. X-10 shows a lower Pu-242/Pu-240 ratio which indicates a harder spectrum over the PWR. This trend is because of the moderating material used in each of the reactors. Graphite has a lower moderating power when compared to water which pushes the spectrum slightly higher for X-10.

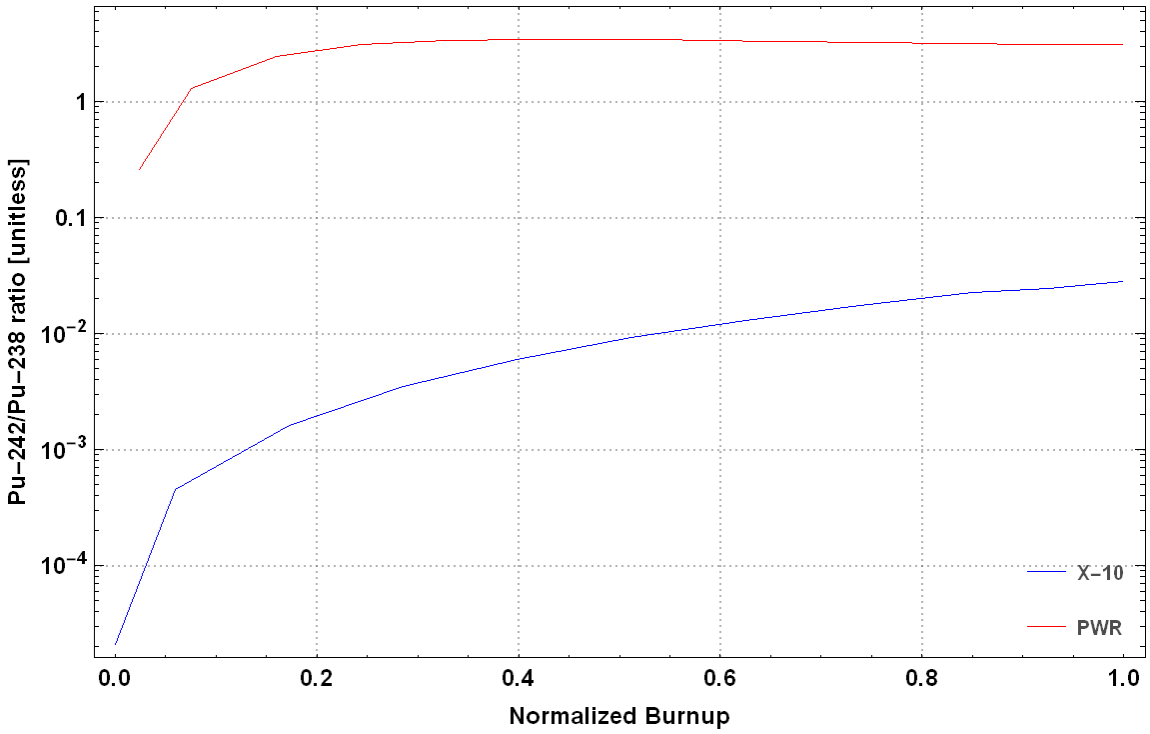

Figure 5.11: Pu-242/Pu-238 ratio with normalized burnup comparison between reactor types.

Figure 5.11 combines neutron spectrum and enrichment level into one ratio and illustrates a radical difference between a production reactor and a commercial reactor.

CHAPTER 6

OVERALL CONCLUSIONS AND RECOMMENDATIONS

Forensically analyzing reactors from the Manhattan Project Era enables the researcher to gain computational nuclear forensic intelligence (CNFI) into production reactor characteristics and signature byproducts. The X-10 reactor provides a solid basis for study because of the fundamental production neutronics that paved the way for the nation's first weapons campaign. Computational forensic assessment of this reactor was completed using several neutron transport codes. These codes differed in transport methods and cross-section evaluation. For the nuclear forensic researcher, these points were demonstrated throughout this study:

- A survey and assessment of the most available neutronic tools and the subsequent relative accuracy of the code results.
- Emphasis on distinct neutronic characteristics and subsequent signature outputs of production reactors.
- Feasibility of determining in-situ fuel origin within a production reactor and reactor intent (commercial versus military).

These topics highlight the Manhattan Era production reactor traits which are required for any modern day weapons program and the tools available to exploit these characteristics.

6.1 Computational and Forensic Conclusions

For this study, discrete ordinates codes ran slower (due to the level of detail gained) than MC codes but this performance statement was dependent on the user's problem discretization (space, energy and angle). With respect to differing P_N and S_N orders, homogenizing the unit cell with P_3/S_8 performed the fastest for reflected unit cell cases. When compared to P_3/S_{16} case, it performed 75% faster and compared to P_3/S_{16} homogenized case, 50% faster. Interestingly, in both homogenized and heterogeneous unit cell calculations, P_3/S_8 performed the fastest even over P_3/S_6 calculations. The P_3/S_8 heterogeneous calculation ran 21% faster than P_3/S_6 case and 56% faster for the homogeneous case. When compared to MCNP, this was roughly a 35% increase in run time for the discrete ordinates calculation. The eigenvalues calculated for the discrete ordinates and MCNP heterogeneous cases were identical to the 3rd decimal place. For the homogeneous discrete ordinates case, the percent change was 0.36% in the 3rd decimal place. If dominance ratio effects are present, 3D discrete ordinates codes add run time but not at the sacrifice of the eigenvalue. Further optimization on discrete ordinates unit cell calculations should be performed in future work. Lowering P_N order affects the answer more adversely when compared to the changing the quadrature. Optimum spatial discretization would lower run times significantly and could reach MC simulation times.

Unit cell results were very similar across code systems with respect to eigenvalue and burnup problems. With uncertainty added in these measurements, no significant differences exist. Concerning comparative burnup study between a PWR and the X-10, unit cell analysis highlighting the key differences in commercial and production reactors represents the two extremes of neutron spectrum (excluding fast reactors). Discernable

differences between these two reactors can be used for distinguishing average fission spectrum (intent of reactor). Eighth-core analysis on X-10 showed Pu-242/Pu-238 ratio behavior with each zone. Pu-242 is very sensitive to neutron spectrum which, in this case, will narrow down the zone from which the material originated within the reactor. The Sampler module within the Scale package offers a stochastic method to determine nuclear data uncertainty. With these uncertainties the null hypothesis cannot be rejected (values are the same to the 68% confidence interval) in the Pu-242/Pu-238 ratio between zones 1-6. A statistical significance exists (null hypothesis can be rejected to one-sigma confidence) between zones 7 and 8 and could potentially be used for determining inner-core vs. outer-core provenance. This difference in Pu-242/Pu-238 ratio is because of the flux drop off between these locations. This result is significant due to the flat flux profile across the entire core (less than an order of magnitude difference) and indicates the highest flux gradient, between zones 6 and 7, is on the periphery of the core. The Pu-242/Pu-240 ratio behaves similarly to the Pu-242/Pu-238. The difference between the two ratios is highlighted with decay from discharge to present day. Pu-242/Pu-240's null hypothesis cannot be rejected (one-sigma confidence) for the steady state and decayed values. This result is important, because analysis of the decayed ratio gives insight into the steady state ratio which points to operating characteristics. Material provenance with respect to commercial versus military use is distinguishable to a high degree of confidence using the above ratios because of the dramatic spectral differences.

Loading of the X-10 reactor was done manually on a slug by slug basis. This fuel loading scheme adds another area of uncertainty in determining axial slug position with respect to any isotopic ratio or amount. Examining the zone 7 Pu-240/Pu-239 ratio axial

variation, there is only a factor of 3.6 drop in the ratio between the outer slug and inner slug positions. The highest axial flux gradient falls off only by a factor of 1.75. This small gradient (less isotopic variation); the fact the slugs were not at static positions throughout the burnup; and nuclear data uncertainty (perhaps experimental error) makes axial position determination an unlikely result. Determining inner-core versus outer-core does allow the researcher to potentially estimate the overall isotopics because removal and blending of the material would take place at different times because of varying degrees of burnup.

Forensically analyzing a Manhattan Era reactor gives the scientist an understanding into the mechanics and simplistic design that were extremely effective at producing weapon quality plutonium. The X-10 reactor design produced very pure Pu-239 across the history of operation. This weapons grade Pu was attributed to the flat flux profile across the core and is a known spectral signature of production reactors. The spectral profile of production reactors also adds ambiguity when applied to material provenance within the reactor. In this case, the flux drops less than an order of magnitude which in turn produces less statistical significant results (e.g. cannot reject null hypothesis of ratios being equal at different areas within the core). Higher burnup production and commercial reactors demonstrate higher flux gradients which in turn produce statistically significant differences in isotopics. These gradients would allow for different isotopic results and provide a better means for determining material origination within the reactor. The pilot plant for the Manhattan Project, the X-10 reactor, not only shaped the understanding of neutronics but affords the nuclear forensic scientist the opportunity to highlight production reactor characteristics and corresponding signatures.

In turn, these first principle production characteristics apply to any aspiring weapons development program.

6.2 Future Considerations

Further investigations into MC codes dominance ratio effects in production reactors isotopics and fissile isotope creation amounts should be addressed. Discrete ordinates code packages are void of this effect and more spatial granularity can be gained with respect to isotopics and production amounts. Finally, investigations into forensic differences between production reactors of the Manhattan Era and modern day (similar properties of past reactors) reactors calls for study for national security reasons, mainly attribution efforts. Addressing the issues and potential sources of error within these code packages not only aids in CNFI but in reporting answers to policy makers with a level of confidence.

REFERENCES

[1] K. Mayer, M. Wallenius, and I. Ray. "Nuclear Forensics- A Methodology Providing Clues on the Origin of Illicitly Trafficked Nuclear Materials." Analyst The Analyst 130.4 (2005): 433. Web.

[2] D.D. Cowen. The Oak Ridge National Laboratory Graphite Reactor. Tech. Oak Ridge: Central Files Number 53-12-126. Print.

[3] E.J. Boyle, and C. D. Cagle. Fuel Elements for ORNL Graphite Reactor. Tech. no. ORNL CF-52-6-10. N.p.: n.p., 1952. Print.

[4] L. E. Stanford. Safeguard Report on the Proposed Method of Annealing Graphite in the X-10 Reactor. Tech. no. ORNL 2725. Oak Ridge: n.p., 1959. Print.

[5] J. J. Duderstadt, and L. J. Hamilton. Nuclear Reactor Analysis. New York: Wiley, 1976. Print.

[6] M. J. Kristo, D. K. Smith, S. Niemeyer, G. D. Dudder, Model Action Plan for Nuclear 3 Forensics and Nuclear Attribution, Rep. UCRL-TR-202675, Lawrence Livermore National 4 Laboratory, Livermore, CA (2004).

[7] A. Glaser. "Isotopic Signatures of Weapon-Grade Plutonium from Dedicated Natural Uranium-Fueled Production Reactors and Their Relevance for Nuclear Forensic Analysis." Nuclear Science and Engineering Nucl. Sci. Eng. 163.1 (2009): 26-33. Web.

[8] G. Hecht. Being Nuclear: Africans and the Global Uranium Trade. Cambridge, MA: MIT, 2012. Print.

[9] M. A. Levi. Deterring State Sponsorship of Nuclear Terrorism. New York: Council on Foreign Relations, 2008. Print.

[10] D. Reilly, Passive Nondestructive Assay of Nuclear Materials (PANDA), Los Alamos National Laboratory, LA-UR-90-732, 1991.

[11] K. J. Moody, I. D. Hutcheon, and P. M. Grant. Nuclear Forensic Analysis. Boca Raton, FL: CRC, 2005. Print.

[12] The Fallout Analysis Tool (FAT), Oak Ridge National Laboratory.

[13] S. D. Sheppard, Experiment Facilities of the Oak Ridge Graphite Reactor. Tech. no. ORNL-TM-266. Oak Ridge: n.p., 1962. Print.

[14] National Nuclear Energy Series Division VIII-Volume 5 (Published Declassified Volumes). Technical Information Service, Oak Ridge, TN. AECD-2624.

[15] MCNP User's Manual, Version 5. Los Alamos National Laboratory. LA-UR-03-1987. 2003.

[16] ORNL Graphite Reactor: 1943 X-10 Pile - 1963 Research Reactor. Publication no. 3445605702923. Web. <web.ornl.gov/info/reports/1963/3445605702923.pdf>.

[17] G. Sjoden and A. Haghighat, "PENTRAN Code System, Users Guide to Version9.4.X.1 Series," HSW Technologies LLC, (2008).

[18] K. Manalo, T. Plower, T. Mock, M. Rowe, G. Sjoden, "PENBURN User's Guide version 3.5," (2009).

[19] J. S. Levin, and J. W. Weil. Calibration of Control Rod System of the X-10 Reactor. Tech. no. BNL-22 (R-6877). Upton: n.p., 1949. Print.

[20] M. L. Williams, et. al., Sampler: A Module for Statistical Uncertainty Analysis With Scale Sequences (Draft Documentation). Oak Ridge National Laboratory.

[21] A. S. Quist. A History of Classified Activities at Oak Ridge National Laboratory. Tech. no. ORCA-7. 2000. Print.

[22] A. Aronson, H. Ludewig, and L. Cheng. "X-10 Fuel Slugs." Memorandum to Diane Rocco. 4 Apr. 2008. MS. N.p.

[23] B. Petrovic, and A. Haghighat. "Effects of SN Method Numerics on Pressure Vessel Neutron Fluence Calculations." NSE Nuclear Science and Engineering 122.2 (1996): 167-93. Web.

[24] Chang, J.: ENDFPLOT 0.2 - Cross Section Plotter, KAERI. Available at: http://atom.kaeri.re.kr/endfplot.shtml. Retrived 2015.

[25] SCALE: A Comprehensive Modeling and Simulation Suite for Nuclear Safety Analysis and Design, ORNL/TM-2005/39, Version 6.1, Oak Ridge National Laboratory, Oak Ridge, Tennessee, June 2011.